THREE-AXIS ORIENTATION AND STABILIZATION OF A PROBE USING SOLAR PRESSURE

by

Luat T. Nguyen

NGR 22-009-019

CSR T-70-4

CENTER FOR SPACE RESEARCH
MASSACHUSETTS INSTITUTE OF TECHNOLOGY

THREE-AXIS ORIENTATION AND STABILIZATION OF A PROBE USING SOLAR PRESSURE

by

Luat T. Nguyen

CSR T-70-4

THREE-AXIS ORIENTATION AND STABILIZATION OF A PROBE USING SOLAR PRESSURE

by

Luat T. Nguyen

Submitted to the Department of Aeronautics and Astronautics on August 31, 1970 in partial fulfillment of the requirements for the degrees of Master of Science and Engineer in Aeronautics and Astronautics.

ABSTRACT

This thesis report describes an investigation into the possibilities of using solar pressure torques to perform three-axis orientation and stabilization of a small probe. The attitude control system is to maintain one spacecraft axis perpendicular to the ecliptic plane and another axis pointed closely to the sun. This orientation allows the use of a high gain directional antenna which tracks the earth through a single rotation in the ecliptic. The three main elements of the control loop are analyzed: (1) attitude sensing, (2) spacecraft dynamics, (3) control torque production. A workable design is evolved which satisfies all the attitude control requirements while retaining the features of simplicity and low weight.

Thesis Supervisor: John V. Harrington
Title: Professor of Aeronautics and Astronautics

ACKNOWLEDGMENTS

I wish to thank Professor John V. Harrington, Thesis Supervisor, who made this work possible. I wish also to express my deepest appreciation to Mr. Richard H. Baker, who was my immediate supervisor, and Mr. William W. Cooper for the generosity with which they gave of their time and for their guidance, helpful suggestions and ideas, many of which appear in this thesis. Thanks also are due to Mrs. Hannah Irving for typing the final manuscript.

TABLE OF CONTENTS

LIST OF ILLUSTRATIONS

CHAPTER 1

INTRODUCTION

In the past, solar photon pressure acting on a body in space has been regarded as an undesirable disturbance which can cause trajectory errors as well as tax the attitude control system. For example, on the Mariner II Venus mission, solar pressure imbalance torques accounted for about half of the total gas consumed. More recently, the idea of actually using solar pressure to advantage has gained prominence. Investigations have been made into its possible use both as a propulsive system, solar sailing, and as control torques for attitude control. The advantages in using solar radiation pressure are obvious: (1) It provides a practically limitless source of momentum, or to put it in propulsive terms the system has an infinite specific impulse; and (2) Like the gravity gradient, it has an inherent reference direction toward which a spacecraft can be oriented and maintained. These characteristics make the concept especially desirable for long duration missions. The principal drawback in using solar pressure is the rather minute magnitude of the pressure itself, at one A.U. it is only about .46 dynes/m^2.

Thus, solar sailing is impractical except for the longest missions. However, solar pressure acting at long enough moment arms can provide appreciable torques for spacecraft attitude control. Several studies have been made into the feasibility of such schemes but by far the most detailed investigation was carried out for the Sunblazer program. Here, the objective is to put a small, light spacecraft into a heliocentric orbit for the purpose of making certain scientific measurements. The principal attitude control requirement is to keep one axis always facing the sun. There are several reasons for this desired orientation:

(1) Solar cell power is maximized when all cells are in a plane facing the sun.

(2) Antenna patterns can be maximized for a sun-oriented spacecraft.

(3) Some solar experiments may require that the spacecraft point closely to the sun.

(4) Thermal control is simplified for a spacecraft with one side always facing the sun.

Initial orientation and long term stabilization was achieved using only solar radiation pressure torques. The spacecraft configuration is shown in Figure 1.1. The attitude control system consists of four reflecting vanes, rotatable about their longitudinal axis. The torques

produced by such vanes are derived in Apprendix A. Rotations of the vanes allowed direct control over θ, i.e., sun-pointing. However, there is no direct roll control, the spin rate being allowed to vary between .1 RPM and 19 RPM. Thus, this design is essentially a two axis stablized system. It is the objective of this thesis to investigate the possibility of carrying this design one step further, that is, to a fully three-axis stabilized system. The overriding reason for going to three-axis stabilization is that it allows the use of a high-gain directional antenna. For this case, where the orbital plane is essentially coincident with the ecliptic, control of roll about the sun-pointed axis will allow a directional antenna to track earth by a single rotation in the ecliptic plane. It was determined that the best antenna configuration for this application is a stacked pair of three-element Yagis. Parabolic dish configurations were rejected due to the requirement of a large dish size at the frequency of operation. Studies resulted in an optimum design for the Yagi antenna structure as shown in Figure 1.2. Mechanical and electrical specifications are shown in the following table.

Mechanical Specifications

$2h_R = .51\lambda$ $\qquad$ $S_F = .17\lambda \leftrightarrow .23\lambda$

$2h_F = .5\lambda$ $\qquad$ $S_{FD} = .16\lambda \leftrightarrow .19\lambda$

$2h_D = .44\lambda$ $\quad d = .75\lambda \rightarrow .9\lambda$

$\rho_R = \rho_F = \rho_D = .0037\lambda$

Electrical Specifications

A. Individual 3-element Yagi

$\theta^a_h = 57°$ $\quad \lambda$ = wavelength

$\theta^a_v = 75°$ $\quad \theta^a$ = beamwidth

Gain = 9.65 dB over omnidirectional

B. Stacked Yagis

$\theta^a = 47°$

Gain = 12.65 dB over omnidirectional

The antennas rotate in the ecliptic plane through γ to track the earth as shown in Figure 1.3. The attitude control requirements are thus:

(1) Maintain one axis, z , pointing closely to the sun.

(2) Maintain another body axis, x , pointing closely perpendicular to the ecliptic plane.

Control of both axes should be within 10° of optimum to avoid losses in antenna pattern. Having defined the requirements, the problem can now be divided into three major areas:

(1) Attitude sensing

(2) Initial orientation

(3) Long term stabilization

Within this framework, two configurations were studied: (1) a completely despun spacecraft and; (2) a dual spin spacecraft. It must be emphasized that the prime objective of the Sunblazer design was to have a very lightweight, low-cost spacecraft -- the final configuration weighed only twenty-eight pounds. This study was carried out with the same objectives in mind; minimum weight and simplicity were sought at all times.

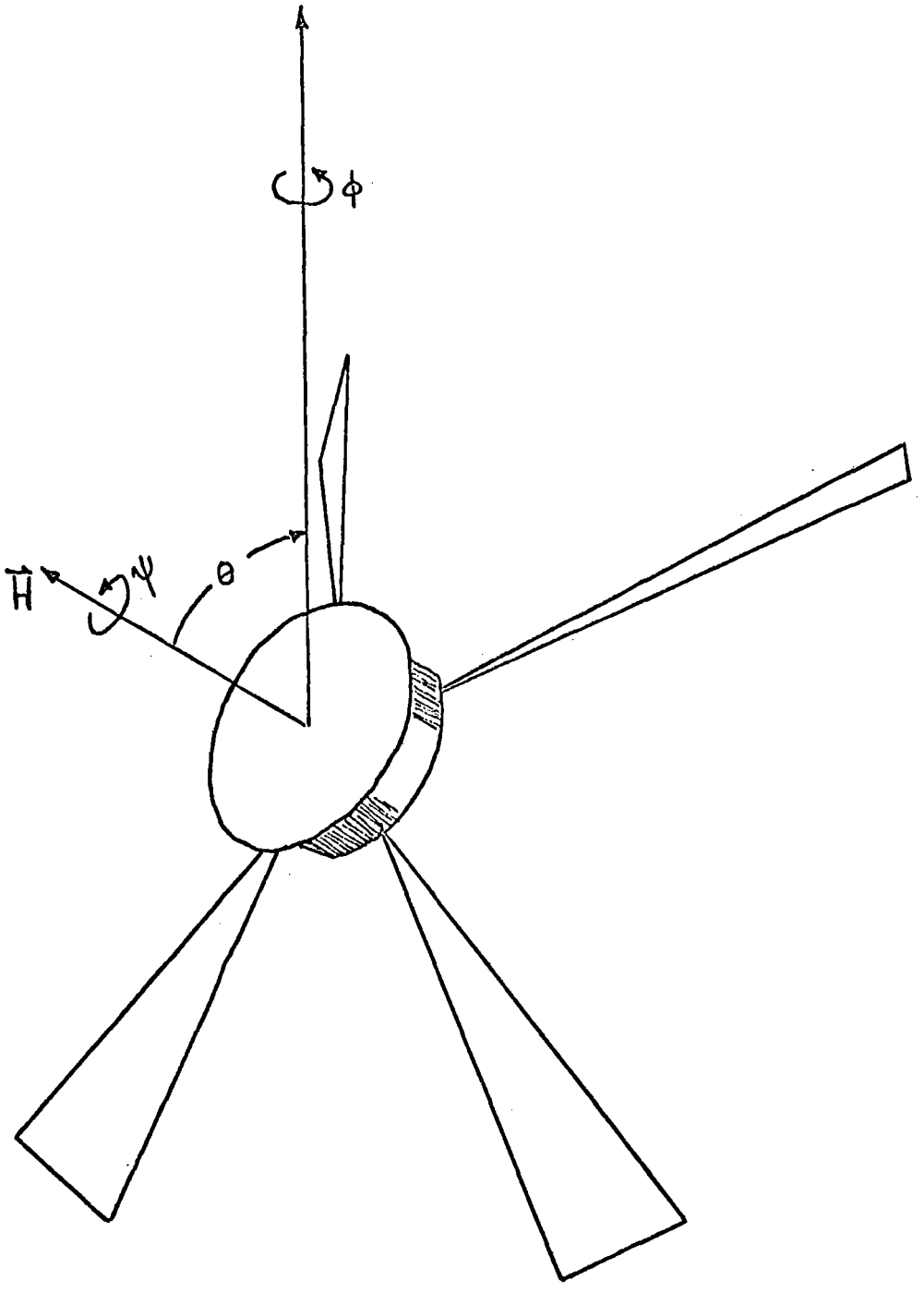

Figure 1.1 Sunblazer spacecraft

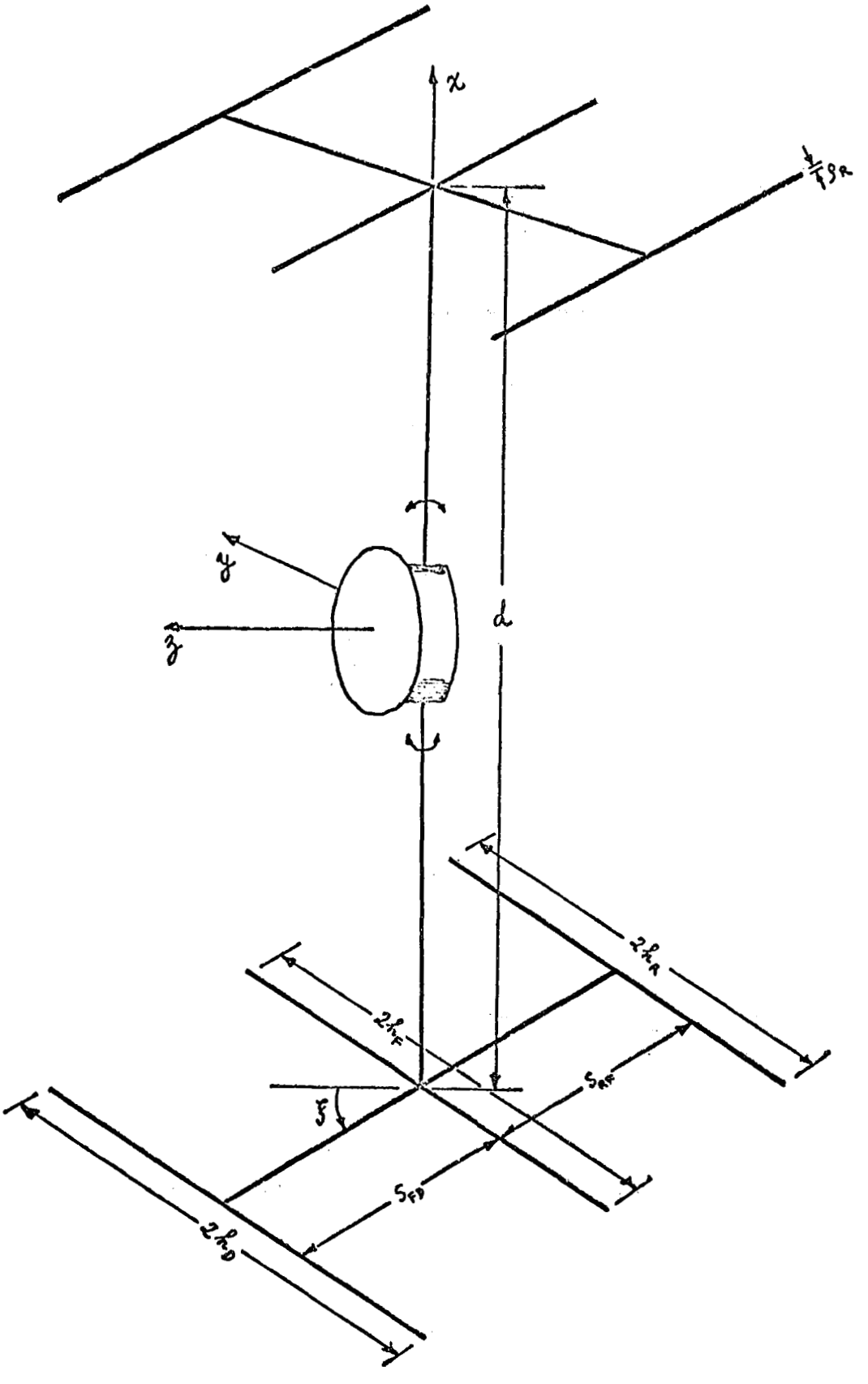

Figure 1.2 Antenna configuration

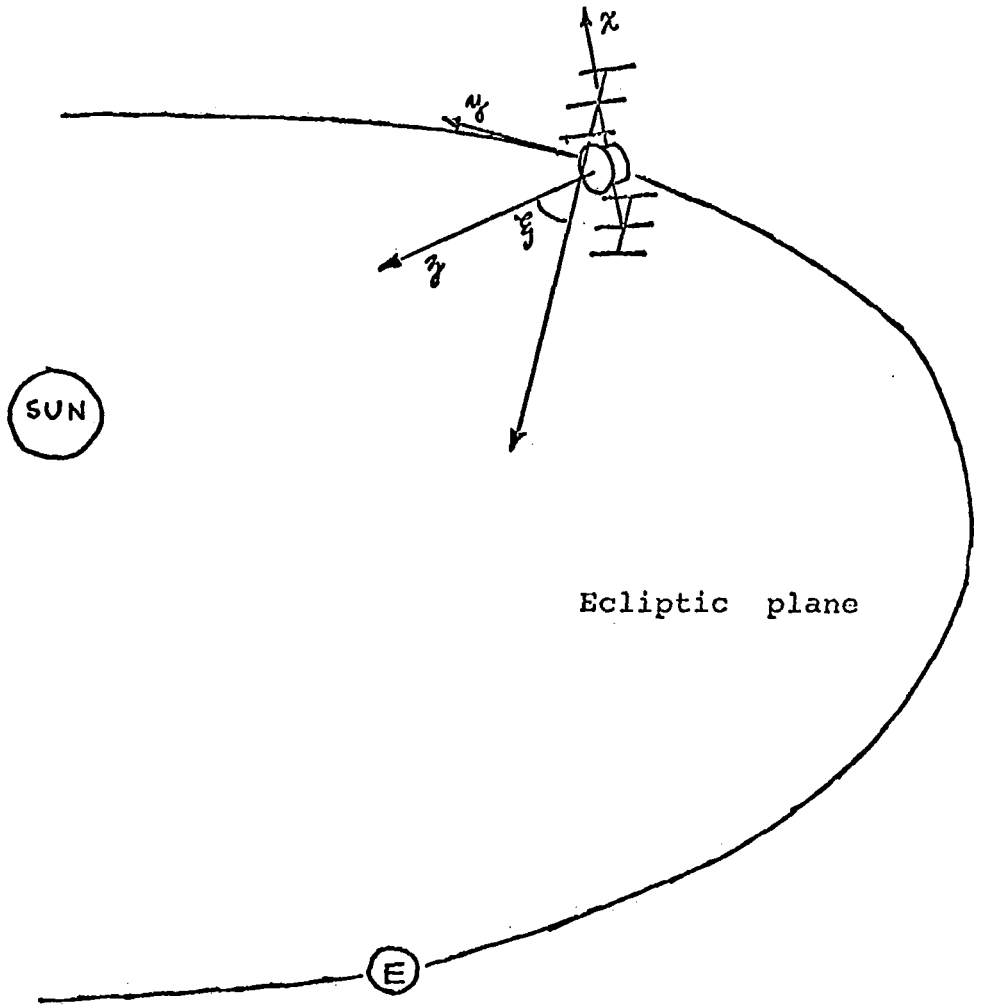

Figure 1.3 Antenna orientation requirements

CHAPTER 2

GENERAL DYNAMICS OF A SPINNING BODY

2.1 General

The Sunblazer probe is to be launched into its solar orbit by a five stage Scout booster. The spacecraft initial conditions at separation from the final stage are assumed to be a spin rate of 200 RPM at an angle of 60° from the sun. Therefore, to investigate the dynamics of such a spacecraft, one must first have an understanding of the basics of rotational motion.

The basic equations for gyrodynamic motion are Euler's equations:

$$I_{x_p}\dot{\omega}_{x_p} + \omega_{y_p}\omega_{z_p}(I_{z_p} - I_{y_p}) = N_{x_p} \qquad (2\text{-}1)$$

$$I_{y_p}\dot{\omega}_{y_p} + \omega_{x_p}\omega_{z_p}(I_{x_p} - I_{z_p}) = N_{y_p} \qquad (2\text{-}2)$$

$$I_{z_p}\dot{\omega}_{z_p} + \omega_{x_p}\omega_{y_p}(I_{y_p} - I_{x_p}) = N_{z_p} \qquad (2\text{-}3)$$

where x_p, y_p, z_p are the principal axes of the body. Study of the motion can now be divided into two general areas: (1) Torque free motion where $\vec{N} = 0$, and (2) Motion in which torques act on the body.

2.2 Torque Free Motion

With the simplification that the body is symmetric so that $I_{x_p} = I_{y_p} = I_t$, the above equations become:

$$I_t \dot{\omega}_{x_p} + \omega_{y_p}\omega_{z_p}(I_{z_p} - I_t) = 0 \qquad (2\text{-}4)$$

$$I_t \dot{\omega}_{y_p} + \omega_{x_p}\omega_{z_p}(I_t - I_{z_p}) = 0 \qquad (2\text{-}5)$$

$$I_{z_p}\dot{\omega}_{z_p} = 0 \qquad (2\text{-}6)$$

The first result for the motion follows from Equation (2-6):

$$\omega_{z_p} = \text{constant} \qquad (2\text{-}7)$$

Define $$\Omega = \frac{I_{z_p} - I_t}{I_t}\omega_{z_p} \qquad (2\text{-}8)$$

Then Equations (2-4) and (2-5) can be written as:

$$\dot{\omega}_{x_p} + \Omega\omega_{y_p} = 0 \qquad (2\text{-}9)$$

$$\dot{\omega}_{y_p} - \Omega\omega_{x_p} = 0 \qquad (2\text{-}10)$$

A solution may be found to these coupled simultaneous equations by multiplying the second equation by i and adding it to the first:

$$(\dot{\omega}_{x_p} + i\dot{\omega}_{y_p}) - i\Omega(\omega_{x_p} + i\omega_{y_p}) = 0 \qquad (2\text{-}11)$$

If we define

$$\lambda \equiv \omega_{x_p} + i\omega_{y_p} \qquad (2\text{-}12)$$

then $$\dot{\lambda} - i\Omega\lambda = 0 \qquad (2\text{-}13)$$

with the solution $$\lambda(t) = Ae^{i\Omega t} \qquad (2\text{-}14)$$

Thus, $$\omega_{x_p} + i\omega_{y_p} = A\cos\Omega t + iA\sin\Omega t \qquad (2\text{-}15)$$

where $$A = \text{const.} = \sqrt{\omega_{x_p}^2 + \omega_{y_p}^2} \equiv \omega_t \qquad (2\text{-}16)$$

and therefore, $$\omega_{x_p}(t) = \omega_t\cos\Omega t \qquad (2\text{-}17)$$

$$\omega_{y_p}(t) = \omega_t\sin\Omega t \qquad (2\text{-}18)$$

Since ω_{3_p} = constant, the magnitude of $\vec{\omega}$ is also constant.

$$|\vec{\omega}| = \omega = \sqrt{\omega_t^2 + \omega_{3_p}^2} = \text{const.} \qquad (2\text{-}19)$$

Equations (2-17) and (2-18) are the parametric equations of a circle, so that the projection of the vector $\vec{\omega}$ onto the plane describes a circle with time, as shown in Figure 2.1.

Since we are considering force-free motion, the angular momentum vector $\vec{H}$ must be a constant, fixed in space. An additional constant of the motion is that the rotational kinetic energy is constant:

$$T = \frac{1}{2}\vec{\omega}\cdot\vec{H} = \text{const.} \qquad (2\text{-}20)$$

Since $\vec{H}$ is constant, Equation (2-20) requires that $\vec{\omega}$ move in such a manner that its projection on the stationary angular momentum vector is constant. Thus, $\vec{\omega}$ "nutates" about and makes a constant angle with the vector $\vec{H}$, the rate of nutation being given by Ω. The motion can be visualized as a rolling of the "body cone" on the "space cone" which is fixed in space by the vector $\vec{H}$, Figure 2.2. From geometry,

$$\tan\theta' = \frac{I_t\,\omega_t}{I_{3_p}\,\omega_{3_p}} = \frac{H_t}{H_{3_p}} \qquad (2\text{-}21)$$

Thus θ' is simply a function of the ratio of the transverse angular momentum to the spin momentum. θ' is called the "nutational amplitude" because it is a direct measure of the magnitude of the "wobble".

2.3 Torqued Motion

Note that the equations used so far have all been referred to the body-fixed axes which move with the body and hence tells us nothing about how the body moves in space. This is perfectly acceptable when studying torque free motion since the angular momentum vector remains fixed in space while the body simply nutates around it. However, when studying the case where torques act on the body, it is more convenient and illuminating to define a coordinate system with a reference external to the body -- in this particular case, the sun. Define three coordinate systems as shown in Figure 2.3. $\{X_s, Y_s, Z_s\}$ is a system, call it "s", with origin fixed at the center of gravity of the spacecraft with the Z_s-axis pointed at the sun, Y_s-axis in the ecliptic plane, and X_s-axis perpendicular to the ecliptic. $\{X, Y, Z\}$ is an axes system, call it "k", which, though it moves with the body, does not rotate with it about Z. $\{x, y, z\}$ are body-fixed coordinates, "b". The three systems are related through the standard Euler angles (ϕ, θ, ψ) as defined:

First rotation $$\begin{Bmatrix} X \\ y_1 \\ Z_s \end{Bmatrix} = A \begin{Bmatrix} X_s \\ Y_s \\ Z_s \end{Bmatrix}$$

$$A = \begin{bmatrix} \cos\phi & \sin\phi & 0 \\ -\sin\phi & \cos\phi & 0 \\ 0 & 0 & 1 \end{bmatrix} \qquad (2\text{-}22)$$

Second rotation $$\begin{Bmatrix} X \\ Y \\ Z \end{Bmatrix} = B \begin{Bmatrix} X \\ y_1 \\ Z_s \end{Bmatrix}$$

$$B = \begin{bmatrix} 1 & 0 & 0 \\ 0 & \cos\theta & \sin\theta \\ 0 & -\sin\theta & \cos\theta \end{bmatrix} \qquad (2\text{-}23)$$

Third rotation $$\begin{Bmatrix} x \\ y \\ z \end{Bmatrix} = C \begin{Bmatrix} X \\ Y \\ Z \end{Bmatrix}$$

$$C = \begin{bmatrix} \cos\psi & \sin\psi & 0 \\ -\sin\psi & \cos\psi & 0 \\ 0 & 0 & 1 \end{bmatrix} \qquad (2\text{-}24)$$

For the total rotation

$$\begin{Bmatrix} x \\ y \\ z \end{Bmatrix} = CBA \begin{Bmatrix} X_s \\ Y_s \\ Z_s \end{Bmatrix} \qquad (2\text{-}25)$$

where

$$CBA = \begin{bmatrix} c\phi c\psi - s\phi s\psi c\theta & s\phi c\psi + c\phi s\psi c\theta & s\psi s\theta \\ -c\phi s\psi - s\phi c\psi c\theta & -s\phi s\psi + c\phi c\psi c\theta & c\psi s\theta \\ s\phi s\theta & -c\phi s\theta & c\theta \end{bmatrix} \quad (2\text{-}26)$$

As defined, the Euler angles are useful in describing the attitude of the spacecraft with respect to the sunline; θ specifies the angle between the spin axis and the sun line, the precession angle, ϕ, specifies rotation about the sun line, and ψ specifies rotation about the spin axis. The "k" axes system is very suitable for studying the motion of the spacecraft. Since the X-axis is always perpendicular to the plane containing the spin axis and the sun line, torques acting along this axis will cause the spin axis to precess about the sun line. This torque is analogous to the gravity torque acting on a spinning top, causing it to precess about the local vertical. Because the X-axis is coincident with the $\dot{\theta}$ direction, N_X torques can never effect θ. The Y-axis, on the otherhand, lies in the plane containing the sun line and the spin axis and is in fact perpendicular to the latter. Thus torques along this axis will erect the spin axis toward (or away from) the sun. Since the Z-axis corresponds to the spacecraft spin axis, N_Z torques

will only change the magnitude of the angular momentum, not its direction. For these reasons, the N_X, N_Y, and N_Z torques are referred to as the precession, erection, and spin torques respectively.

With these definitions, we can proceed to develop the equations of motion in the "k" axes system. Once again, the spacecraft is assumed symmetric, with $I_x = I_y = I_t$. Following the derivation from the Sunblazer report [1], the basic equation of motion when referred to the rotating frame of reference "k" becomes:

$$\dot{\vec{H}} = \vec{N} - (\vec{\omega}_{sk} + \vec{\omega}_{is}) \times \vec{H} \qquad (2\text{-}27)$$

where $\vec{\omega}_{sk}$ = angular velocity of "k" system with respect to the "s" system

$\vec{\omega}_{is}$ = angular velocity of "s" system with respect to inertial space, i.e. the orbital angular rate.

These rates can be expressed in terms of the Euler angles as:

$$\vec{\omega}_{sk} = \vec{\imath}_k \dot{\theta} + \vec{\jmath}_k \dot{\phi} s\theta + \vec{k}_k \dot{\phi} c\theta \qquad (2\text{-}28)$$

$$\vec{\omega}_{is} = \omega_{is}(\vec{\imath}_k \cos\phi - \vec{\jmath}_k c\theta s\phi + \vec{k}_k s\theta s\phi) \qquad (2\text{-}29)$$

And also:

$$\vec{H} = \vec{\imath}_k I_t \dot{\theta} + \vec{\jmath}_k I_t \dot{\phi} s\theta + \vec{k}_k I_z (\dot{\psi} + \dot{\phi} c\theta) \qquad (2\text{-}30)$$

So that:

$$\dot{\vec{H}} = \vec{\imath}_K I_t \ddot{\theta} + \vec{\jmath}_K I_t(\ddot{\phi} s\theta + \dot{\phi}\dot{\theta} c\theta) + \vec{k}_K I_z \frac{d}{dt}(\dot{\psi} + \dot{\phi} c\theta) \tag{2-31}$$

$$\vec{\omega}_{sK} \times \vec{H} = \vec{\imath}_K \left[I_z \dot{\phi} s\theta (\dot{\psi} + \dot{\phi} c\theta) - I_t \dot{\phi}^2 s\theta\, c\theta \right] + \vec{\jmath}_K \left[I_t \dot{\phi}\dot{\theta} c\theta - I_z \dot{\theta}(\dot{\psi} + \dot{\phi} c\theta) \right] \tag{2-32}$$

$$\vec{\omega}_{is} \times \vec{H} = \omega_{is} \left\{ -\vec{\imath}_K \left[I_z c\theta\, s\phi (\dot{\psi} + \dot{\phi} c\theta) + I_t \dot{\phi} s^2\theta\, s\phi \right] - \vec{\jmath}_K \left[I_z c\phi (\dot{\psi} + \dot{\phi} c\theta) - I_t \dot{\theta} s\theta\, s\phi \right] + \vec{k}_K \left[I_t \dot{\phi} s\theta\, c\phi + I_t \dot{\theta} c\theta\, s\phi \right] \right\} \tag{2-33}$$

Putting equations (2-31), (2-33) into (2-27), we obtain:

$$I_t \ddot{\theta} - I_t \dot{\phi}^2 s\theta c\theta + I_z \dot{\phi} \omega_z s\theta = N_x - (\vec{\omega}_{is} \times \vec{H})_x \tag{2-34}$$

$$I_t(\ddot{\phi} s\theta + 2\dot{\phi}\dot{\theta} c\theta) - I_z \dot{\theta} \omega_z = N_y - (\vec{\omega}_{is} \times \vec{H})_y \tag{2-35}$$

$$I_z \frac{d\omega_z}{dt} = N_z - (\vec{\omega}_{is} \times \vec{H})_z \tag{2-36}$$

where

$$\omega_z = \dot{\psi} + \dot{\phi} c\theta \tag{2-37}$$

and $(\vec{\omega}_{is} \times \vec{H})$ is given by (2-33).

Equations (2-34) to (2-37) are the complete, general dynamical equations describing the motion of an inertially symmetric spacecraft in a solar orbit. For our case, the precessional torques caused by solar pressure are so small that for spin rates above about .1 r/min, the nutational and precessional motions are essentially uncoupled; that is, the dynamics of the spacecraft can be considered as a fast torque free nutation superimposed upon a very slow and steady torqued precession of the angular momentum vector about the sun line. Thus to analyze

the two motions separately we define two intermediate axes systems which when combined bring us back to the "b" system. These axes and the Euler rotations which describe them are shown in Figure 2.4. They are defined as follows: (1) Rotations from the "s" system through ϕ_{AV}, θ_{AV} to get $\{X_{AV}, Y_{AV}, Z_{AV}\}$, the precession "p" axes; then (2) Rotations through ϕ', θ' to get $\{X', Y', Z'\}$, the nutation "n" axes, and finally a rotation through ψ' to arrive at "b", the body-fixed axes as defined earlier.

Using these new axes and the corresponding dynamical equations it is possible to arrive at the torque free results derived earlier:

From (2-34) $I_t \ddot{\theta}' - I_t \dot{\phi}'^2 s\theta' c\theta' + I_z \dot{\phi}' \omega_{z'} s\theta' = 0$ (2-38)

From (2-35) $\dot{\theta}' = 0$ (2-39)

From (2-36) $\omega_{z'} = \text{const.}$ (2-40)

$(\vec{\omega}_{is} \times \vec{H})$ is neglected when studying nutations because the nutation period is so short that any coupling with $\vec{\omega}_{is}$ can be neglected. Equation (2-38) gives the nutation rate as:

$$\dot{\phi}' = \frac{I_z}{I_t c\theta'} \omega_{z'}$$

Earlier, the nutation rate with respect to body coordinates was derived as:

$$\Omega = \frac{I_z - I_t}{I_t} \omega_{z_p} \qquad (2\text{-}8)$$

If we convert to the nutation coordinates $\{X', Y', Z'\}$, we find:

$$\dot{\phi}' = (\Omega + \omega_{3_p})/c\theta'$$

$$= \left(\frac{I_z - I_t}{I_t}\omega_{3_p} + \omega_{3_p}\right)/c\theta'$$

$$\dot{\phi}' = \frac{I_z}{I_t c\theta'}\omega_{z'}$$

which is exactly the same result as Equation (2-41).

The "high" spin rate case ($\omega_z \gtrsim .1$ r/min) also allows much simplification of the precessional equations. In this case, the precession rate is very much smaller than the spin rate ω_z so that the following assumptions are valid:

$$\omega_z \simeq \dot{\psi} >> \dot{\phi}, \dot{\theta} \qquad (2\text{-}42)$$

$$\dot{\phi} = 0 \qquad (2\text{-}43)$$

$$\ddot{\theta} = 0 \qquad (2\text{-}44)$$

Applying these simplifications to Equation (2-33), the coupling with the orbital rate becomes:

$$\vec{\omega}_{is} \times \vec{H} \simeq \omega_{is}\left[-\vec{\tau}_K I_z \dot{\psi} c\theta s\phi - \vec{j}_K I_z \dot{\psi} c\phi\right] \qquad (2\text{-}45)$$

Equations (2-42) to (2-45) applied to the dynamical equations (2-34) to (2-37) lead to the precessional equations for "high" spin rates:

$$I_z \omega_z \dot{\phi} s\theta = N_X + I_z \omega_z \omega_{is} c\theta s\phi \qquad (2\text{-}46)$$

$$I_z \omega_z \dot{\theta} = -N_Y - I_z \omega_z \omega_{is} c\phi \qquad (2\text{-}47)$$

$$I_z \dot{\omega}_z = N_z \qquad (2\text{-}48)$$

Note that these equations verify the description of torqued precession described earlier; that is, the precession rate, $\dot{\phi}$, is dependent on torques acting along the X-axis, whereas the erection rate, $\dot{\theta}$, is dependent on torques acting along the Y-axis. These "high" spin rate equations rest basically on the precept that at high enough spin rates, the angular momentum of the spacecraft is so large compared to the applied torques that the rate at which the momentum vector moves is very small -- thus the assumptions $\dot{\psi} >> \dot{\phi}, \dot{\theta}$. The motion is therefore a steady ($\dot{\theta}' << 1$) nutation superposed on a steady ($\dot{\theta}_{AV} << 1$) precession. The lowest spin rate at which these assumptions are still valid can be seen by examining equation (2-34). If we use this "steady" motion assumption, $\ddot{\theta}$ is ignored, thus the equation becomes a quadratic in $\dot{\phi}$:

$$(I_z - I_t) s\theta c\theta \dot{\phi}^2 + I_z s\theta \dot{\psi} \dot{\phi} - N_X = 0 \qquad (2\text{-}49)$$

Solving for $\dot{\phi}$:

$$\dot{\phi} = \frac{-I_z s\theta \dot{\psi} \pm \sqrt{I_z^2 s^2\theta \dot{\psi}^2 + 4(I_z - I_t) s\theta c\theta N_x}}{2(I_z - I_t) s\theta c\theta} \qquad (2\text{-}50)$$

For solar pressure torques, $N_x < 0$ (see Appendix A). Thus the assumption of steady motion is valid only if:

$$I_z^2 s^2\theta \dot{\psi}^2 > -4(I_z - I_t) s\theta c\theta N_x$$

$$\omega_z^{crit} \simeq \dot{\psi} > \frac{2}{I_z}\left[-N_x(I_z - I_t)\cot\theta\right]^{1/2} \qquad (2\text{-}51)$$

For typical values: $N_x = -20$ dyne-cm.

$I_t = 3 \times 10^6$ gm-cm^2

$I_z = 4.2 \times 10^6$ gm-cm^2

$\theta = 5°$

$$\omega_z^{crit} \simeq .079 \text{ r/min}$$

Thus, it appears that the "high" spin rate assumption is valid for spin rates about about .1 r/min.

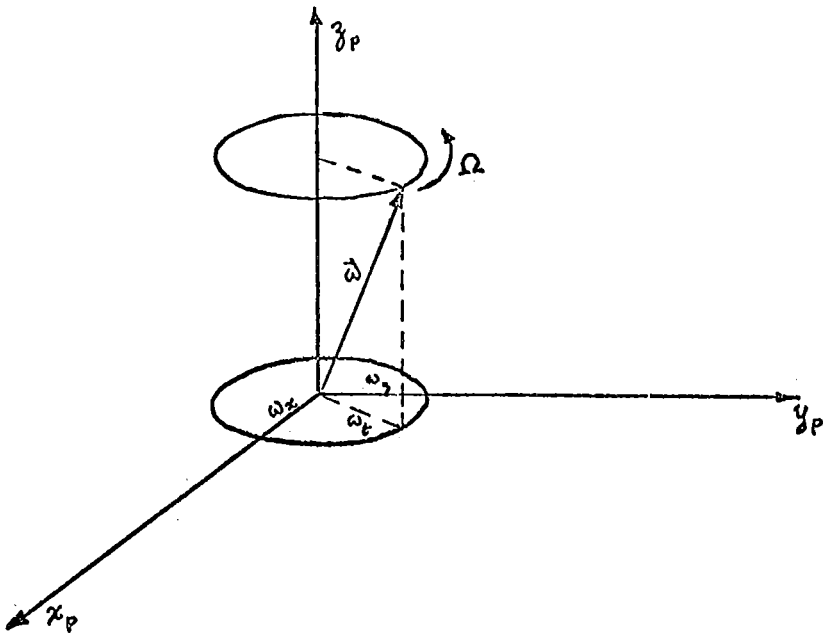

Figure 2.1 Nutational motion

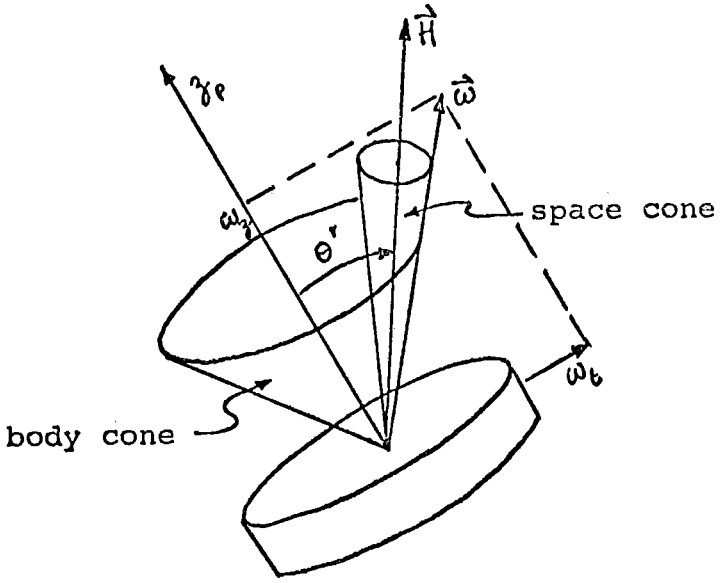

Figure 2.2 Nutation visualization ($I_z > I_t$)

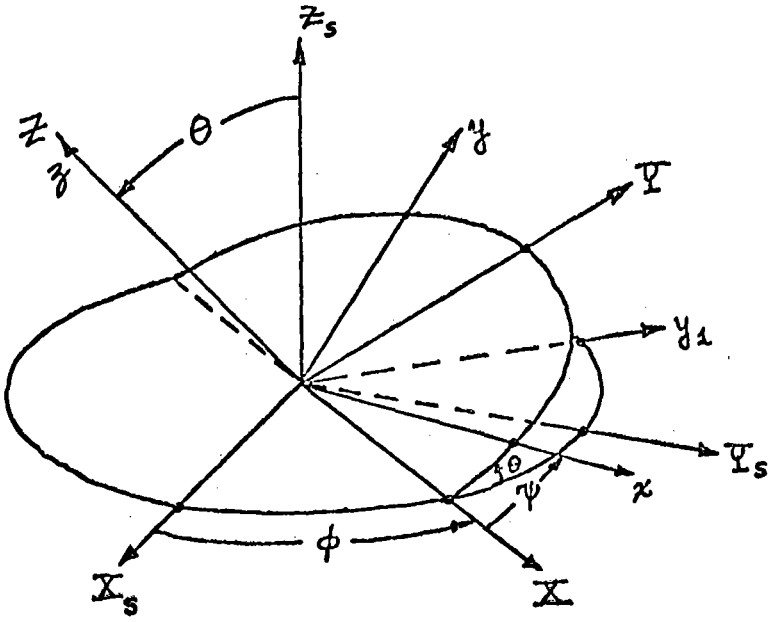

Figure 2.3 Definition of "s", "k", and "b" axes and Euler rotations

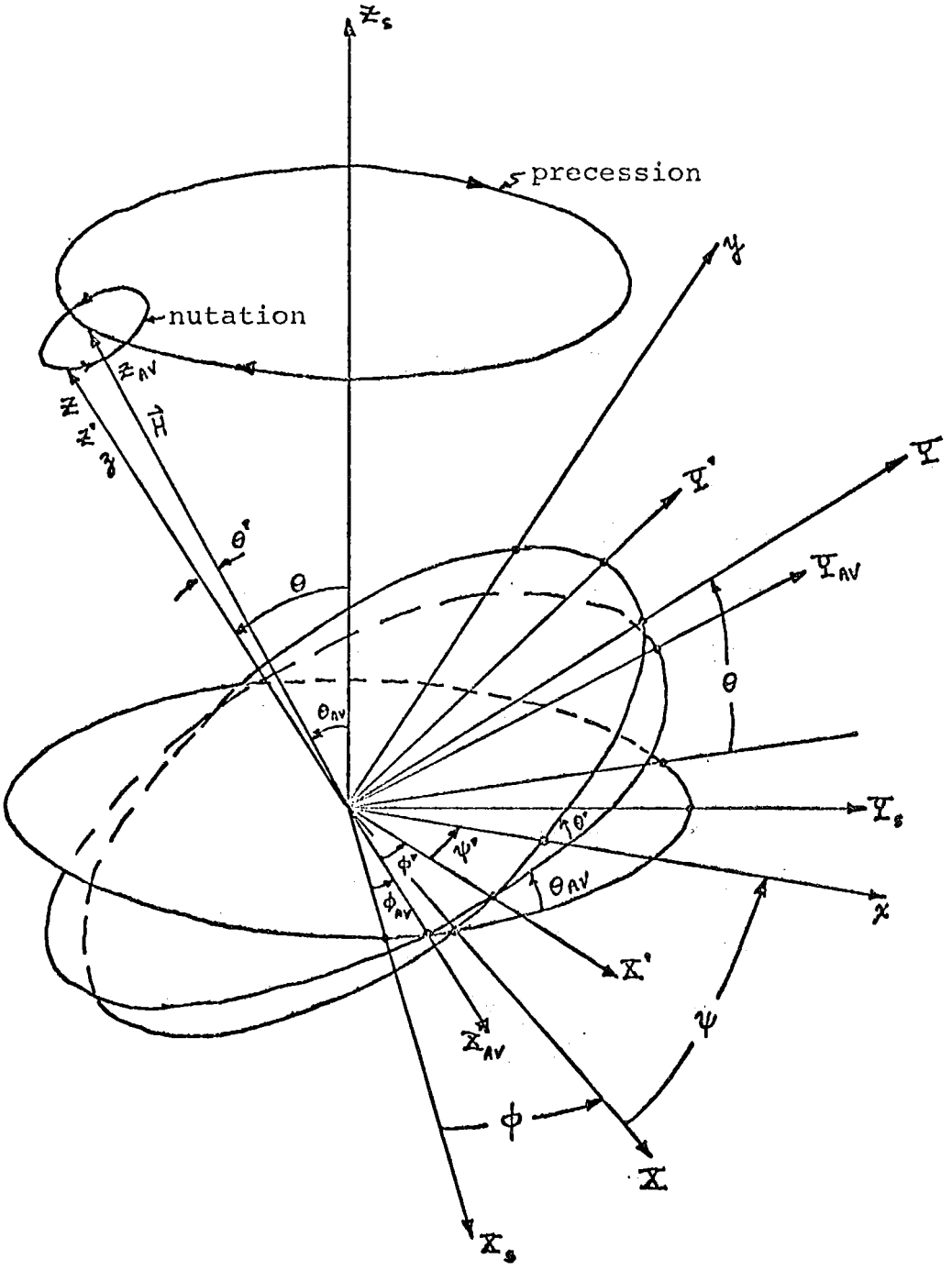

Figure 2.4 Definition of "p" and "n" axes and Euler rotations

CHAPTER 3

ATTITUDE SENSING

3.1 General Considerations

In order to perform three-axis attitude control, it is required that two distinct vectors from the spacecraft to known directions be defined thus permitting complete specification of the spacecraft attitude. Since one body axis must always be maintained pointing closely to the sun, it is obvious that one of the required vectors should be the solar radiation vector. Measurement of the solar aspect, essentially the angle θ, makes possible the achievement of the first requirement, sun-pointing. Another vector is then necessary to determine roll orientation. Conceptually, this second vector could be one of several possible vectors. Let's first analyze the first vector measurement and determine how much information one can extract by simply "looking" at the sun.

3.2 Solar Radiation Vector Measurement

In the last chapter, it was determined that the attitude of the spacecraft with respect to the sun line

is completely specified with the knowledge of the three Euler angles ϕ, θ, ψ. The solar radiation vector will allow the measurement of the last two quantities, θ and ψ. The precession angle, ϕ, which is measured in the plane perpendicular to the sun line of course cannot be determined. (If it could, we would have complete knowledge of the spacecraft attitude and the second vector measurement would not be necessary.)

There are several possible solar sensor configurations for the measurement of θ and ψ. Consider the one shown in Figure 3.1. The sensor consists of a circular detector made up of many individual tiny photodetectors. A pin hole or a lens mounted on the z axis at a distance h above the detector plane focuses the sun on the detectors. Thus the radial distance, r, of the image point from the center of the detector gives θ :

$$r = h \tan \theta \qquad (3\text{-}1)$$

The azimuthal angle, ψ_s, measured by the detector gives ψ, where, as shown in Figure 3.3:

$$\psi_s = \psi + \frac{\pi}{2}$$

Thus, for example, if the spacecraft is spinning uniformly with the spin axis at an angle from the sun line, the image

will trace out a circle on the detector face; the radius of the circle giving θ, and position on the circle giving ψ. Note, however, that both the θ and ψ resolutions decrease as θ decreases. For example, for individual detectors of size .01 in. by .01 in., the worst θ resolution would occur right next to the center:

$$h \tan\theta = .01$$

$$\theta_{MIN}^{res} = \tan^{-1}\left(\frac{.01}{h}\right) \qquad (3\text{-}3)$$

for h = 2 in.

$$\theta_{MIN}^{res} = 17'$$

The resolution in ψ is given by:

$$\psi^{res} \simeq \frac{.01}{r} = \frac{.01}{h\tan\theta} \qquad (3\text{-}4)$$

for h = 2 in., and $\theta = 5°$

$$\psi^{res} \simeq 3.25°$$

Also, the maximum θ that can be measured with this configuration is limited by the allowable size of the sensor. For example, for a sensor radius of 3.5 in., the maximum θ that will be detected is:

$$\theta_{MAX} = \tan^{-1}\left(\frac{3.5}{2}\right)$$

$$\theta_{MAX} = 60° 20'$$

To circumvent this drawback, a hollow spherical cup detector could be used, as shown in Figure 3.4. The θ resolution would be the same for all θ :

$$\theta^{res} = \frac{.01}{R}$$

The ψ resolution at small θ is about the same as that for the planar detector:

$$\psi^{res} = \frac{.01}{R \sin\theta}$$

However, the maximum measurable θ would theoretically be 90°. Optically, the hemispherical cup would be preferred over the planar design because the detectors would always be a constant distance from the pin hole or lens.

For either design, however, sensor resolution in ψ limits the minimum allowable θ to about 2°. This point must be taken into consideration in the design of the θ control loop.

It would also be very desirable to be able to sense nutational motion. To do this, requires the ability to determine the Euler rotations ϕ_{AV}, θ_{AV}, ϕ', θ', ψ' which describe the "p" and "n" axes as defined earlier. Again, since ϕ_{AV} is measured in the plane perpendicular to the sun line, it cannot be deduced from a solar measurement. The question remains as to whether it is possible to

extract θ_{AV}, ϕ^*, θ^*, and ψ^* from the actual sensor measurement of θ and ψ. Since the five rotations through ϕ_{AV}, θ_{AV}, ϕ^*, θ^*, ψ^* are equivalent to the three rotations ϕ, θ, ψ, we can obtain relationships between these quantities by equating their corresponding rotation matrices:

$$\begin{Bmatrix} x \\ y \\ z \end{Bmatrix} = \begin{bmatrix} c\phi_{AV} & s\phi_{AV} & 0 \\ -s\phi_{AV}c\theta_{AV} & c\phi_{AV}c\theta_{AV} & s\theta_{AV} \\ s\phi_{AV}s\theta_{AV} & -c\phi_{AV}s\theta_{AV} & c\theta_{AV} \end{bmatrix} \cdot \tag{3-7}$$

$$\begin{bmatrix} c\phi^*c\psi^* - s\phi^*s\psi^*c\theta^* & s\phi^*c\psi^* + c\phi^*s\psi^*c\theta^* & s\psi^*s\theta^* \\ -c\phi^*s\psi^* - s\phi^*c\psi^*c\theta^* & -s\phi^*s\psi^* + c\phi^*c\psi^*c\theta^* & c\psi^*s\theta^* \\ s\phi^*s\theta^* & -c\phi^*s\theta^* & c\theta^* \end{bmatrix} \begin{Bmatrix} X_s \\ Y_s \\ Z_s \end{Bmatrix}$$

Also,

$$\begin{Bmatrix} x \\ y \\ z \end{Bmatrix} = \begin{bmatrix} c\phi c\psi - s\phi s\psi c\theta & s\phi c\psi + c\phi s\psi c\theta & s\psi s\theta \\ -c\phi s\psi - s\phi c\psi c\theta & -s\phi s\psi + c\phi c\psi c\theta & c\psi s\theta \\ s\phi s\theta & -c\phi s\theta & c\theta \end{bmatrix} \begin{Bmatrix} X_s \\ Y_s \\ Z_s \end{Bmatrix} \tag{3-8}$$

Equating the two equivalent rotation matrices gives three independent equations:

$$c\theta = c\theta^*c\theta_{AV} - c\phi^*s\theta^*s\theta_{AV} \tag{3-9}$$

$$s\theta s\psi = s\phi^*c\psi^*s\theta_{AV} + c\phi^*s\psi^*c\theta^*s\theta_{AV} + s\psi^*s\theta^*c\theta_{AV} \tag{3-10}$$

$$s\theta c\psi = -s\phi^*s\psi^*s\theta_{AV} + c\phi^*c\psi^*c\theta^*s\theta_{AV} + c\psi^*s\theta^*c\theta_{AV} \tag{3-11}$$

Equations (3-10) and (3-11) can be rewritten as:

$$s\theta s\psi = \frac{s\theta_{AV}}{2}(1+c\theta')s(\psi'+\phi') + \frac{s\theta_{AV}}{2}(c\theta'-1)s(\psi'-\phi') + c\theta_{AV}s\theta's\psi' \qquad (3\text{-}12)$$

$$s\theta c\psi = \frac{s\theta_{AV}}{2}(1+c\theta')c(\psi'+\phi') + \frac{s\theta_{AV}}{2}(c\theta'-1)c(\psi'-\phi') + c\theta_{AV}s\theta'c\psi' \qquad (3\text{-}13)$$

These equations allow a further insight into the effect of nutations on the sensor measurement. Noting that the only cyclic terms on the right hand side involve $(\psi'+\phi')$, $(\psi'-\phi')$, and ψ', if we plot $s\theta c\psi$ on one axis and $s\theta s\psi$ on the other (these quantities essentially describe the motion of the solar trace on the sensor face), it can be seen that the result is made up of a sum of three vectors of differing amplitudes, which are functions of θ_{AV} and θ'; the vectors rotating with the frequencies $(\dot{\psi}'+\dot{\phi}')$, $(\dot{\psi}'-\dot{\phi}')$, and $\dot{\psi}'$, (Figure 3.5). Thus it is clear that when nutations are present, the sun's image will no longer trace out a circle on the detector, but instead a more irregular shape depending on the nutational amplitude, θ'. Figures 3.6, 3.7, 3.8 show the results for three different values of θ'. Note that in the first two cases where θ' is less than θ_{AV} the trace always moves in a counterclockwise motion, correctly indicating positive spin rate. However, in the last case where θ' is larger than θ_{AV}, the average direction is clockwise, and the sensor would incorrectly indicate a negative rate. Here is one factor among many which

indicates a need for eliminating nutations.

Returning to Equations (3-9), (3-10), and (3-11) and noting that the left hand side are known quantities measured by the sensor, there remains three equations in four unknowns θ_{AV}, ϕ', θ', and ψ'. However, in the first equation, the only cyclic term is $c\phi'$, thus it is obvious that $\theta(t)$ oscillates between the extreme values $(\theta_{AV}-\theta')$ and $(\theta_{AV}+\theta')$ at the frequency $\dot{\phi}'$. Hence it is possible to determine ϕ', θ_{AV}, and θ' from the measured θ time history, as seen in Figure 3.9.

$$\theta_{AV} = \frac{\theta_{MAX} + \theta_{MIN}}{2} \tag{3-14}$$

$$\theta' = \frac{\theta_{MAX} - \theta_{MIN}}{2} \tag{3-15}$$

$$\dot{\phi}' = \frac{\pi}{\Delta t} \quad , \quad \phi' = \int \frac{\pi}{\Delta t}\, dt \tag{3-16}$$

where θ_{MAX} is the largest measured value of θ, θ_{MIN} is the smallest, and Δt is the time between peaks in θ.

Thus, all that remains is to solve for ψ' using either Equation (3-10) or (3-11). Unfortunately these equations involve trigonometric functions of ψ' and ϕ' hence in general cannot be readily solved for ψ'. However, for $\theta' \ll 1$ (very small nutations), the equations simplify to:

$$\begin{aligned} s\psi &\simeq s\phi' c\psi' + c\phi' s\psi' = s(\phi' + \psi') \\ \psi &\simeq \phi' + \psi' \end{aligned} \tag{3-17}$$

Hence, we can obtain ψ' as:

$$\psi' = \psi - \phi' \tag{3-18}$$

The requirement that θ' be very small again indicates a need for control of nutations.

3.3 Second Vector Measurement

Conceptually, the second required vector could be one of several possibilities, namely:

(1) the apparent local solar wind bulk velocity vector

(2) the local magnetic field vector

(3) the earth to spacecraft vector (from a radio uplink)

(4) the earth to spacecraft vector (from an IR sensor)

(5) a vector from a star sensor

(6) energetic particles velocity vector

Of these, (2) can be ignored because the magnetic field direction is too variable. Item (6) is roughly coincident with the solar radiation vector and hence will not be considered further.

Considerable work has been done on star trackers and earth IR sensors. Star trackers in particular have proven their accuracy and reliability in actual missions.

Both of these methods, however, require much complex equipment and thus tend to be rather heavy. For example, the Canopus sensor used on Mariner weighly about seven pounds and consumed a little less than five watts of power. For our application a less sophisticated tracker is required which would bring the weight down to perhaps five pounds. This is still a very large penalty when compared to the weight of the entire spacecraft. Thus these methods are to be avoided if possible.

Consider item 1, the apparent solar wind velocity vector. The observed solar wind flux at the earth has run typically from 10^7 to 2×10^9 protons/cm^2-sec. These limits correspond to densities and velocities from 4 protons/cm^3 and 250 km/sec to 40 protons/cm^3 and 500 km/sec. The spacecraft radial and tangential components of velocity for a 3/4 year solar orbit are shown roughly in Figure 3.10. The radial velocity is always small relative to the wind velocity and hence can be ignored. Assuming a radial flow of plasma, the aberration angle measured at the spacecraft would be

$$\epsilon = \tan^{-1}\left(\frac{v_T}{v_{sw}}\right) \qquad (3\text{-}19)$$

where v_t = spacecraft tangential velocity

v_{sw} = solar wind velocity

The expected values of ϵ versus heliocentric distance are shown in Figure 3.11. Note that the aberration angle can vary between 2° and 8°, thus the system would have to work over this range of angles. The difficulty in using this method lies in the angular fluctuation of the plasma direction. Satellite measurements show that the instantaneous velocity vector fluctuates about its average direction by typically $\pm$10°. Presumably, the out of plane angular fluctuations would be comparable, however, little is known about this. Note that this value is larger than the expected aberration angles ϵ. The magnitude of the direction variation, particularly the out of plane fluctuation, makes this method too unreliable for use in roll sensing.

Next, consider the use of the earth to spacecraft vector from a radio uplink. Spacecraft roll attitude could be deduced using standard phase comparison methods of an RF signal from earth. However, tracking is carried out only about three hours per day, thus if this were the sole roll sensing method used, the spacecraft would essentially have no roll reference for the remaining twenty-one hours. However, this method appears most promising as a roll "updating" source which would correct roll drift approximately once a day and bring the spacecraft back to the desired orientation. A further advantage

with a radio uplink is that it also allows ground control of antenna rotation to track earth. This would be accomplished by sending a command to the spacecraft every several days to rotate its antenna by a certain angular increment, say 2° or 3°, thus eliminating the need for an on board preprogrammed control of antenna rotation.

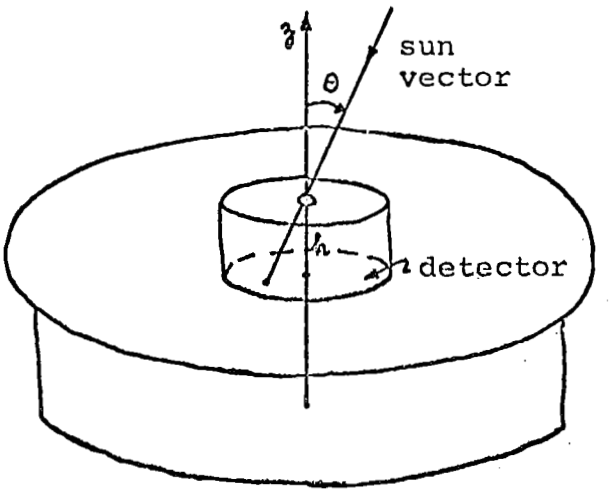

Figure 3.1 Sensor schematic

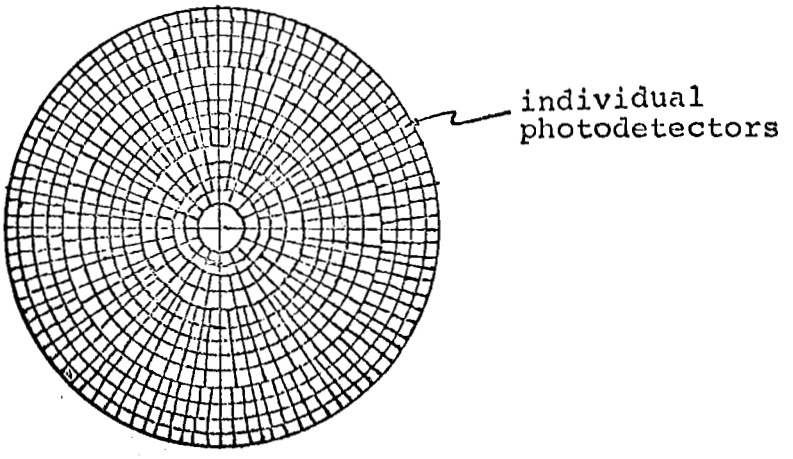

Figure 3.2 Detector face

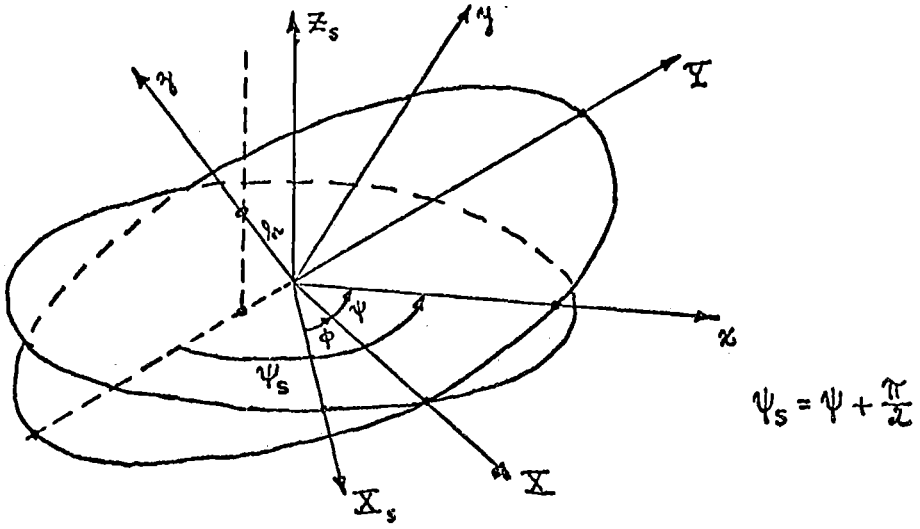

Figure 3.3 Sensor measurement of ψ_s

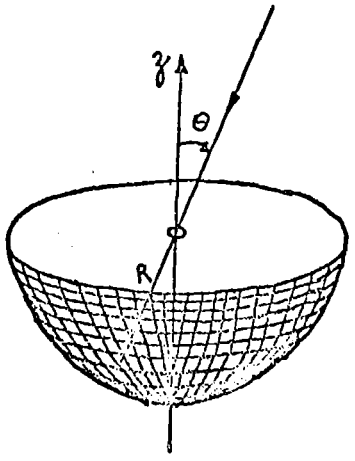

Figure 3.4 Hemispherical detector

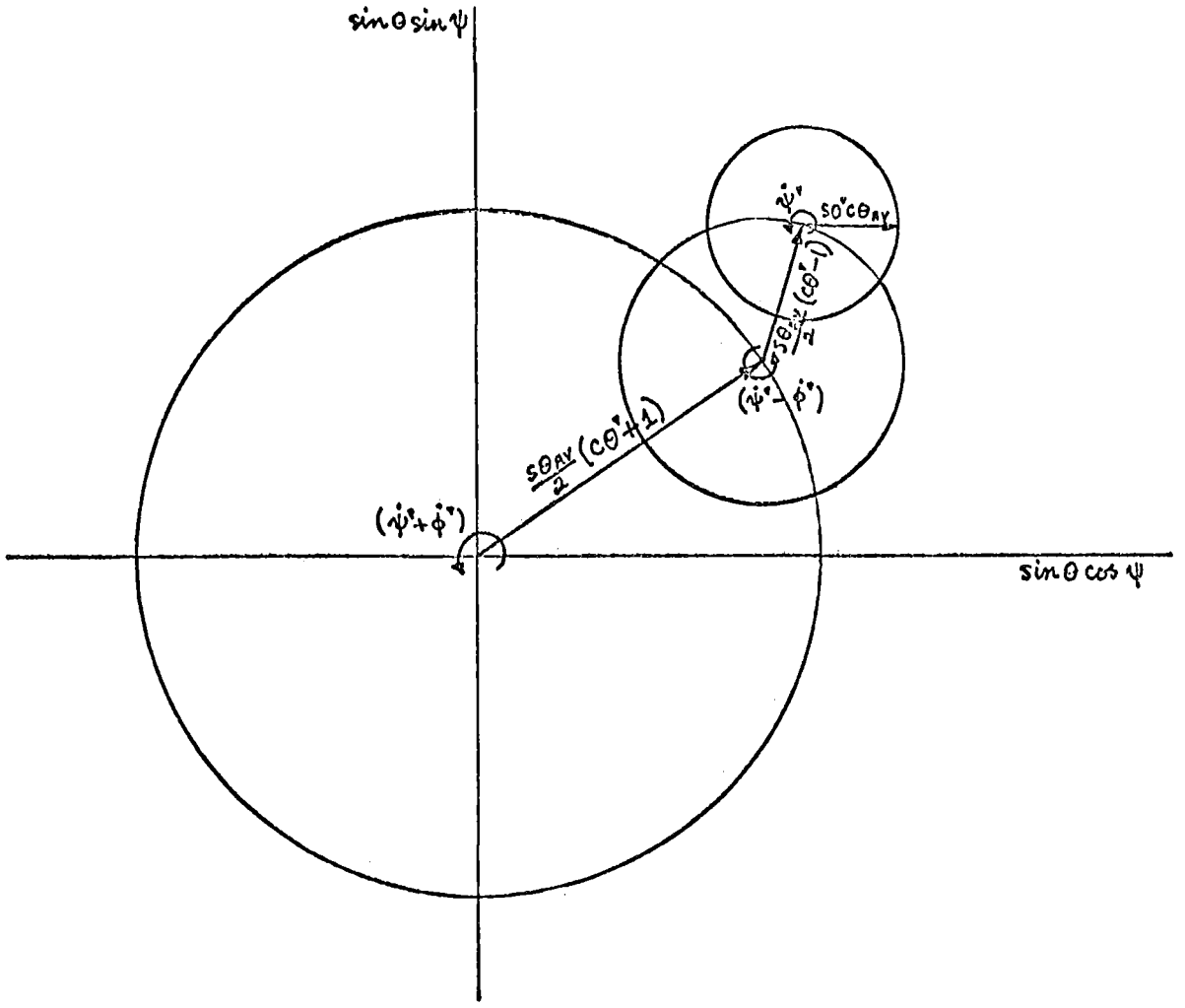

Figure 3.5 Vector representation of sensor trace

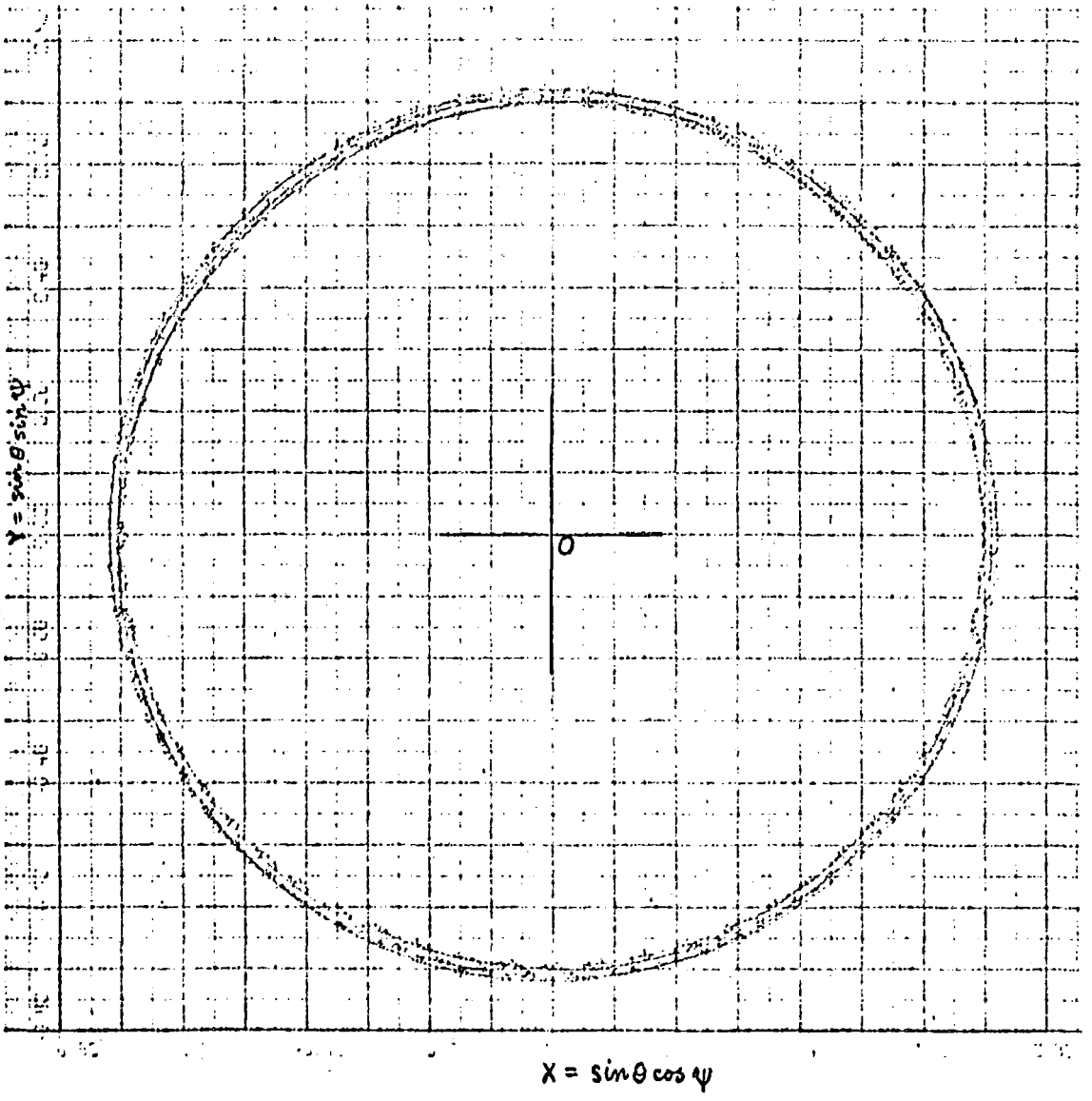

Figure 3.6 Solar trace on sensor face (θ_{AV}= 45°, θ^{*}= 1°)

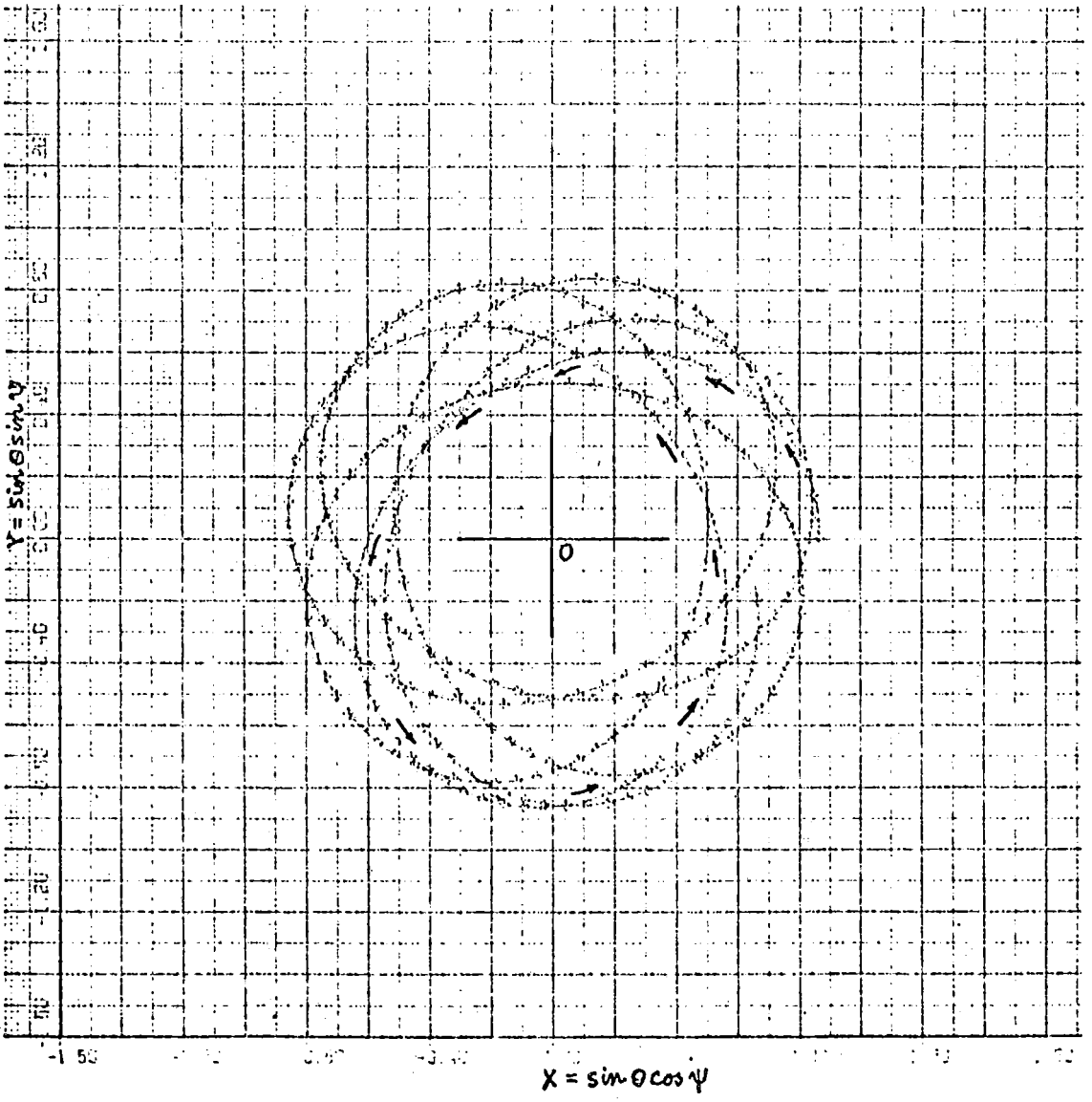

Figure 3.7 Solar trace on sensor face (θ_{AV} = 45°, θ^{*} = 15°)

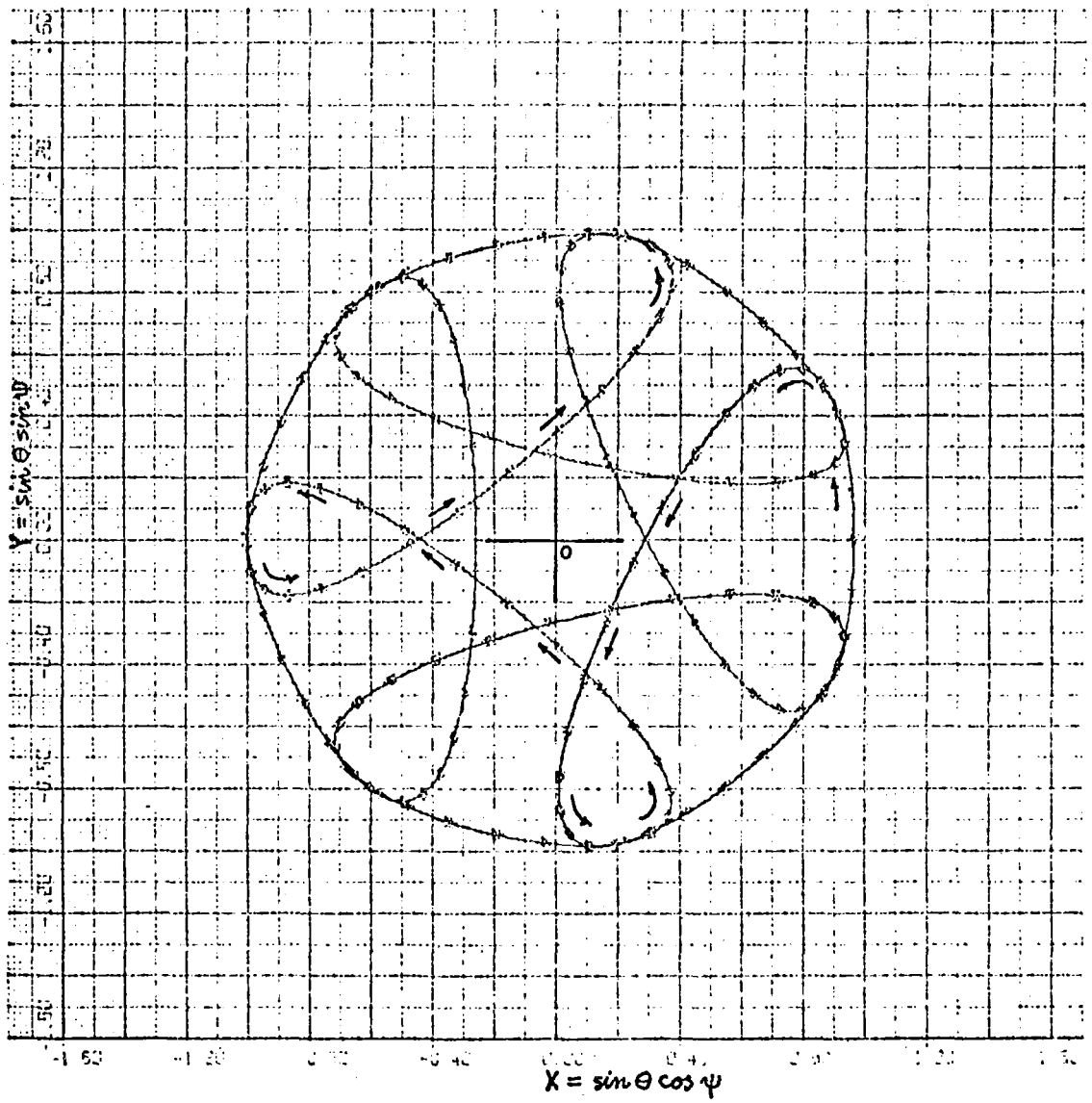

Figure 3.8 Solar trace on sensor face (θ_{AV} = 45°, θ' = 60°)

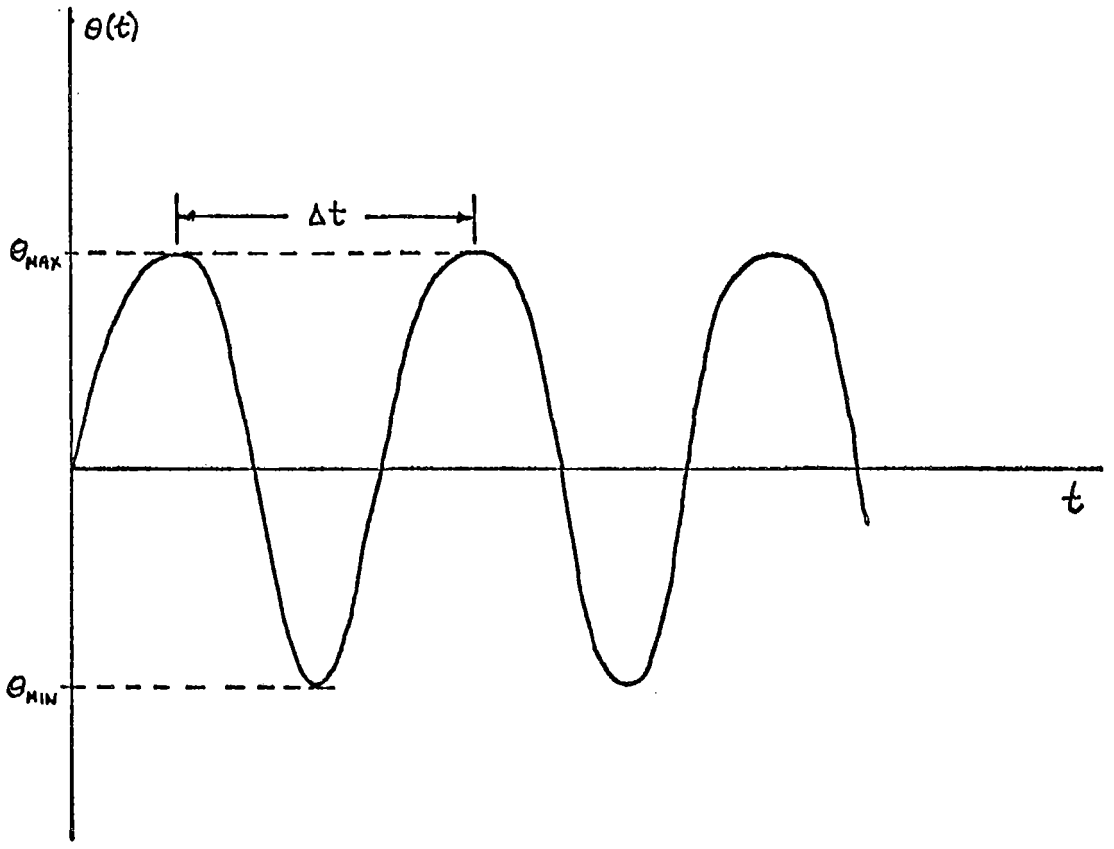

Figure 3.9 Determination of θ_{AV}, θ', ϕ' from θ time history

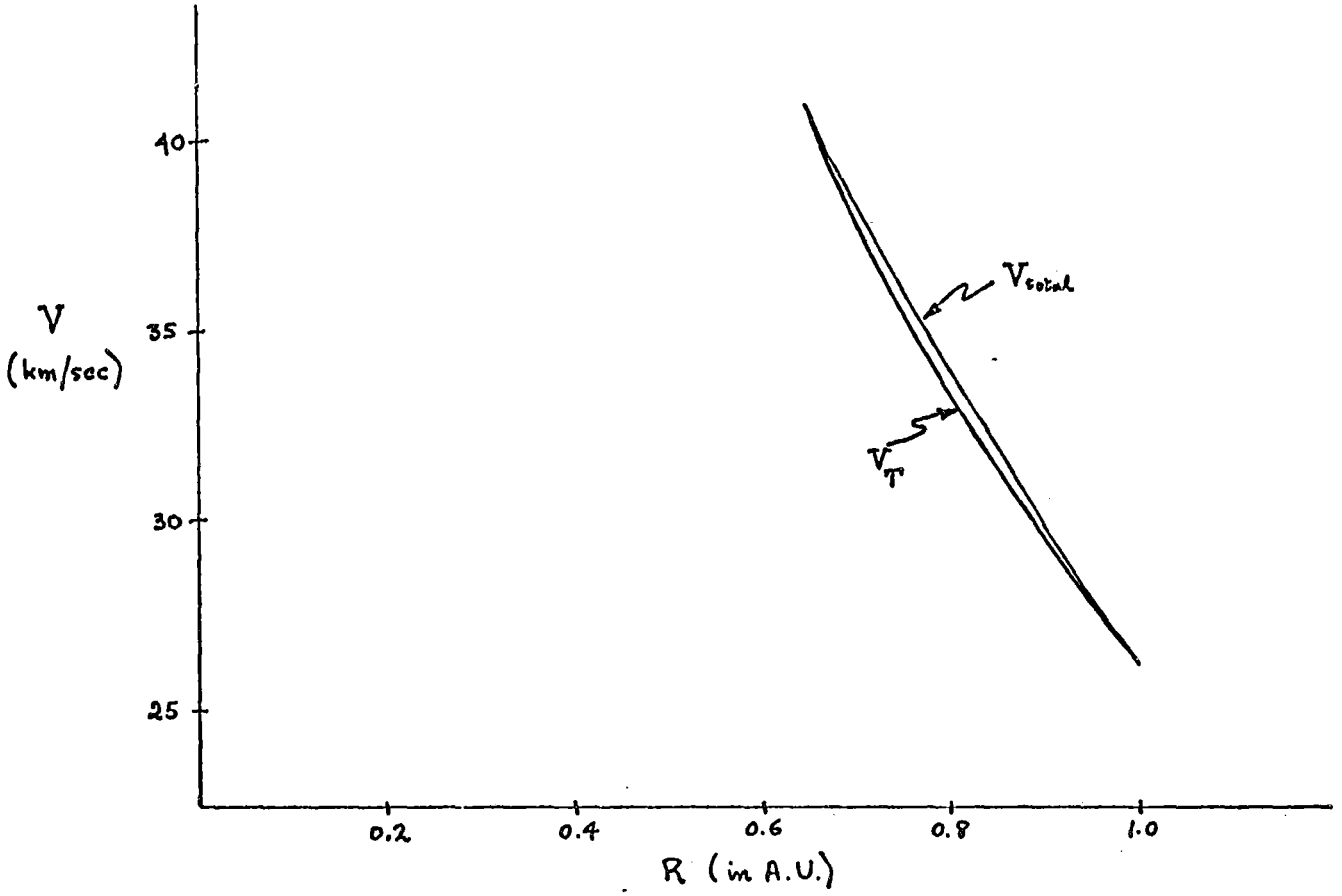

Figure 3.10 Spacecraft velocity for 3/4 year orbit

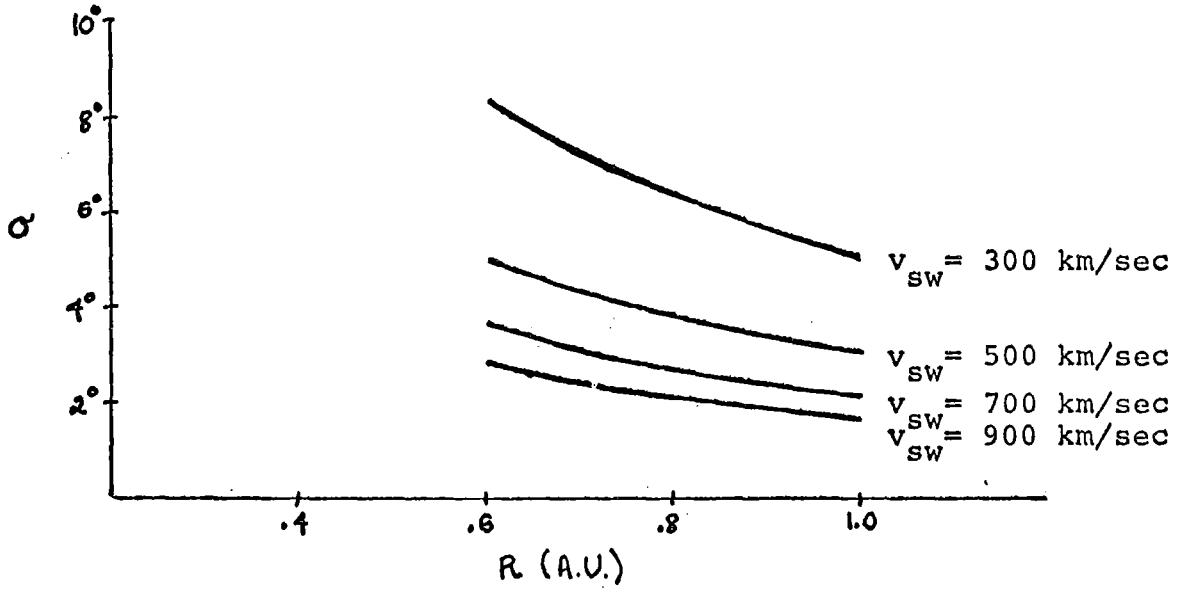

Figure 3.11 Expected aberation angles

CHAPTER 4

DESPUN SPACECRAFT CONFIGURATION

4.1 Spacecraft Configuration

The first configuration that was studied was one that would be completely despun, so that it was essentially a non-spinning Sunblazer. Once the spacecraft was oriented properly this sttitude would be maintained through the use of movable solar pressure vanes. For example, consider one possible configuration shown in Figure 4.1. Assume that initial despin and orientation has been accomplished such that the body axis z is pointed closely to the sun, and such that the ①-③ vanes lie in the ecliptic plane whereas the ②-④ vanes are perpendicular to it. The ②-④ vanes are rotatable about their longitudinal axes whereas the ①-③ pair can be rotated about axes which are perpendicular both to z. and to the individual sail longitudinal axis. Thus by varying their pitch angles, the ②-④ pair would produce roll torques for maintaining roll attitude whereas the ①-③ pair would produce restoring torques by varying their cant angles to maintain sun-pointing. Ideally, then, this scheme appears workable for long term

stabilization. There remains the major problem of initial despin and orientation.

4.2 General Considerations in Initial Despin and Orientation

The initial conditions after separation are assumed to be an initial spin rate of 200 r/min, initial angle between spacecraft angular momentum vector and sun line of 60°, and an initial nutation amplitude of 10°:

$$\omega_{z_0} \simeq 200 \text{ r/min} \tag{4-1}$$

$$\theta_{AV_0} \simeq 60^\circ \tag{4-2}$$

$$\theta_0' \simeq 10^\circ \tag{4-3}$$

Thus, it is obvious that the first task is to despin the spacecraft from its initial rate of 200 r/min down to zero. The next step would be to achieve sun pointing, that is, reduce θ_{AV} to some value less than 10°. Finally, proper roll orientation would be achieved such that the antenna rotation axis is perpendicular to the ecliptic.

To analyze the first problem, consider the despinning of the spacecraft prior to the deployment of sails or antennas. Thus, the spacecraft is essentially an inertially symmetric cylindrical body with no torques

acting on it except the despin torque. The initial despin can most quickly be achieved by the use of a yo-yo device. Inability to predice the exact value of initial spin rate makes it impossible to design a yo-yo to despin the spacecraft to precisely zero. However such a device can be used to bring the spin rate down from the 200 r/min initial value to perhaps 2 r/min where another despin device must take over. In this case, it appears that the use of microthrusters would be desirable. Tiny motors, perhaps using a subliming propellant and weighing on the order of tens of grams could do the job of final despin from 2 r/min to zero. Remembering that the spacecraft is initially nutating with an amplitude $\theta^* = 10°$, it is necessary to analyze its effect on the despin process. In the earlier analysis of nutations, the following result was found:

$$\tan \theta^* = \frac{I_t \omega_t}{I_3 \omega_3} = \frac{H_t}{H_3} \qquad (2\text{-}21)$$

The nutation amplitude is simply proportional to the ratio of the transverse angular momentum to the spin momentum. Thus as the despin motors decrease the spin momentum, θ^* will grow until the spin rate, ω_3, goes to zero at which time $\theta^* = 90°$ and the spacecraft tumbles about a transverse axes at the rate ω_t. It is thus imperative that the nutation be damped out as the spacecraft is being despun.

4.3 Despin With Passive Nutation Damping

We next examine the possibilities of passive damping. Most dampers are designed to be most effective at a specific spin rate, that is, they are tuned to a specific driving frequency. These dampers have highly "peaked" dissipation characteristics; they're very effective at their tuned frequency but are very poor dissipators at other frequencies. In this case, since the spin rate is constantly decreasing, it is more desirable to have a damper which is more effective over the entire spin interval. The viscous damper has this characteristic. Consider the configuration shown in Figure 4.2 where two microthrusters provide a constant despin torque and a viscous damper mounted parallel to the spacecraft spin axis damp nutations. The condition for a stable despin is $\dot{\theta}' < 0$. Remembering Equation (2-21), this means that the damper must decrease the transverse angular rate proportionately as fast as the thrusters are reducing the spin rate. Thus we should be able to find a stability condition in terms of the thruster and damper characteristics. This is done by invoking the energy sink approximation to the motion, in which the damper is modeled as a passive device which simply extracts energy from the dynamic system. Using this approximation:

$$\vec{H} = I_t \omega_x \vec{i}_b + I_t \omega_y \vec{j}_b + I_z \omega_z \vec{k}_b \tag{4-1}$$

$$H^2 = I_t^2 \omega_t^2 + I_z^2 \omega_z^2 \tag{4-2}$$

$$T = \frac{1}{2}\left[I_t \omega_t^2 + I_z \omega_z^2\right] \tag{4-3}$$

And from geometry

$$\sin^2\theta' = \frac{I_t^2 \omega_t^2}{H^2} \tag{4-4}$$

From (4-2) $$I_t^2 \omega_t^2 = H^2 - I_z^2 \omega_z^2 \tag{4-5}$$

Using (4-3) $$I_z^2 \omega_z^2 = I_z\left[2T - I_t \omega_t^2\right] \tag{4-6}$$

Therefore, (4-5) becomes

$$\omega_t^2 = \frac{H^2 - 2 I_z T}{I_t (I_t - I_z)} \tag{4-7}$$

Substituting for ω_t^2 in Equation (4-4)

$$\sin^2\theta' = \frac{I_t}{I_z - I_t}\,\frac{(2 I_z T - H^2)}{H^2} \tag{4-8}$$

Differentiating with respect to time

$$\dot{\theta}' = \frac{1}{\sin\theta\cos\theta}\left[\frac{I_t I_z}{(I_z - I_t)}\,\frac{(H\dot{T} - 2T\dot{H})}{H^3}\right] \tag{4-9}$$

Thus for $I_t' < I_z$, the stability requirement $\dot{\theta}' < 0$ gives

$$\dot{T} < \frac{2T}{H}\dot{H} \tag{4-10}$$

Since $\dot{T} < 0$ and $\dot{H} < 0$, the stability requirement can be written as

$$|\dot{T}| > \frac{2T}{H}|\dot{H}| \tag{4-11}$$

For this case,

$$\dot{T} = -M\omega_z + \dot{T}_{damper} \tag{4-12}$$

where M is the despin torques exerted by the thrusters.

And $$\dot{H} = -M$$

Using Equations (4-2) and (4-3):

$$\frac{2T}{H} = \left[\frac{I_z}{I_t}\tan^2\theta' + 1\right]\omega_z\cos\theta' \tag{4-14}$$

Therefore, Equation (4-11) becomes

$$|\dot{T}_{damper}| > \left[\frac{I_z}{I_t}\omega_z\cos\theta'\tan^2\theta' + \omega_z\cos\theta' - \omega_z\right]|M| \tag{4-15}$$

Equation (4-15) represents the stability criteria in terms of the damper energy dissipation rate and the magnitude of the despin torque. Now, to find $\dot{T}_{damper}$ we must find the body acceleration at the damper due to the nutation. Let $\vec{R}$ be the vector from the spacecraft center of mass to the damper attachment point P:

$$\vec{R}_p = x_p\vec{\imath}_b + z_p\vec{k}_b \tag{4-16}$$

The angular velocity with respect to the body-fixed axes can be written in terms of the nutation Euler angles as

$$\omega_x = \dot{\theta}'c\psi' + \dot{\phi}'s\psi's\theta' \tag{4-17}$$

$$\omega_y = \dot{\phi}'c\psi's\theta' - \dot{\theta}'s\psi' \tag{4-18}$$

$$\omega_z = \dot{\psi}' + \dot{\phi}'c\theta' \tag{4-19}$$

Differentiating:

$$\dot{\omega}_x = \left(\ddot{\theta}'c\psi' - \dot{\theta}'\dot{\psi}'s\psi' + \ddot{\phi}'s\psi's\theta' + \dot{\phi}'\dot{\psi}'c\psi's\theta' + \dot{\phi}'\dot{\theta}'s\psi'c\theta'\right) \tag{4-20}$$

$$\dot{\omega}_y = \left(\ddot{\phi}'c\psi's\theta' - \dot{\phi}'\dot{\psi}'s\psi's\theta' + \dot{\phi}'\dot{\theta}'c\psi'c\theta' - \ddot{\theta}'s\psi' - \dot{\theta}'\dot{\psi}'c\psi'\right) \tag{4-21}$$

$$\omega_z = \left(\ddot{\psi}' + \ddot{\phi}'c\theta' - \dot{\phi}'\dot{\theta}'s\theta'\right) \tag{4-22}$$

The absolute acceleration at P is

$$\vec{a}_p = \frac{d\vec{\omega}_b}{dt} \times \vec{R}_p + \vec{\omega}_b \times (\vec{\omega}_b \times \vec{R}_p) \tag{4-23}$$

Applying Equations (4-16) to (4-22) to (4-23):

$$a'_x = z_p\ddot{\phi}'s\theta'c\psi' + 2z_p\dot{\phi}'\dot{\theta}'c\theta'c\psi' - z_p\ddot{\theta}'s\psi' - x_p\dot{\phi}'^2s^2\theta'c^2\psi' + 2x_p\dot{\phi}'\dot{\theta}'s\theta's\psi'c\psi' \tag{4-24}$$
$$- x_p\dot{\theta}'^2s^2\psi' - x_p\dot{\psi}'^2 - x_p\dot{\psi}'\dot{\phi}'c\theta' - x_p\dot{\phi}'\dot{\psi}'c\theta' - x_p\dot{\phi}'^2c^2\theta' + z_p\dot{\phi}'^2c\theta's\theta's\psi'$$

$$a'_y = -z_p\ddot{\theta}'c\psi' - z_p\ddot{\phi}'s\theta's\psi' - 2z_p\dot{\phi}'\dot{\theta}'c\theta's\psi' + x_p\ddot{\psi}' + x_p\dot{\phi}'\dot{\theta}'s\theta' - \tag{4-25}$$
$$x_p\dot{\phi}'\dot{\theta}'s\theta' + x_p\dot{\phi}'\dot{\theta}'s\theta'c^2\psi' + x_p\dot{\phi}'^2s^2\theta's\psi'c\psi' - x_p\dot{\theta}'^2c\psi's\psi'$$
$$- x_p\dot{\phi}'\dot{\theta}'s\theta's^2\psi' + z_p\dot{\phi}'^2c\theta's\theta'c\psi'$$

$$a'_z = -x_p\ddot{\phi}'s\theta'c\psi' - 2x_p\dot{\phi}'\dot{\theta}'c\theta'c\psi' + x_p\ddot{\theta}s\psi' + 2x_p\dot{\theta}'\dot{\psi}'c\psi' - z_p\dot{\theta}'^2 \tag{4-26}$$
$$- x_p\dot{\phi}'^2s\theta'c\theta's\psi' - z_p\dot{\phi}'^2s^2\theta' - z_p\dot{\phi}'^2s^2\theta'c^2\psi' + 2x_p\dot{\phi}'\dot{\psi}'s\theta's\psi'$$

Since the damper is mounted parallel to the z axis, we are only interested in the a_y component. Using the assumption that the nutation amplitude is small and that it changes very little over one cycle:

$$\theta' \ll 1 \tag{4-27}$$

$$\dot{\theta}', \ddot{\theta}' \ll \dot{\phi}', \dot{\psi}' \tag{4-28}$$

Equation (4-26) can be simplified to

$$a_y' \simeq \chi_p (2\theta'\dot{\phi}'\dot{\psi}' - \theta'\dot{\phi}'^2) \sin\psi' \tag{4-29}$$

Note that the acceleration is cyclic in ψ'.

The nutation rate was found earlier as

$$\dot{\phi}' = \frac{I_z}{I_t c\theta'} \omega_{z'} \tag{2-41}$$

Hence $$\dot{\psi}' = \omega_{z'} - \dot{\phi}' c\theta' = \left(1 - \frac{I_z}{I_t}\right) \omega_{z'}$$

Applying these two equations to (4-29):

$$a_y' \simeq \chi_p D \omega_{z'}^2 \theta' [3D-2] \sin(D-1)\omega_{z'} t \tag{4-30}$$

where $$D \equiv \frac{I_z}{I_t}$$

The equation of motion for the damper mass is:

$$m\ddot{d}_m + b(\dot{d}_m - \dot{d}_p) = 0$$

$$m\ddot{\delta}_m + b\dot{\delta}_m = -m\ddot{d}_p \qquad (4-31)$$

where $\ddot{d}_p = a_z^p$

and $\delta_m = d_m - d_p$ = relative displacement of damper mass, m.

Writing the driving acceleration as

$$\ddot{d}_p = A \sin\omega t \qquad (4-32)$$

Taking the Laplace transform of (4-31):

$$\delta(s) = -\frac{A\omega}{s(s+\sigma)(s^2+\omega^2)} \qquad (4-33)$$

where $\sigma \equiv \frac{b}{m}$ (4-34)

Taking the inverse transform gives a steady state solution:

$$\delta(t) = -A\omega\left[\frac{1}{\sigma\omega^2} - \frac{\cos(\omega t - \psi)}{\omega^2(\sigma^2+\omega^2)^{1/2}}\right] \qquad (4-35)$$

where $\psi = \tan^{-1}\frac{\omega}{\sigma}$ (4-36)

The power dissipated by the damper is given by $b(\delta(t))^2$.

$$\left|\dot{T}^{\text{inst.}}_{\text{damper}}\right| = \frac{bA^2\sin^2(\omega t - \psi)}{(\sigma^2+\omega^2)} \qquad (4-37)$$

The average power loss is then

$$\left|\dot{T}_{damper}\right| = \frac{1}{2}\frac{bA^2}{(\sigma^2+\omega^2)} \tag{4-38}$$

From Equation (4-30):

$$A = \chi_p D \omega_{z'}^2 \theta' (3D-2) \tag{4-39}$$

$$\omega = (D-1)\omega_{z'} \tag{4-40}$$

Therefore, the energy dissipation rate becomes:

$$\left|\dot{T}_{damper}\right| = \frac{1}{2}\frac{b\chi_p^2 D^2 \omega_{z'}^4 \theta'^2 (3D-2)^2}{\left[\sigma^2+(D-1)^2\omega_{z'}^2\right]} \tag{4-41}$$

Putting this result into the stability condition, Equation (4-15)

$$\frac{1}{2}\frac{b\chi_p^2 D^2 \omega_3^4 \theta'^2 [3D-2]^2}{\left[\sigma^2+(D-1)^2\omega_{z'}^2\right]} > \left[D\omega_3 c\theta' \tan^2\theta' + \omega_3 c\theta' - \omega_3\right]|M| \tag{4-42}$$

Using the assumption $\theta' \ll 1$, the right hand side simplifies to give

$$\begin{aligned} D\omega_3 c\theta' \tan^2\theta' + \omega_3 c\theta' - \omega_3 &\simeq \omega_3\left[D\theta'^2 + 1 - \frac{\theta'^2}{2} - 1\right] \\ &\simeq \omega_3 \theta'^2 \left[D - \frac{1}{2}\right] \end{aligned} \tag{4-43}$$

Thus Equation (4-42) becomes

$$\frac{1}{2}\frac{b\chi_p^2 D^2 \omega_3^3 [3D-2]^2}{\left[\sigma^2+(D-1)^2\omega_3^2\right]} > \left[D-\frac{1}{2}\right]|M| \tag{4-44}$$

Note that for any given system, the only variable in the above relation is the spin rate ω_z. Thus it is obvious that the above inequality cannot always be satisfied as ω_z goes to zero. Writing (4-44) as an equality results in an equation which can be solved for ω_z^*, the spin rate below which the motion diverges:

$$b\, x_p^2 D^2 [3D-2]^2 \omega_z^{*3} - 2(D-1)^2(D-\tfrac{1}{2})|M|\omega_z^{*2} - 2\sigma^2(D-\tfrac{1}{2})|M| = 0 \quad (4\text{-}45)$$

For most systems, ω_z^* will be small so we can make the assumption that $(D-1)^2\omega_z^{*2} << \sigma^2$, then ω_z^* is simply

$$\omega_z^{*3} \simeq \frac{2(D-\frac{1}{2})|M|\, b}{m^2 x_p^2 D^2 (3D-2)^2} \quad (4\text{-}46)$$

Note that as expected, ω_z^* varies directly with the despin torque and inversely with the squares of the damper mass and the distance from the spacecraft center of mass. For typical values:

$|M| = 40$ dyne-cm. $\qquad m = 1$ gm.

$D = \frac{I_z}{I_t} = 1.5 \qquad x_p = 20$ cm.

$b = 1$ dyne-sec/cm.

$$\omega_z^* \simeq 2.4 \text{ r/min}$$

To get an idea of the best that can be expected from passive dampers, similar calculations were carried out for a tuned pendulous damper as shown in Figure 4.3. It is assumed that as the spin rate decreases, the spring and damping constants also change to keep the damper always tuned. Lim's [6] analysis of this damper resulted in the following expression for power dissipation:

$$|\dot{T}_{damper}| = \left|\frac{1}{2} m\ell^2 \theta'^2 (1+\delta) D(D-1)(D-2)\omega_z^3/a\right| \qquad (4\text{-}47)$$

where $\delta = \dfrac{x_p}{\ell}$

$a = \dfrac{\theta_o'}{\alpha_m}$

θ_o' = maximum θ' expected

α_m = maximum allowable damper deflection

ℓ = length of pendulum arm

The resulting expression for the critical spin rate is

$$\omega_z^{*2} = \left|\frac{2(M)[D-\frac{1}{2}]\,a}{m\ell^2(1+\delta)D(D-1)(D-2)}\right| \qquad (4\text{-}48)$$

For typical values:

$D = 1.5$ $\qquad$ $\alpha_m = 60°$

$x_p = 20$ cm. $\qquad$ $m = 2$ gm.

$\ell = 40$ cm. $\qquad$ $|M| = 40$ dyne·cm.

$\theta_o' = 20°$

$$\omega_z^* \simeq 1.22 \text{ r/min}$$

4.4 Actively Pitched Thrusters

With the failure of passive damping to provide a stable despin, the next step was to investigate the possibility of active nutation damping. This can be accomplished by pitching the thrusters so that they produce transverse torques as well as despin torque, as shown in Figure 4.4. Pitching of the thrusters can be controlled to accomplish all three objectives: (1) despin, (2) sun-pointing, and (3) active nutation damping. To determine a workable pitching scheme, the torque requirements must first be determined. Returning to the equations of motion developed earlier, (2-34) to (2-37), the nutational equations are:

$$I_t\ddot{\theta}' - I_t\dot{\phi}'^2 s\theta' c\theta' + I_3\dot{\phi}'\omega_{z'} s\theta' = N_{x'} \qquad (4\text{-}49)$$

$$I_t(\ddot{\phi}' s\theta' + 2\dot{\phi}'\dot{\theta}' c\theta') - I_3\dot{\theta}'\omega_{z'} = N_{y'} \qquad (4\text{-}50)$$

$$I_3\frac{d\omega_{z'}}{dt} = N_{z'} \qquad (4\text{-}51)$$

$$\omega_{z'} = \dot{\psi}' + \dot{\phi}' c\theta'$$

If we once again use the assumption of steady motion, $\ddot{\theta}'$ can be ignored and the effect of the thruster torque over one cycle is negligible so that the nutation rate is still the torque free result:

$$\dot{\phi}' = \frac{I_3\,\omega_{z'}}{I_t\,c\theta'} \qquad (2\text{-}41)$$

Solving for $\dot{\theta}'$ in Equation (4-50) gives:

$$\dot{\theta}' = \frac{I_t \ddot{\phi}' s\theta' - N_{Y'}}{I_3 \omega_{z'} - 2 I_t \dot{\phi}' c\theta'} \tag{4-52}$$

Differentiating (2-41) to get $\ddot{\phi}'$:

$$\ddot{\phi}' = \frac{N_{z'} c\theta' + I_3 \omega_{z'} \dot{\theta}' s\theta'}{I_t c^2\theta'} \tag{4-53}$$

Substituting Equations (2-41) and (4-53) into (4-52):

$$\dot{\theta}' = \frac{N_{Y'} - N_{z'} \tan\theta'}{I_3 \omega_{z'} (1 + \tan^2\theta')} \tag{4-54}$$

This equation shows two separate effects that torques have on the nutation amplitude. The first is due to torques acting along the Y' axis; a negative $N_{Y'}$ tends to reduce nutations. The second effect is that due to the despin torque. As described earlier, nutations will grow as the spin rate is decreased simply because the nutation is proportional to the ratio of transverse angular momentum to spin momentum:

$$\tan\theta' = \frac{I_t \omega_t}{I_3 \omega_3}$$

$N_{Y'}$ effects ω_t while $N_{z'}$ effects ω_3. Thus Equation (4-57) gives the condition for stable despin ($\dot{\theta}' < 0$):

$$N_{Y'} < N_{z'} \tan\theta'$$

or since both $N_{y'}$ and $N_{z'}$ are negative:

$$|N_{y'}| > |N_{z'}| \tan\theta' \tag{4-55}$$

This condition simply states that for nutations to decrease the $N_{y'}$ torque must be large enough in proportion to the $N_{z'}$ torque to keep the ratio of transverse to spin momentum always decreasing.

The precessional equations for "high" spin rate gives the following result:

$$\dot{\theta}_{AV} = -\frac{N_{Y_{AV}}}{I_3 \omega_{z_{AV}}} \tag{4-56}$$

Thus to reduce θ_{AV} a positive $N_{Y_{AV}}$ torque is required. For two thrusters mounted on the $+\chi$ and $-\chi$ axes and pitched at an angle $\pm\eta$, the torques are as follows:

$$N_{x'} = -M \sin\eta \sin\psi' \tag{4-57}$$

$$N_{y'} = M \sin\eta \cos\psi' \tag{4-58}$$

$$N_{z'} = -M \cos\eta \tag{4-59}$$

Transforming to precessional coordinates:

$$N_{x_{AV}} = -M\sin\eta(c\phi's\psi' - s\phi'c\psi'c\theta') - M\cos\eta\, s\phi's\theta' \tag{4-60}$$

$$N_{Y_{AV}} = M\sin\eta(-s\phi's\psi' + c\phi'c\theta'c\psi') + M\cos\eta\, c\phi's\theta' \tag{4-61}$$

$$N_{z_{AV}} = -M\cos\eta \tag{4-62}$$

It is assumed that a passive damper has brought θ' down from its initial value to 10° to some very small angle, so that $\theta' << 1$. With this assumption, Equations (4-60) to (4-62) simplify to:

$$N_{x_{AV}} \simeq -M \sin\eta \sin(\psi' + \phi') \simeq -M \sin\eta \sin\psi \qquad (4\text{-}63)$$

$$N_{Y_{AV}} \simeq M \sin\eta \cos(\psi' + \phi') \simeq M \sin\eta \cos\psi \qquad (4\text{-}64)$$

$$N_{Z_{AV}} = -M \cos\eta \qquad (4\text{-}65)$$

Remembering that the requirement for reduction of nutation, θ', requires a negative $N_{Y'}$ torque where $N_{Y'}$ is given by Equation (4-58). Thus this requirement is met if η is switched such that $\sin\eta \cos\psi'$ is always negative. The condition to reduce θ_{AV} requires that $N_{Y_{AV}}$ always be positive; thus η must be switched so that $\sin\eta \cos\psi$ always remains positive.

$$\dot{\theta}' < 0 \quad \Rightarrow \quad \sin\eta \cos\psi' < 0 \qquad (4\text{-}66)$$

$$\dot{\theta}_{AV} < 0 \quad \Rightarrow \quad \sin\eta \cos\psi > 0 \qquad (4\text{-}67)$$

Note that they are not always compatible; hence one possible switching scheme would be to switch between $\pm\eta_0$ when the two requirements are compatible, and to set $\eta = 0$ when they are not, as shown in the following table:

$c\psi$ \ $c\psi'$	+	−
+	$\eta = 0$	$\eta = +\eta_0$
−	$\eta = -\eta_0$	$\eta = 0$

The above scheme will achieve all three objectives: despin, sun-pointing, and nutation damping as long as the assumption of steady precession and nutation are valid. For thrusters producing 40 dyne-cm of torque, and $\eta_0 = 10°$, it was determined that the minimum spin rate for validity of these assumptions is approximately .5r/min. Thus, whereas with passive damping nutations can be controlled only down to about 2 r/min, with this active scheme we can do so down to about half an r/min. Therefore, using this scheme, we can expect to reach the following conditions: (a) z axis pointing closely to the sun, $\theta_{AV} < 10°$; (b) very small nutation amplitude, $\theta' \ll 1$ (c) $\omega_z \simeq .5$ r/min. At this point, the switching thrusters scheme will no longer work and η must be set to zero to produce only a despin torque. It was hoped that in the final stage of despin from .5 r/min to zero, the restoring vane torques would prevent the motion from diverging too much and that the resulting motion would be a simple libration which could be damped out by moving the vanes as described earlier. Further analysis showed that this does not happen.

4.5 Final Despin

To investigate the motion at $\omega_3 = 0$, consider the configuration shown in Figure 4.5. For unpitched vanes ($\beta=0$), the torques produced are purely restoring, that is, only N_X torques are generated. Since the X-axis is always perpendicular to both the Z_s-axis and the Z-axis, the component of the total angular momentum along these two axes must be constant in time:

$$H_{Z_s} = I_t \sin^2\theta\,\dot{\phi} + I_3 \omega_Z \cos\theta = \text{const.} \tag{4-68}$$

$$H_Z = I_Z(\dot{\psi} + \dot{\phi}\cos\theta) = I_3\omega_Z = \text{const.} \tag{4-69}$$

In order for the motion to be a true libration, it must pass through $\theta=0$. Thus for this condition, the above equations give

$$H_{Z_s} = I_3(\dot{\psi} + \dot{\phi}) = I_3\omega_Z \tag{4-70}$$

$$H_Z = I_3\omega_Z \tag{4-71}$$

Therefore, $H_{Z_s} = H_Z = \text{constant}$ (4-72)

Thus for $\omega_Z = 0$

$$H_{Z_s} = H_Z = 0 \tag{4-73}$$

Hence, Equation (4-68) gives:

$$\dot{\phi} = 0 \qquad (4\text{-}74)$$

$$\dot{\psi} = 0 \qquad \text{always}$$

The conclusion is that for the condition $\omega_z = 0$, the motion will pass through $\theta = 0$ if and only if the motion is a true libration. The condition for librational motion is $\omega_z = \dot{\psi} = \dot{\phi} = 0$, as seen above. However, for our case where we are despinning from some initial value of ω_z down to $\omega_z = 0$, the precession rate, $\dot{\phi}$, does not approach zero as ω_z goes to zero; on the contrary, $\dot{\phi}$ tends to increase in magnitude as the spin rate decreases. Thus it is evident that when $\omega_z = 0$ is reached, $\dot{\psi}$ and $\dot{\phi}$ will not be zero and librational motion is not possible.

$$\omega_z = \dot{\psi} + \dot{\phi}\cos\theta = 0$$

$$\dot{\psi} = -\dot{\phi}\cos\theta \qquad (4\text{-}75)$$

$$\dot{\psi} \neq 0 \qquad \dot{\phi} \neq 0$$

Thus the general solution, at $\omega_z = 0$ is given by:

$$\dot{\phi} = \frac{H_{z_s}}{I_t \sin^2\theta} \qquad (4\text{-}76)$$

$$\dot{\psi} = -\frac{H_{z_s}\cos\theta}{I_t \sin^2\theta} \qquad (4\text{-}77)$$

$$H_{z_s} \neq 0 \qquad (4\text{-}78)$$

An analytic solution which completely describes the motion in this final stage of despin is not possible, so a computer program was used to numerically integrate the complete general equations of motion that were derived earlier:

$$I_t\ddot{\theta} - I_t\dot{\phi}^2 s\theta c\theta + I_z\dot{\phi}\omega_z s\theta = N_x - (\vec{\omega}_{is}\times\vec{H})_x \qquad (2\text{-}34)$$

$$I_t(\ddot{\phi}s\theta + 2\dot{\phi}\dot{\theta}c\theta) - I_z\dot{\theta}\omega_z = N_y - (\vec{\omega}_{is}\times\vec{H})_y \qquad (2\text{-}35)$$

$$I_z\frac{d\omega_z}{dt} = N_z - (\vec{\omega}_{is}\times\vec{H})_z \qquad (2\text{-}36)$$

$$\omega_z = \dot{\psi} + \dot{\phi}c\theta \qquad (2\text{-}37)$$

The spacecraft is assumed to have the configuration shown in Figure 4.5 where the microthrusters provide despin torque and the unpitched reflecting vanes produce only restoring torques, N_x. The parameters used are shown below:

Moments of Inertia: $I_t = 2.8\times10^6$ gm-cm^2 , $I_z = 4.65\times10^6$ gm-cm^2

Vane constants: $\alpha = 70^\circ$

$\beta = 0^\circ$

Area = .125 m^2

Thruster despin torque: $M = 40$ dyne-cm.

In the program, the thrusters are cut-off when $\omega_z \leq 0$ is first reached. The first run was made assuming no initial nutation; the initial conditions used were:

$\theta_o = 7°$ $\qquad$ $\omega_{x_o} = 0$

$\phi_o = 0°$ $\qquad$ $\omega_{y_o} = 0$

$\psi_o = 0°$ $\qquad$ $\omega_{z_o} = .15$ r/min

The resulting motion of the spacecraft z axis about the sun line is plotted in $\theta - \phi$ coordinates in Figure 4.6. Note that initially the motion is a very slow precession. However, as the spin rate falls below $\sim .1$ r/min, the applied N_x torques produced by solar pressure on the vanes are sufficiently large in comparison to the angular momentum of the spacecraft to cause a nutation to build up in addition to the precession. Note that at this low spin rate, the nutation rate becomes comparable to the precession rate making it impossible to separate and distinguish between the two motions. This coupling becomes more pronounced as the spin rate decreases. At $\omega_z = 0$, the thrusters are cut off so that the only torque acting is the restoring torque due to solar pressure on the vanes. The resulting motion is a pseudo libration-precession of the spacecraft z axis about the sun line. The open elliptical paths are traversed at approximately the libration rate (~50 minutes). Note that because there was no initial nutation, θ never exceeds the initial value of 7°.

The next case studied assumed an initial nutation amplitude of about 30'. This is a more realistic condition than the above because if we assume active nutation control down to 1 r/min, the residual amplitude at that point can be expected to be on the order of about half a degree. The initial conditions used were:

$\theta_0 = 7°$ $\qquad$ $\omega_{x_0} = .01$ r/min

$\phi_0 = 0°$ $\qquad$ $\omega_{y_0} = 0$ r/min

$\psi_0 = 0°$ $\qquad$ $\omega_{z_0} = 1.0$ r/min

The resulting motion is plotted in Figure 4.7. Note that initially the motion is very well described by the "high" spin rate approximation -- a superposition of a fast torque free nutation on a slow torqued precession. The plot shows that as expected, the nutation amplitude increases as the spin rate decreases. Once again, when ω_z goes to zero and the thrusters are cut-off, the resulting motion can be described as a pseudo libration-precession about the sun at approximately the libration rate. Note, however, that because there was an initial nutation, the motion is more irregular and diverged considerably from the initial value of $\theta = 7°$ to a maximum value of about 30°.

A third case was run with initial conditions based on the assumption of passive nutation damping down to 2 r/min with no further damping after that point. Thus the initial conditions used were:

$\theta_o = 7°$ $\qquad$ $\omega_{x_o} = .02$ r/min

$\phi_o = 0$ $\qquad$ $\omega_{y_o} = 0$

$\psi_o = 0$ $\qquad$ $\omega_{z_o} = .15$ r/min

Again, the motion at $\omega_z = 0$ is an irregular libration-precession with the period of about fifty minutes, (Figure 4.8). However, due to a larger initial nutation, the motion diverged considerably to a maximum of $\theta \simeq 83.5°$! These results emphasize the critical need to control nutations at very low spin rates.

4.5 Difficulties With the Despun Configuration

It appears that the completely despun configuration contains inherent difficulties which may be very difficult to overcome. The first is the sensing problem. Since the scheme requires that $\omega_z = 0$ be detected, the sensing method used must be able to measure ω_z accurately. Remembering that $\omega_z = \dot{\psi} + \dot{\phi} c\theta$ and that a sun sensor can only measure ψ and not ϕ, we see that in the "high" spin rate regime, $|\dot{\phi}| << |\dot{\psi}|$, so that $\omega_z \simeq \dot{\psi}$ and hence a solar measurement of $\dot{\psi}$ gives an excellent indication of ω_z. However, as the spin rate approaches zero, $|\dot{\phi}|$ becomes comparable to $|\dot{\psi}|$ so that solar sensing cannot be used to detect $\omega_z = 0$. Thus another sensing device would be required, adding to spacecraft complexity and weight.

The second difficulty is the need for complete nutation control at low spin rates. The above results showed that even tiny residual nutations can cause wildly diverging motions when ω_z goes to zero. Associated with this problem is that of how to damp out these motions to achieve the required initial orientation. Both of these problems could possibly be solved with the use of a much more complex control scheme, but again, the entailing weight and complexity make this solution less than desirable.

The final and most inherent drawback of a completely despun configuration is its sensitivity to disturbance. Unlike a spinning configuration which possesses an inherent "stiffness" due to its angular momentum, the despun spacecraft is very susceptible to impulsive torque disturbances such as micro-meteoritic impact or outgassing from a malfunctioning component. Thus even if it were possible to initially despin and orient the spacecraft, any disturbance would necessitate a re-orientation during which time the signal received at earth would be diminished or lost.

In view of its many inherent drawbacks, the despun configuration did not appear promising and was not investigated further.

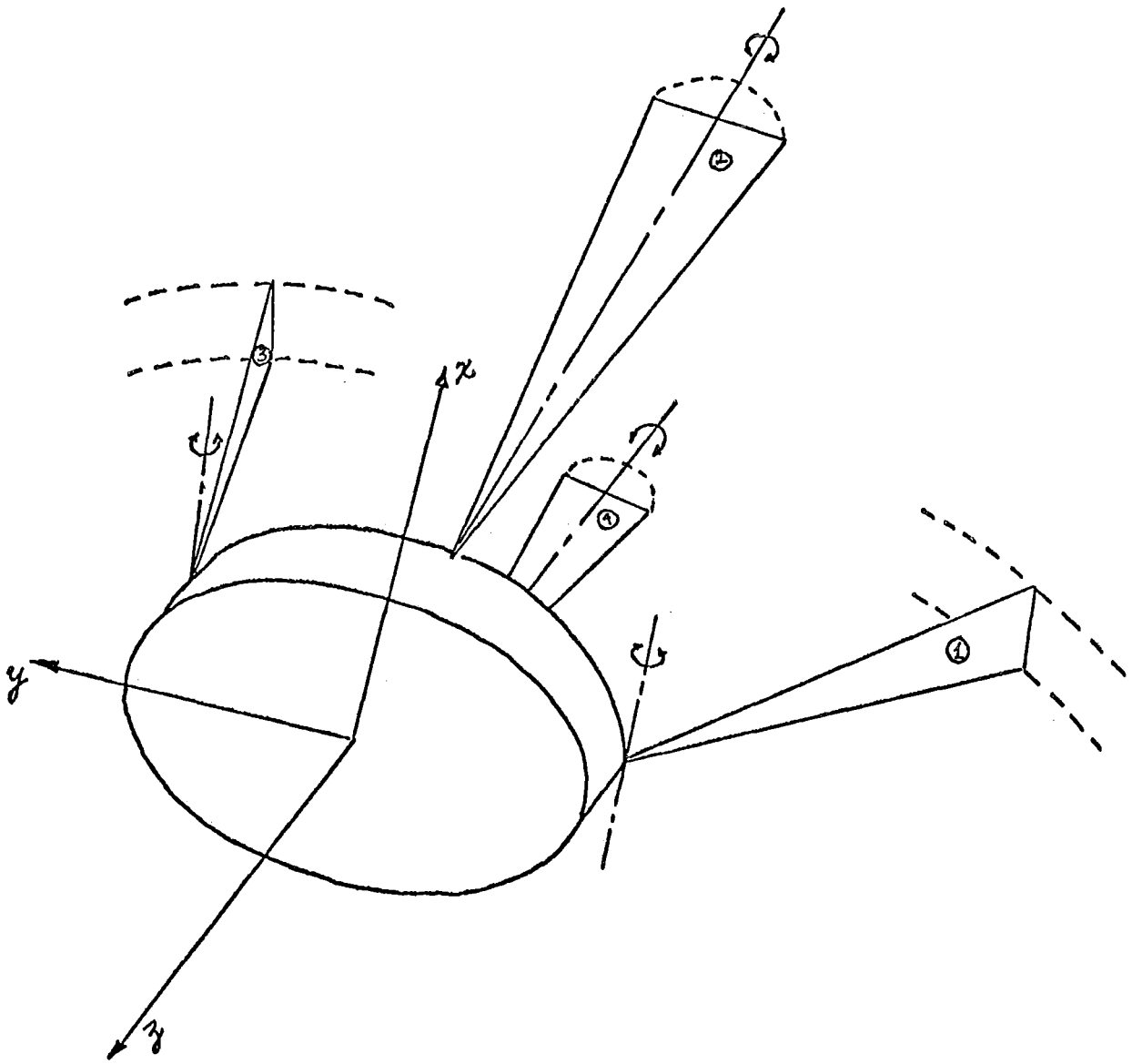

Figure 4.1 Possible despun configuration

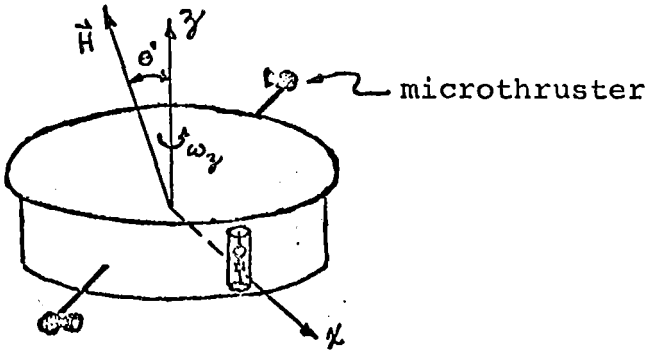

Figure 4.2 Despin scheme with viscous nutation damping

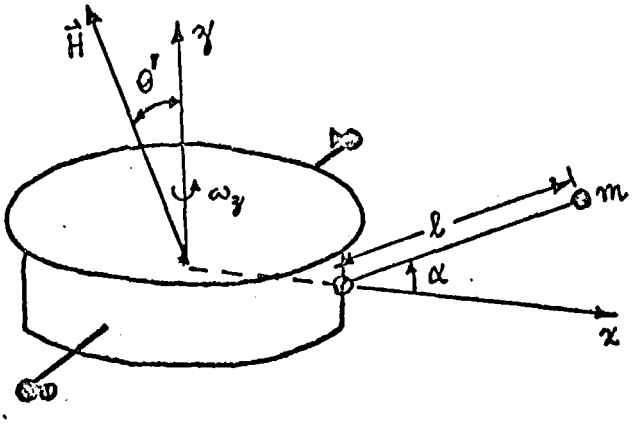

Figure 4.3 Despin scheme with tuned pendulous damper

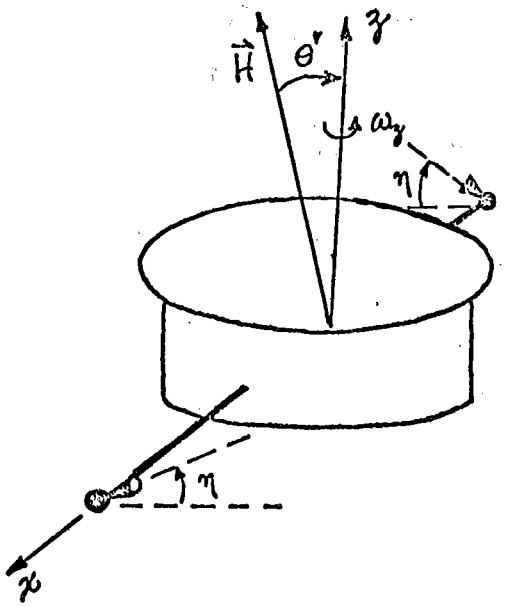

Figure 4.4 Initial orientation scheme using pitched thrusters

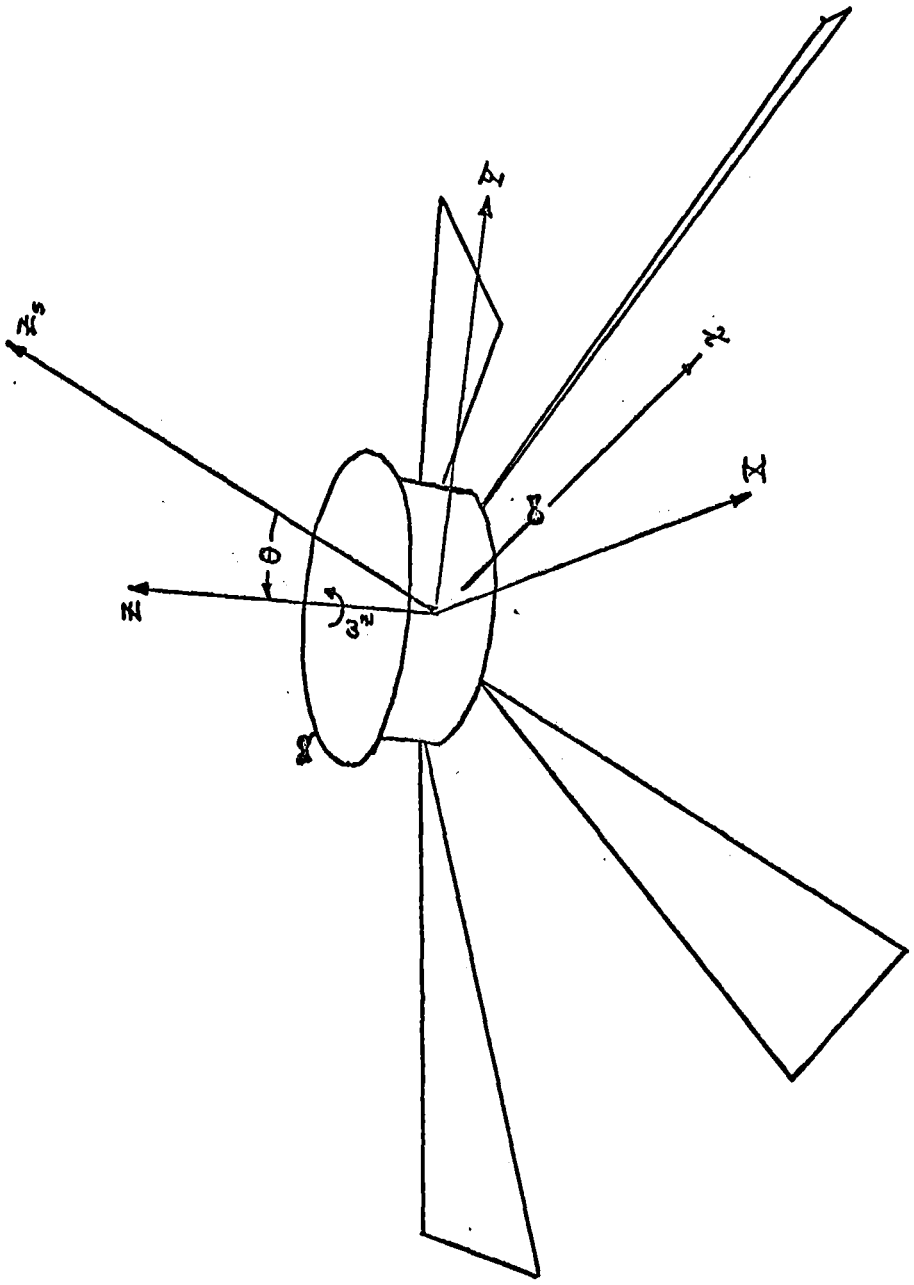

Figure 4.5 Final despin configuration

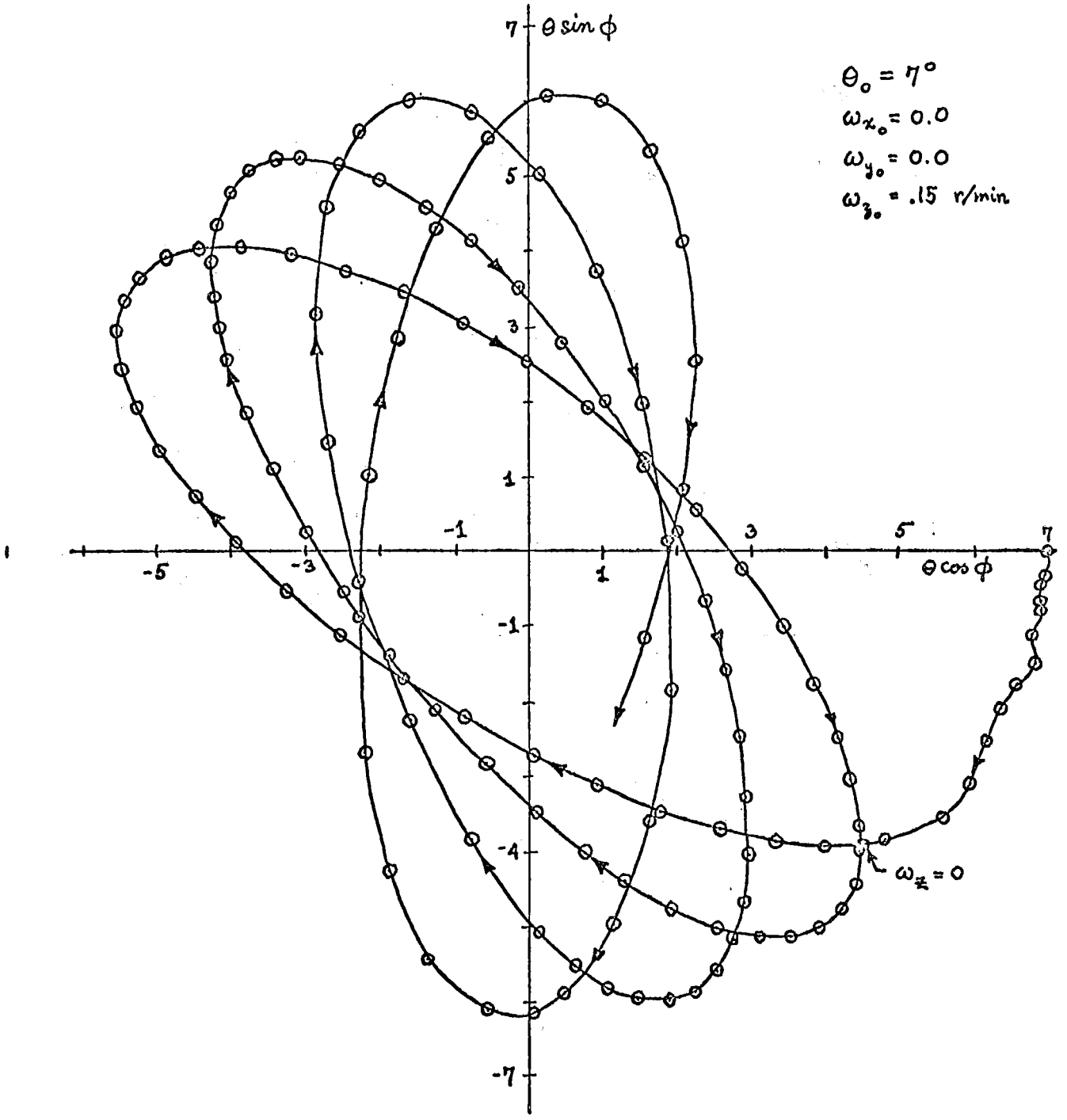

Figure 4.6 Spacecraft motion at final stage of despin

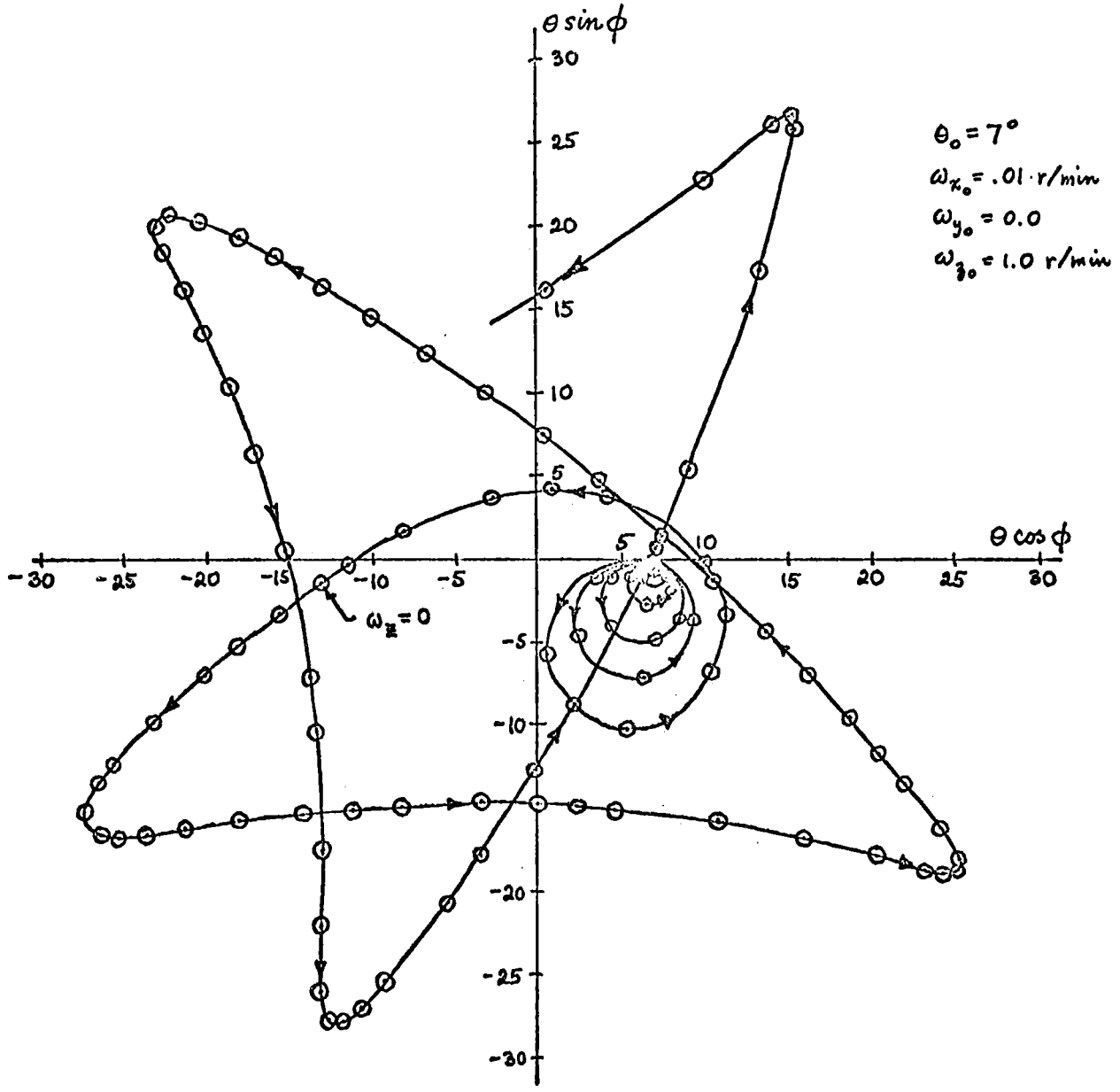

Figure 4.7 Spacecraft motion at final stage of despin

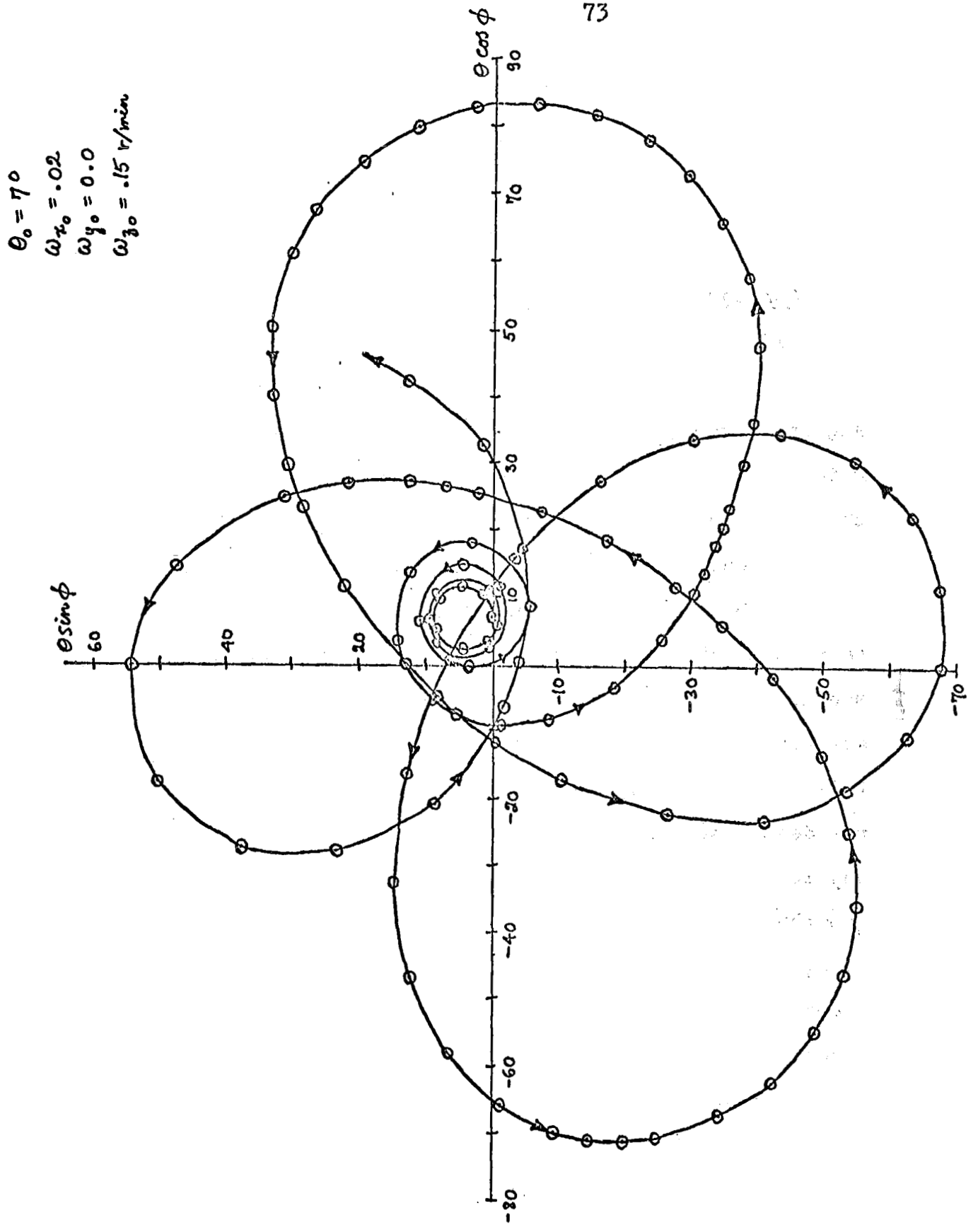

Figure 4.8 Spacecraft motion at final stage of despin

CHAPTER 5

DUAL SPIN CONFIGURATION

5.1 Configuration Description

All the difficulties in the despun configuration stem from the basic condition that the spacecraft has no angular momentum (aside from that due to orbital rate which is negligible). However, it was required to despin the spacecraft in order to maintain proper antenna orientation. The classic solution to these two conflicting requirements is a dual spin configuration where the section of the spacecraft on which the antennas are mounted is completely despun while the remainder of the spacecraft is maintained at some high spin rate. For this configuration, all the difficulties encountered in the despun spacecraft are eliminated. The sensing of ω_z is greatly simplified because for a spinning configuration, $\omega_z \simeq \dot{\psi}$ thus solar sensing of $\dot{\psi}$ is an excellent approximation to ω_z. The effect of nutations on spacecraft dynamics become far less critical because the nutational and precessional motions become uncoupled (assuming that the spinning section has sufficient angular momentum) and the overall dynamics can be modeled as a fast torque

free nutation superposed on a very slow torqued motion ("high" spin rate approximation). Any existing nutation can be damped out by passive dampers. The final advantage of the dual spin configuration is that it is less vulnerable to disturbance torques.

There are basically two possible dual spin configurations. The first is one in which the spacecraft is simply divided into two sections, one spinning and one despun. Such a design is shown in Figure 5.1 where section B containing the antennas is despun while section A containing the sails is maintained spinning at a high rate. The difficulty with this configuration is that the required bearing between A and B would be subjected to the space environment and therefore presents lubrication problems. Also, the bearing would have to be electrically conducting in order to provide power for section A. Since failure of the bearing would be catastrophic to the mission, a second configuration as shown in Figure 5.2 appears more desirable. Here, the entire spacecraft is despun except for a small contained momentum wheel. In this case, the entire momentum wheel system would be sealed and hence free from the effects of the space environment. Another minor advantage of this design is that the momentum wheel has essentially no energy dissipation; in the earlier configuration, any flexible parts in the spinning section,

such as the sails, provide energy dissipation which adversely effect the nutational stability of the spacecraft. This topic will be discussed in a later section. The principal disadvantage of the momentum wheel system is the weight penalty due to the momentum wheel itself. Whereas in the earlier configuration, components of the basic spacecraft provide the spin inertia, this second design requires a separate wheel which serves no purpose except to provide spin inertia. It was decided that because bearing reliability is so critical to the success of the mission, the greater reliability of the momentum wheel system far outweighed the penalty in extra weight involved.

Before proceeding to study the dynamics of such a configuration, the moments of inertia of the spacecraft must first be determined. The spacecraft can be divided into three separate components: (1) an inertially symmetric body, (2) an inertially symmetric momentum wheel, and (3) a pair of rotatable yagi antennas.

$$[I]_{s/c} = [I]_{body} + [I]_{wheel} + [I]_{antennas} \qquad (5\text{-}1)$$

where these inertias are calculated with respect to the body-fixed axes $\{x, y, z\}$. First of all, it is obvious that as the antennas rotate to track earth, their inertias with respect to the "b" system will change. The effect of

the rotation is to make the body axes no longer principal. In fact, they will be principal axes only for $\xi = 0, \frac{\pi}{2}, \pi, \ldots, n\frac{\pi}{2}$, where ξ is measured from the z axis. In general, rotation of the antennas through some angle ξ introduces product of inertia terms. Because the rotation is about the x-axis, this axis is always principal. In general, then, the inertia matrix of the entire spacecraft will be:

$$[I]_{s/c} = \begin{bmatrix} I_t & 0 & 0 \\ 0 & I_t & 0 \\ 0 & 0 & I_z \end{bmatrix} + \begin{bmatrix} B & 0 & 0 \\ 0 & B & 0 \\ 0 & 0 & C \end{bmatrix} + \begin{bmatrix} I_x^a & 0 & 0 \\ 0 & I_y^a(\xi) & J_{yz}^a(\xi) \\ 0 & J_{yz}^a(\xi) & I_z^a(\xi) \end{bmatrix}$$

$$= \begin{bmatrix} I_x & 0 & 0 \\ 0 & I_y(\xi) & J_{yz}^a(\xi) \\ 0 & J_{yz}^a(\xi) & I_z(\xi) \end{bmatrix} \qquad (5\text{-}2)$$

The antenna inertias as a function of the antenna dimensions and the rotation angle ξ are worked out in Appendix C. It turns out that because the antennas are so massive, their inertias dominate. Typical values are:

$$I_y^a \simeq 2.9 \times 10^8$$
$$I_x^a \simeq .372 \times 10^8$$
$$I_z^a \simeq 3 \times 10^8$$
$$J_{yz}^a \lesssim 6 \times 10^6$$

5.2 Momentum Wheel Specifications and the Roll Control Loop

The purpose of the momentum wheel is two fold: first, it provides the spacecraft with the required angular momentum; and secondly, it serves as a momentum source-sink which exchanges spin momentum with the main body to counteract roll disturbance torques. The minimum required angular momentum is determined by three factors: (1) the required "stiffness" to disturbances; (2) passive damping efficiency; and (3) validity of "high" spin rate equations. The last requirement is, the more important one; the wheel must provide enough angular momentum so that "steady" precession and nutation are possible thus avoiding the coupling between the two motions which results in the wild gyrations seen in the study of the despun configuration at very low spin rates. For this dual spin configuration, the dynamical equations are identical to those derived earlier except for the additional spin momentum term due to the wheel. Thus equations (2-34) to (2-37) written for this configuration becomes (for the moment, still assuming a symmetric spacecraft):

$$I_x \ddot{\theta} - I_x \dot{\phi}^2 s\theta c\theta + (I_3 \omega_3 + C\Omega_z)\dot{\phi} s\theta = N_x - (\vec{\omega}_{is} \times \vec{H})_x \quad (5\text{-}3)$$

$$I_x(\ddot{\phi} s\theta + 2\dot{\phi}\dot{\theta} c\theta) - (I_3 \omega_z + C\Omega_z)\dot{\theta} = N_y - (\vec{\omega}_{is} \times \vec{H})_y \quad (5\text{-}4)$$

$$\frac{d}{dt}(I_3 \omega_z + C\Omega_z) = N_z - (\vec{\omega}_{is} \times \vec{H})_z \quad (5\text{-}5)$$

where I_x is the transverse inertia of the entire spacecraft while I_z is the spin inertia of the spacecraft without the wheel, C is the spin inertia of the wheel, and Ω_z is the wheel spin rate. Optimally, $\omega_z = 0$ so that the equations become:

$$I_x\ddot{\theta} - I_x\dot{\phi}^2 s\theta c\theta + C\Omega_z\dot{\phi}s\theta = N_x - (\vec{\omega}_{is}\times\vec{H})_x \qquad (5\text{-}6)$$

$$I_x(\ddot{\phi}s\theta + 2\dot{\phi}\dot{\theta}c\theta) - C\Omega_z\dot{\theta} = N_y - (\vec{\omega}_{is}\times\vec{H})_y \qquad (5\text{-}7)$$

$$C\frac{d\Omega_z}{dt} = N_z - (\vec{\omega}_{is}\times\vec{H})_z \qquad (5\text{-}8)$$

The wheel spin momentum now plays exactly the same role as $I_z\omega_z$ did in the single-spin configuration. It was determined earlier that a lower limit of .1 r/min would ensure the validity of the "high" spin rate assumption. Adding a factor of safety, let us say that the minimum allowable equivalent ω_z is .3 r/min. This gives us the minimum spin angular momentum which the wheel must provide. Assuming $I_z = 3\times10^8$ gm-cm² then:

$$C\Omega_{z_{min}} = (3\times10^8)(.03)$$
$$= 9\times10^6 \text{ gm-cm}^2/\text{sec}$$

Take $\Omega_{z_{min}} = 5000$ r/min, then:

$$C = 1.8\times10^4 \text{ gm-cm}^2$$

Assume the following wheel configuration:

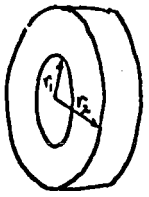

$r_1 = 3$ cm.
$r_2 = 6$ cm.

Then $$m \frac{(r_1^2 + r_2^2)}{2} = C$$

$$m = 800 \text{ gm.}$$

Thus, a momentum wheel weighing about two pounds is required. Assume that the motor saturates at 10^4 r/min, then the wheel operates within the interval 5000 r/min to 10^4 r/min. When either of these limits is reached, a correcting torque must be provided to keep the wheel speed within the allowed interval. Thus in the dual spin application, the momentum wheel operates about a bias instead of about zero as in more conventional applications.

The nutation rate is now given by:

$$\dot{\phi}' = \frac{C\Omega_z}{I_x C\theta'} \tag{5-9}$$

$$\dot{\psi}' = -\frac{C\Omega_z}{I_x} \tag{5-10}$$

Thus, .03 rad/sec $\lesssim |\dot{\psi}'| \lesssim$ .06 rad/sec. The damper can therefore be tuned to this range of frequencies.

For the study and design of the roll control loop, the following model can be used:

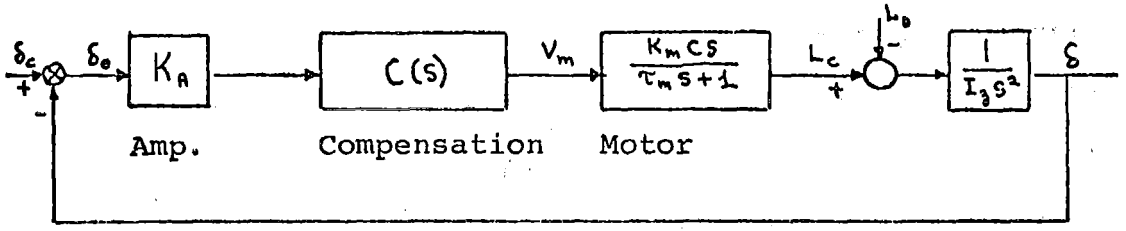

Two types of compensation were studied and compared: (1) an integrator system, and (2) a lead compensation system. The latter was rejected because for a constant disturbance torque, $L_D(s) = \frac{L_o}{s}$, the roll error grows with time. The following integrator compensation system appeared superior:

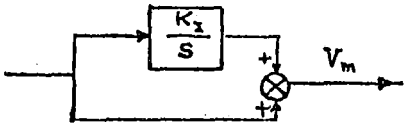

The open loop transfer function is:

$$\frac{\delta(s)}{\delta_e(s)} = \frac{K_A K_m C (K_I + s)}{I_y \tau_m s^2 (s + \frac{1}{\tau_m})} \qquad (5\text{-}11)$$

Thus, for stability,

$$K_I < \frac{1}{\tau_m} \qquad (5\text{-}12)$$

The response to a disturbance torque is:

$$\frac{\delta_e(s)}{L_D(s)} = \frac{\tau_m s + 1}{I_y s^2 (\tau_m s + 1) + K_A K_m C (K_I + s)} \qquad (5\text{-}13)$$

For a step disturbance $L_D = \frac{L_o}{s}$:

$$\delta_e \Big|_{s.s.} = \frac{L_o}{K_A K_m K_I C} \qquad (5\text{-}14)$$

By specifying a maximum allowable roll error for a specific disturbance torque, the forward loop gain $K_A K_m K_I$ is determined with the restriction that $K_I < \frac{1}{\tau_m}$. Specification of other dynamic parameters such as the damping ratio further defines the individual gains. Design of the roll control loop is a straight forward application of linear theory and will not be shown here. In the final stage of initial orientation, the roll error would normally be very large, resulting in a very large error signal to the roll loop. This situation would also occur if the RF roll reference uplink is used approximately every twenty four hours to correct the error build-up due to sensor inaccuracy. These large error signals would saturate the motor amplifier. Thus a non-linear analysis was also undertaken to determine the system response to large signals. The motor was modeled as an ideal relay and the "switching time" method used. It was found that for roll errors as great as 40°, the settling time was on the order of tens of minutes which is perfectly acceptible. The methods used in this analysis are well documented in references (10) and (11) and hence will not be shown here.

5.3 Spacecraft Dynamics

The momentum wheel is designed to provide sufficient angular momentum so that the "high" spin rate approximation

to the motion is valid. The dynamics of the spacecraft can therefore be modeled as a sum of two uncoupled motions, a fast torque-free nutation about the angular momentum vector superposed on a slow torqued motion of the angular momentum vector. Thus, we are allowed to analyze the two motions separately.

Nutations are not as critical to the motion of a dual spin spacecraft as they are to the despun configuration. For the spacecraft with spin, a passive damper mounted on the spacecraft body provides more than adequate nutation control. The only factor which requires investigation is stability; it must be determined whether the damper actually damps out nutation or whether it reenforces it, causing the motion to diverge. For single spin bodies with energy dissipation, the well known major axis rule applies -- only spin about the major axis of inertia is stable. If we were to apply this rule to our case, we would conclude that the system is not always stable, for as the antennas rotate, the spin axis ceases to be the major inertia axis. Investigations into the stability of dual spin bodies have shown that the "major axis" rule does not apply to such configurations. In fact, the result is that when the body to which the damper is attached is at rest (while the rotating wheel contains no energy

dissipation), a dual spin system is assymptotically stable regardless of its inertia distribution. For the worst case, where the body containing the damper is spinning in inertial space and the wheel is at rest, the stability condition reduces to the above "major axis" spin requirement. Thus the general conclusion is that damping on the despun portion of a dual spin system adds to the stability whereas energy dissipation in the spinning portion is detrimental to stability.

A stability analysis for the specific spacecraft configuration is shown in Appendix B. The equations of motion are satisfied by the following solution:

$$\begin{aligned} \omega_x &= \omega_y = \omega_z = 0 \\ Z &= 0 \\ \Omega &= \Omega_s \end{aligned} \tag{5-15}$$

where $\vec{\omega}$ is the angular velocity of the main spacecraft body referred to body-fixed axes, Ω is the spin rate of the momentum wheel, and Z is the displacement from equilibrium of the damper mass. The stability conditions for this solution are:

$$I_x > \frac{md^2}{1-\mu} \tag{B-60}$$

$$I_y > \frac{I_{yz}^2}{I_z - C} \tag{B-61}$$

Both conditions are always met for the given configuration.

When studying torqued motion, only the spin momentum of the wheel need be considered. Because the non-spinning body is essentially stationary, its inertia can be ignored. Thus, the "high" spin rate equations derived earlier are valid, giving:

$$C\Omega\dot{\phi}\sin\theta = N_x + C\Omega\omega_{is}\cos\theta\sin\phi \tag{5-16}$$

$$C\Omega\dot{\theta} = -N_y - C\Omega\omega_{is}\cos\phi \tag{5-17}$$

$$C\dot{\Omega} = N_z \tag{5-18}$$

To find the equilibrium point of the motion, set $\dot{\phi} = \dot{\theta} = 0$.

$$\sin\phi = -\frac{N_x(\theta)}{C\Omega\omega_{is}C\theta} \tag{5-19}$$

$$\cos\phi = -\frac{N_y(\theta)}{C\Omega\omega_{is}} \tag{5-20}$$

Hence, $$1 = \left(\frac{N_x^2(\theta)}{C^2\theta} + N_y^2(\theta)\right)\frac{1}{C^2\Omega^2\omega_{is}^2} \tag{5-21}$$

For solar pressure torques on vanes, the erecting and precession components are well approximated by

$$N_x(\theta) \simeq K_x S\theta C\theta \tag{5-22}$$

$$N_y(\theta) \simeq K_y S\theta C\theta \tag{5-23}$$

Thus (5-21) becomes:

$$S^2\theta^*\left(K_x^2 + K_y^2 C^2\theta^*\right) = C^2\Omega^2\omega_{is}^2$$

For small θ^*:

$$\theta^* \simeq \frac{C\Omega\omega_{is}}{\sqrt{K_x^2 + K_y^2}} \qquad (5\text{-}24)$$

And

$$\cos\phi^* = -\frac{N_y(\theta^*)}{C\Omega\omega_{is}} \qquad (5\text{-}25)$$

Thus, for a precessing spacecraft such as Sunblazer where $N_y << H\omega_{is}$, the equilibrium position is $\phi^* \sim 90°$ and $\theta^* \sim 5°$ which means that the average position of the spin axis is several degrees above the ecliptic as it precesses about the sun line.

Remembering that with sun sensing alone, a measurement of ϕ is not possible. Thus precession is undesirable from an attitude sensing viewpoint. If we could therefore eliminate precession and determine the resulting spacecraft equilibrium position, the need for an additional roll sensing device would be eliminated since for $\dot{\phi} = 0$, $\omega_z = \dot{\psi}$ and hence a solar measurement of θ and ψ will completely specify the spacecraft attitude. To eliminate precession, N_x must be zero. Equations (5-16) and (5-17) become:

$$C\Omega\omega_{is}\cos\theta^*\sin\phi^* = 0 \qquad (5\text{-}26)$$

$$C\Omega\omega_{is}\cos\phi^* = -N_y \simeq -K_y s\theta^* c\theta^* \qquad (5\text{-}27)$$

Thus for sufficiently large N_Y:

$$\phi^* = 180^\circ \tag{5-28}$$

$$\theta^* \cong \frac{C\Omega\omega_{is}}{K_Y} \tag{5-29}$$

The equilibrium position for a non-precessing spacecraft is therefore z in the ecliptic making a small angle θ^* with the sun line. This result can be intuitively reasoned as follows. If there are no torques acting on the spacecraft, the momentum vector would remain pointed in the same direction in inertial space as the spacecraft orbits the sun, resulting in loss of sun pointing as shown below:

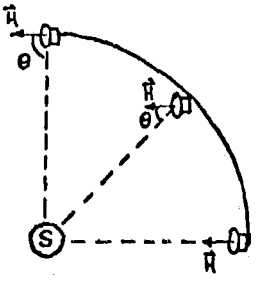

Thus, if the spacecraft is to be maintained sun pointing without precessing a sufficiently large erecting torque (equal to the spin momentum times the orbital angular rate) is required. Since N_Y is proportional to θ (for small θ) this results in an equilibrium position $\phi^* = 180^\circ$ and $\theta = \theta^*$ as derived above. Simply because we know that the spacecraft z axis lies in the ecliptic plane, a simple solar measurement of θ and ψ allows complete

determination of the spacecraft attitude thus eliminating the need for a second vector measurement. Note that since the wheel spin rate varies between 5000 r/min and 10^4 r/min, the equilibrium point will vary between θ^* corresponding to the lower spin momentum state and $\theta^{**} \sim 2\theta^*$ corresponding to $\Omega = 10^4$ r/min.

5.4 Production of Control Torques

The control torques required are an erecting torque to maintain sun-pointing, and a spin torque N_z to desaturate the wheel. The required N_Y is

$$N_Y = c\Omega\omega_{is} \simeq 4.8 \text{ dyne-cm.} \tag{5-30}$$

The control requirements are: (1) maintain θ in the interval $2° \leq \theta \leq 10°$ and (2) maintain wheel speed in the interval 5000 r/min $\leq \Omega \leq 10^4$ r/min. The lower limit on θ stems from the fact that sensor sensitivity in ψ decreases rapidly as θ becomes small and in fact at $\theta = 0$, solar measurement of ψ is lost completely. These two distinct attitude control requirements necessitate the ability to generate N_Y and N_z independently of each other.

Using pairs of identical vanes such as on Sunblazer results in coupled N_Y and N_z torques, that is, for a

negative pitch angle, negative erecting and spin torques are generated, whereas for positive pitch, the reverse occurs. The reason for this coupling can be seen as follows. Consider a pair of vanes mounted on opposite sides of the spacecraft and pitched at some angle β :

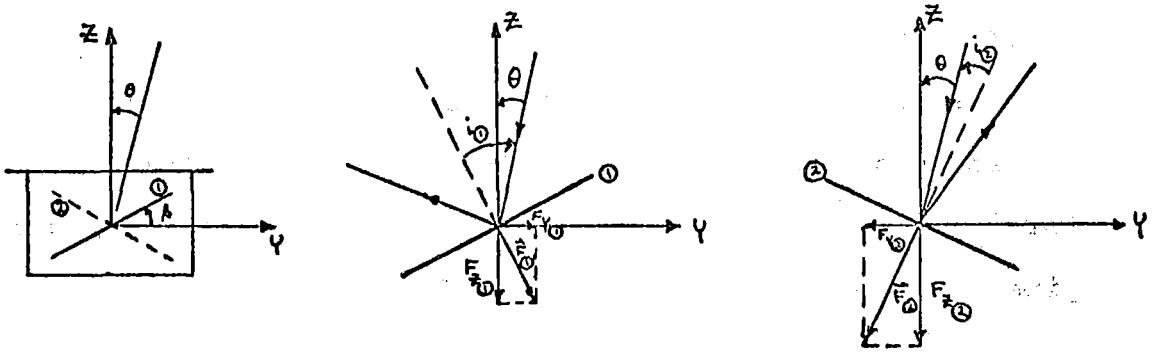

Light reflecting off the vanes create resulting forces $\vec{F}_{①}$ and $\vec{F}_{②}$. The components $F_{Y_{①}}$ and $F_{Y_{②}}$ reenforce to produce a roll torque; $F_{Z_{①}}$ and $F_{Z_{②}}$, on the other hand, create opposite erecting torques, however they do not cancel since $|F_{Z_{②}}| > |F_{Z_{①}}|$ due to the fact that $i_{②} < i_{①}$. Thus it is possible to produce roll torque without also producing an erecting torque only if $\theta = 0$. If we controlled the pitch angles of the vanes independently so that $i_{①} = i_{②}$ always, N_Y would be zero, however a net precession torque results which is unacceptible. The difficulty in separating the roll and erecting torques when using vanes is that only a single reflection occurs so that a "bias" results when θ is not zero and the N_Y torques

created by the pair of opposite vanes do not cancel. This prompted an investigation into light pipes which essentially transmit light by total internal reflection. One can think of such light pipes as nozzles through which light, a flux of momentum, is carried and then discharged. These "nozzles" which are mqde up of many individual fibers (~50μm in diameter) can be rotated to give torques about any desired direction. Because so many reflections occur within the fibers, the above "bias" for θ not zero is eliminated. Consider two sets of light pipes mounted on opposite sides of the spacecraft:

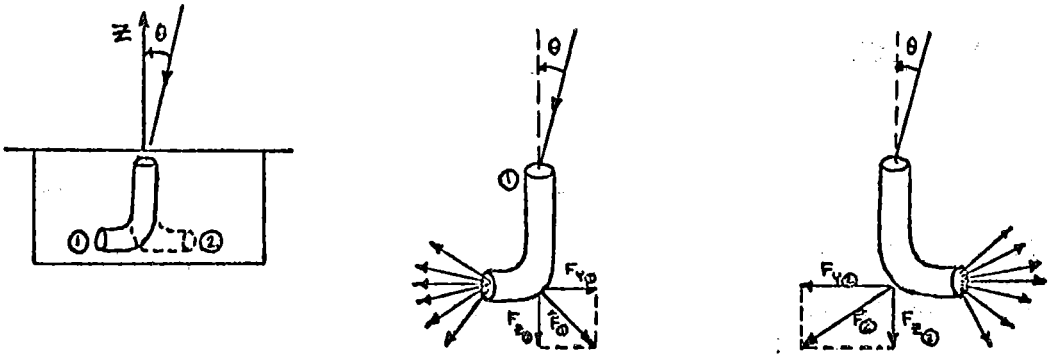

Experimentally, it is found that the illuminance on the exit face appears quite uniform independent of the angle of incidence θ. This is due to the many reflections which occur within the fibers which tend to average out the directional bias at the entrance face. Thus, in this case, $F_{z_①} = F_{z_②}$, and only a roll torque is produced.

To determine the feasibility of such a system, its drawbacks must be investigated. The two principal weaknesses are: (1) light collection ability, and (2) efficiency. Consider first the problem of efficiency. There are three loss mechanisms involved here: (1) reflection losses upon entering and leaving the fiber; (2) absorption losses within the fiber; and (3) reflection losses at the walls of the fiber.

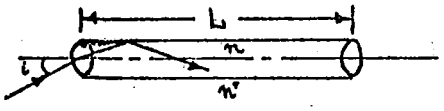

Reflection losses always occur whenever light passes between two media of differing indices of refraction, hence these losses are inevitable. Figure 5.3 shows the fractional intensity of the reflected light as a function of the angle of incidence for glass of index of refraction 1.52. Thus to keep this loss below 10%, the angle of incidence should be kept smaller than 45°.

Next, consider the effect of absorption. The transmissivity $\tau(i)$ for a ray inclined at an angle i is given by:[18]

$$\tau(i) = \exp\left[\frac{-\alpha L n}{(n^2 - \sin^2 i)^{1/2}}\right] \qquad (5\text{-}31)$$

where α is the absorption coefficient of the fiber material.

Note that the expression is exponential in αL, hence a short fiber with a very low α is desirable. For most glasses, $\alpha \sim 1\%/\text{in.}$

Now we include the losses due to imperfect reflections within the fiber. These losses can be caused by irregularities or defects along the wall or even by films of dirt or grease on the fiber surface. Due to these factors, a percentage α' is lost at every reflection. The transmission expression becomes

$$\tau(i) = (1-\alpha')^{\eta} \cdot \exp\left[\frac{-\alpha L n}{\sqrt{n^2 - \sin^2 i}}\right] \qquad (5\text{-}32)$$

where η = number of reflections suffered by a given ray. The transmission of a uniform ray of light may thus be calculated by numerical integration. It can be shown that for a 10° incident cone of light in a fiber 50μm in diameter and 50 cm. long (n=1.5, α =1%/cm), the transmission is 60% when there are no reflection losses (α'=0). However, when α'=1%, the light transmission falls to only 4%. This indicates the importance of keeping reflection losses as low as possible. Thus, at best, we can expect about 60% of the light hitting the entrance face of the fiber to emerge at the exit. A further loss in effective force produced is incurred due to the fact that the light emerges uniformly in all directions. This could cause a fractional loss of 1/3

(assuming isotropic emergence). Thus, only 40% of the incident momentum flux actually ends up producing torque in this system.

Because the light pipes are rather inefficient, a high concentration of light must be sent through them to produce appreciable forces. Consider the configuration shown in Figure 5.4, where parabolic reflecting dishes concentrate light on the fiber pipes. Note that light bouncing off the dish produces undesired torques. The dishes must be designed so that its center of pressure is exactly level with the spacecraft center of mass, i.e. $z_{cp} = d$, so that no net torque is exerted by the dishes. In order to produce positive or negative roll torques, the fiber pipe can be made to rotate parallel to the z axis as shown in Figure 5.5. Another difficulty with this system is that the parabolic dishes become very inefficient light collectors when they are not pointed directly at the sun; for $\theta = 5°$, over half the concentration is lost.

To assess the performance that can be expected from such a system, the dishes are assumed to have a radius of 20 cm., and the distance from the light pipes to the center of mass was assumed to be 50 cm. Using these figures along with the expected efficiency as discussed above, it was found that the maximum roll torque

that can be expected is less than 2 dyne-cm. It is concluded that because of low overall efficiency, light pipe systems for producing control torques do not appear promising.

Solar pressure vanes still seem to be the simplest and most efficient (minimum weight to torque produced) means of producing control torques. Their inherent drawback is in their inability to generate roll and erecting torques independently of each other. However, a design was found to circumvent this difficulty. In Appendix A, equations are derived for the torques produced by solar pressure on vanes. The "averaged" torques (averaged over ψ) are given by:

reflected:
$$\vec{N}_r^{av} = \text{Area}(1-\text{emiss})\frac{2I}{C}\Big[-\vec{\imath}_K(s^2\alpha\, c\alpha\, c^3\beta\, r_1 + s\alpha\, c\beta(1-s^2\alpha\, c^2\beta)z_1)s\theta c\theta - \vec{\jmath}_K(s^2\alpha\, s\beta\, c^2\beta\, r_1)s\theta c\theta + \vec{k}_K(s^2\alpha\, s\beta\, c^2\beta + s\beta(\tfrac{1}{2} - \tfrac{3}{2}s^2\alpha\, c^2\beta)s^2\theta)r_1\Big]$$

absorbed:
$$\vec{N}_a^{av} = \text{Area}\cdot abs\cdot\frac{I}{C}\Big[\vec{\imath}_K(z_1 s\alpha\, c\beta - \tfrac{r_1}{2}c\alpha\, c\beta)s\theta c\theta + \vec{\jmath}_K(-\tfrac{r_1}{2}s\beta s\theta\, c\theta) + \vec{k}_K(\tfrac{r_1}{2}s\beta\, s^2\theta)\Big]$$

reradiated:
$$\vec{N}_{rr}^{av} = C_r\left\{\vec{\jmath}_K\left[\tfrac{1}{2}(az_1 + br_1 cA)\frac{a\,s\theta}{\left(\frac{\omega}{\omega_{opt}} + \frac{\omega_{opt}}{\omega}\right)}\right] + \vec{k}_K r_1 s\beta\, c\theta\right\}$$

where
$$C_r = \frac{2}{3}\frac{I}{C}\cdot\text{Area}\cdot abs\cdot\frac{(\text{emiss}\,1 - \text{emiss}\,2)}{(\text{emiss}\,1 + \text{emiss}\,2)}$$

$$b = s\alpha c\beta \qquad r_1 = r_o + \ell_o s\alpha$$
$$a = \sqrt{1-b^2} \qquad z_1 = \ell_o c\alpha$$
$$A = \tan^{-1}\left(\frac{s\beta}{c\alpha \cdot c\beta}\right)$$

For uncanted vanes, $\alpha = 90°$, resulting in the following:

$$b = c\beta \qquad z_1 = 0$$
$$a = s\beta \qquad r_1 = r_o + \ell_o \qquad (5\text{-}33)$$
$$A = \frac{\pi}{2}$$

The averaged torques become:

$$\vec{N}_r^{av} = K_r\left[-\vec{i}_K(s\beta c^2\beta r_1)s\theta c\theta + \vec{k}_K(s\beta c^2\beta + s\beta(\tfrac{1}{2} - \tfrac{3}{2}c^2\beta)s^2\theta)r_1\right]$$
$$\vec{N}_a^{av} = K_a\left[\vec{i}_K(-\tfrac{r_1}{2}s\beta c\theta s\theta) + \vec{k}_K(\tfrac{r_1}{2}s\beta s^2\theta)\right] \qquad (5\text{-}34)$$
$$\vec{N}_{rr}^{av} \simeq C_r\left[\vec{k}_K r_1 s\beta c\theta\right]$$

where $K_r \equiv \text{Area}(1-\text{emiss})\frac{2I}{C}$ and $K_a \equiv \text{Area}\cdot\text{abs.}\cdot\frac{I}{C}$

Thus for uncanted sails ($\alpha = 90°$) there is no precession torque, as desired. The total erecting and spin torques produced are:

$$N_Y^{AV} = -s\beta\left[K_r c^2\beta r_1 s\theta c\theta + \frac{K_a}{2} r_1 c\theta s\theta\right] \qquad (5\text{-}35)$$

$$N_Z^{AV} = s\beta\left[K_r r_1 c^2\beta + r_1(\tfrac{1}{2} - \tfrac{3}{2}c^2\beta)K_r s^2\theta + \frac{K_a}{2} r_1 s^2\theta + C_r r_1 c\theta\right] \qquad (5\text{-}36)$$

Thus, a positive vane pitch ($\beta > 0$) results in a negative erecting torque and a positive spin torque, while the reverse occurs for $\beta < 0$. These "averaged" results can be used in studying the initial orientation phase when the spacecraft is spinning uniformly. For the steady-state phase, the sails are essentially stationary and hence

the full unaveraged equations must be used. Consider four vanes spaced 90° apart as shown below:

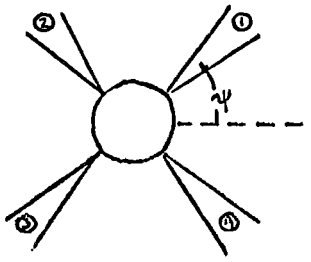

Thus: $\psi_{②} = \psi + \frac{\pi}{2}$

$\psi_{③} = \psi + \pi$

$\psi_{④} = \psi + \frac{3\pi}{2}$ (5-37)

Using the results of Appendix A and Equations (5-37):

Reflected torque:

$$\vec{N}_r(\psi) = K_r\left[s^2\theta(s^2\beta c^2\psi - c^2\beta) - 2s\theta c\theta s\beta c\beta c\psi + c^2\beta\right]\left\{\vec{\imath}_K(-r_1 c\beta s\psi) + \vec{\jmath}_K(r_1 c\beta c\psi) + \vec{k}_K r_1 s\beta\right\}$$
$$+ K_r\left[s^2\theta(s^2\beta s^2\psi - c^2\beta) + 2s\theta c\theta s\beta c\beta s\psi + c^2\beta\right]\left\{\vec{\imath}_K(-r_1 c\beta c\psi) + \vec{\jmath}_K(-r_1 c\beta s\psi) + \vec{k}_K r_1 s\beta\right\}$$
$$+ K_r\left[s^2\theta(s^2\beta c^2\psi - c^2\beta) + 2s\theta c\theta s\beta c\beta c\psi + c^2\beta\right]\left\{\vec{\imath}_K(r_1 c\beta s\psi) + \vec{\jmath}_K(-r_1 c\beta c\psi) + \vec{k}_K r_1 s\beta\right\} \quad (5\text{-}38)$$
$$+ K_r\left[s^2\theta(s^2\beta s^2\psi - c^2\beta) - 2s\theta c\theta s\beta c\beta s\psi + c^2\beta\right]\left\{\vec{\imath}_K(r_1 c\beta c\psi) + \vec{\jmath}_K(r_1 c\beta s\psi) + \vec{k}_K r_1 s\beta\right\}$$

Adding the components individually,

$$N^r_{x_①} + N^r_{x_③} = K_r\left[2s\theta c\theta s\beta c^2\beta s\psi c\psi r_1 + 2s\theta c\theta s\beta c^2\beta s\psi c\psi r_1\right] \quad (5\text{-}39)$$

$$N^r_{x_②} + N^r_{x_④} = K_r\left[-2s\theta c\theta s\beta c^2\beta s\psi c\psi r_1 - 2s\theta c\theta s\beta c^2\beta s\psi c\psi r_1\right] \quad (5\text{-}40)$$

$$\therefore N^r_x = 0 \quad (5\text{-}41)$$

$$N^r_{y_①} + N^r_{y_③} = K_r\left[-4r_1 s\theta c\theta s\beta c^2\beta c^2\psi\right] \quad (5\text{-}42)$$

$$N^r_{y_②} + N^r_{y_④} = K_r\left[-4r_1 s\theta c\theta s\beta c^2\beta s^2\psi\right] \quad (5\text{-}43)$$

$$\therefore N^r_y = K_r\left[-4r_1 s\theta c\theta s\beta c^2\beta\right] \quad (5\text{-}44)$$

$$N^r_{z_①} + N^r_{z_③} = K_r\left[2s^2\theta(s^2\beta c^2\psi - c^2\beta) + 2c^2\beta\right]r_1 s\beta \quad (5\text{-}45)$$

$$N^r_{z_2} + N^r_{z_4} = K_r\left[2s^2\theta\,(s^2\beta\, s^2\psi - c^2\beta) + 2c^2\beta\right] r_1 s\beta \tag{5-46}$$

$$\therefore\ N^r_z = K_r\left[2r_1 s^2\theta\, s^3\beta + 4 r_1 s\beta\, c^2\beta\, c^2\theta\right] \tag{5-47}$$

Absorbed torque:

$$\begin{aligned}\vec{N}_a(\psi) = {} & K_a\left[-s\theta s\beta c\psi + c\theta c\beta\right]\left\{\vec{\imath}_K(-r_1 c\theta s\psi) + \vec{\jmath}_K r_1 c\theta\, c\psi - \vec{k}_K r_1 s\theta\, c\psi\right\} \\ & + K_a\left[s\theta s\beta s\psi + c\theta c\beta\right]\left\{\vec{\imath}_K(-r_1 c\theta\, c\psi) - \vec{\jmath}_K r_1 c\theta\, s\psi + \vec{k}_K r_1 s\theta s\psi\right\} \\ & + K_a\left[s\theta s\beta c\psi + c\theta c\beta\right]\left\{\vec{\imath}_K(r_1 c\theta s\psi) - \vec{\jmath}_K r_1 c\theta\, c\psi + \vec{k}_K r_1 s\theta\, c\psi\right\} \\ & + K_a\left[-s\theta s\beta s\psi + c\theta c\beta\right]\left\{\vec{\imath}_K(r_1 c\theta\, c\psi) + \vec{\jmath}_K r_1 c\theta\, s\psi - \vec{k}_K r_1 s\theta s\psi\right\}\end{aligned} \tag{5-48}$$

Adding the individual components:

$$N^a_{x_1} + N^a_{x_3} = K_a\left[2r_1 s\theta\, c\theta\, s\beta\, s\psi\, c\psi\right] \tag{5-49}$$

$$N^a_{x_2} + N^a_{x_4} = K_a\left[-2r_1 s\theta\, c\theta\, s\beta\, s\psi\, c\psi\right] \tag{5-50}$$

$$\therefore\ N^a_x = 0 \tag{5-51}$$

$$N^a_{y_1} + N^a_{y_3} = K_a\left[-2r_1 s\theta\, c\theta\, s\beta\, c^2\psi\right] \tag{5-52}$$

$$N^a_{y_2} + N^a_{y_4} = K_a\left[-2r_1 s\theta\, c\theta\, s\beta\, s^2\psi\right] \tag{5-53}$$

$$\therefore\ N^a_y = K_a\left[-2r_1 s\theta\, c\theta\, s\beta\right] \tag{5-54}$$

$$N^a_{z_1} + N^a_{z_3} = K_a\left[2r_1 s^2\theta\, s\beta\, c^2\psi\right] \tag{5-55}$$

$$N^a_{z_2} + N^a_{z_4} = K_a\left[2r_1 s^2\theta\, s\beta\, s^2\psi\right] \tag{5-56}$$

$$\therefore\ N^a_z = K_a\left[2r_1 s^2\theta\, s\beta\right] \tag{5-57}$$

Reradiated torque:

$$\begin{aligned}\vec{N}_{rr}(\psi) = {} & C_r\left\{-s\theta\, s\beta\, c\psi + c\theta\, c\beta\right\}\left\{\vec{\imath}_K(-r_1 c\beta\, s\psi) + \vec{\jmath}_K(r_1 c\beta\, c\psi) + \vec{k}_K r_1 s\beta\right\} \\ & + C_r\left\{s\theta s\beta s\psi + c\theta c\beta\right\}\left\{\vec{\imath}_K(-r_1 c\beta\, c\psi) + \vec{\jmath}_K(-r_1 c\beta s\psi) + \vec{k}_K r_1 s\beta\right\} \\ & + C_r\left\{s\theta s\beta c\psi + c\theta c\beta\right\}\left\{\vec{\imath}_K(r_1 c\beta s\psi) + \vec{\jmath}_K(-r_1 c\beta\, c\psi) + \vec{k}_K r_1 s\beta\right\} \\ & + C_r\left\{-s\theta s\beta s\psi + c\theta c\beta\right\}\left\{\vec{\imath}_K(r_1 c\beta c\psi) + \vec{\jmath}_K(r_1 c\beta s\psi) + \vec{k}_K r_1 s\beta\right\}\end{aligned} \tag{5-58}$$

Adding individual componets:

$$N_{x_{①}}^{rr} + N_{x_{③}}^{rr} = C_r\{2r_1 s\theta\, s\beta\, c\beta\, s\psi\, c\psi\} \tag{5-59}$$

$$N_{x_{②}}^{rr} + N_{x_{④}}^{rr} = C_r\{-2r_1 s\theta\, s\beta\, c\beta\, s\psi\, c\psi\} \tag{5-60}$$

$$\therefore N_x^{rr} = 0 \tag{5-61}$$

$$N_{y_{①}}^{rr} + N_{y_{③}}^{rr} = C_r\{-2r_1 s\theta\, s\beta\, c\beta\, c^2\psi\} \tag{5-62}$$

$$N_{y_{②}}^{rr} + N_{y_{④}}^{rr} = C_r\{-2r_1 s\theta\, s\beta\, c\beta\, s^2\psi\} \tag{5-63}$$

$$\therefore N_y^{rr} = C_r\{-2r_1 s\theta\, s\beta\, c\beta\} \tag{5-64}$$

$$N_{z_{①}}^{rr} + N_{z_{③}}^{rr} = C_r\{2r_1 s\beta\, c\beta\, c\theta\} \tag{5-65}$$

$$N_{z_{②}}^{rr} + N_{z_{④}}^{rr} = C_r\{2r_1 s\beta\, c\beta\, c\theta\} \tag{5-66}$$

$$\therefore N_z^{rr} = C_r\{4r_1 s\beta\, c\beta\, c\theta\} \tag{5-67}$$

Note that four identical vanes, the resultant torques are:

$$N_x = 0 \tag{5-68}$$

$$N_y = K_r[-4r_1 s\theta\, c\theta\, s\beta\, c^2\beta] + K_a[-2r_1 s\theta\, c\theta\, s\beta] + C_r[-2r_1 s\theta\, s\beta\, c\beta] \tag{5-69}$$

$$N_z = K_r[2r_1 s^2\theta\, s^3\beta + 4r_1 s\beta\, c^2\beta\, c^2\theta] + K_a[2r_1 s^2\theta\, s\beta] + C_r[4r_1 s\beta\, c\theta] \tag{5-70}$$

Note that N_y and N_z are independent of ψ and that once again for a given pitch angle, β, the N_y and N_z produced are of opposite signs. Thus, for four identical vanes, it is impossible to control N_y and N_z independently. Actually the system is only required tobe able to generate all the four sign combinations of N_y and N_z: (1) $N_y>0, N_z>0$ (2) $N_y<0, N_z<0$, (3) $N_y>0, N_z<0$, (4) $N_y<0, N_z>0$. This would

allow control of sun pointing and roll independently. Note that with four identical sails only combinations (3) and (4) are possible. The solution to this problem is to use non-identical sails, sails with different absorption-reflection characteristics. The first configuration studied is shown in Figure 5.6 and consists of a pair of reflecting vanes, 2 and 4, and a pair of absorbing vanes, 1 and 3. All four vanes are assumed to be made of mylar, aluminized on one side with absorptivity = 0.2 and emissivity = 0.05, black on another side with absorptivity = emissivity = 0.9. The reflecting vanes show the aluminized face to the sun whereas the absorbing vanes are just reversed. Using these values and the equations derived above, the roll and erecting torques produced by these two pairs of vanes are plotted (Figures 5.7 and 5.8) versus their lengths, l, with their pitch angles, β, as a parameter. Note that for any given length, the erecting torque produced by the absorbing vanes is only a little smaller than that produced by the reflecting vanes; however, the roll torque produced by 1 and 3 is much smaller than that produced by 2 and 4. Thus it seems possible to choose $l_{13} > l_{24}$ such that all four combinations of total torques can be generated:
(1) $N_Y > 0$, $N_Z > 0$ (for $\beta_{13} < 0, \beta_{24} > 0$); (2) $N_Y < 0$, $N_Z < 0$

($\beta_{13}>0$, $\beta_{24}<0$); (3) $N_Y>0$, $N_Z<0$ ($\beta_{13}<0$, $\beta_{24}<0$); and (4) $N_Y<0$, $N_Z<0$ ($\beta_{13}>0$, $\beta_{24}>0$). The only other requirement is that $N_Y \gtrsim 4.8$ dyne-cm for stability as shown in Equation (5-30). Considering only the torques produced (shadowing and exposure of backs of vanes are not considered here), the optimum pitch angles are $\beta_{13}= \pm 80°$ and $\beta_{24}= \pm 35.26°$. Thus, for example, the following choices of vane dimensions are possible:

($\beta_{13} = -80°$, $\beta_{24} = 35.26°$, $\Theta = 5°$, $\Psi = 45°$)

ℓ_{13}(cm.)	ℓ_{24}	N_Y (dyne-cm)	N_Z
250	165	3.3	13.4
230	130	3.35	3.0
260	170	3.8	14.0
260	160	4.3	9.0

Note that for all the above choices, $N_Y(\Theta=5°)<4.8$ dyne-cm, thus the maximum equilibrium point will be greater than 5°.

Looking back at the torque equations derived above, for example (5-39) and (5-40), it is obvious that for four unidentical vanes, the precession torques do not cancel resulting in a net N_X which is undesirable from a sensing viewpoint as discussed earlier. To circumvent this difficulty, consider the configuration shown in Figure 5.9. Note that we now have four identical vanes,

each composed of a reflecting and an absorbing part. The diagram of a single vane shows how the design allows rotation of the two sections independently of each other. Note that the absorbing portion is now trapezoidal in shape. The center of pressure for a trapezoid is:

$$\ell_{cp} = \frac{h(2a + b)}{3(a + b)} \qquad (5\text{-}71)$$

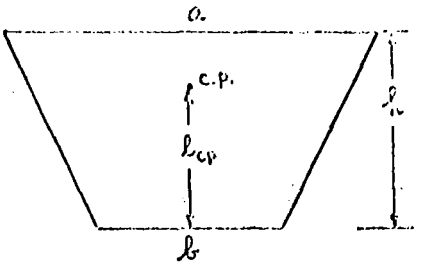

Using this result and the above torque equations for four identical vanes, (5-68), (5-69), and (5-70):

$$N_x = 0$$

The following table shows the results for the most acceptable values of ℓ_{24} and h and the corresponding N_y and N_z.

($\beta_{13} = -80°$, $\beta_{24} = 35.26°$, $\theta = 5°$)

ℓ_{24} (cm.)	Area$_{24}$ (cm^2)	h	Area$_{13}$	N_y	N_z (dyne-cm.)
120	.180	120	.270	2.45	11.56
120	"	130	.301	3.12	10.00
120	.180	150	.366	4.63	6.52
"	"	160	.400	5.47	4.58
130	.211	130	.317	3.11	14.36

ℓ_{24}	$Area_{24}$	ℓ_{13}	$Area_{13}$	N_Y	N_Z
130	.211	140	.350	3.89	12.55
"	"	150	.384	4.73	10.61
"	"	160	.420	5.64	8.53
140	.245	120	.300	2.25	21.32
"	"	130	.333	3.04	19.52
"	"	140	.367	3.88	17.58
"	"	150	.403	4.78	15.50

For example, if we choose ℓ_{24} = 140 cm and ℓ_{13} = 140 cm, then the torques produced by the vanes at θ = 5° are:

β_{24} \ β_{13}	+ 80°	- 80°
+ 35.26°	N_Y = -10.62 N_Z = 51.01	N_Y = 3.88 N_Z = 17.88
-35.26°	N_Y = -3.88 N_Z = -17.58	N_Y = 10.62 N_Z = -51.01

Note that for β_{13} = -80° the N_Y torque produced is always positive independent of β_{24}, and is negative for β_{13} = +80°. For β_{24} = 35.26°, the N_Z torque produced is positive independent of β_{13}, and is negative for β_{24} = -35.26°. Thus, it appears that this vane system meets all the torque production requirements and consequently allows "independent" control of roll and sun pointing.

5.5 Vane Control Scheme for Orientation and Stabilization

As discussed earlier, the expected initial conditions are:

$$\omega_{z_0} \simeq 200 \text{ r/min}$$

$$\theta_0 \simeq 60°$$

$$\theta'_0 \simeq 10°$$

The required end conditions are:

(1) Spacecraft z axis pointed within 10° of the sun, $2° \leq \theta \leq 10°$.

(2) Spacecraft x axis perpendicular to the ecliptic.

(3) 5000 r/min $\leq \Omega \leq 10^4$ r/min.

For design simplicity, it is assumed that the vanes pitch only between two fixed angles, that is, the reflecting vanes switch between $\pm 35.26°$ and the absorbing ones between $\pm 80°$. β_{y_2} is controlled to produce positive or negative erecting torque as needed to maintain θ between 2° and 10°, while β_{z_2} is controlled to produce positive or negative spin torque as needed to maintain wheel speed in the interval 5000 to 10^4 r/min. Specifically, in the steady state after initial orientation, β_{y_2} is switched to -80° whenever θ exceeds 10° to produce a positive erecting torque and hence reduce θ until it reaches 2° at which time β_{y_2} is switched to +80° to drive θ back up. Thus the motion limit cycles in θ between 2° and 10°. A

similar logic controls switching of the reflecting vanes so that the wheel spin rate cycles between 5000 and 10^4 r/min. In order to produce no precession torque, the sails are uncanted ($\alpha = 90°$).

For the initial orientation phase, it is assumed that a yo-yo device is employed to bring the spin rate down from its initial value of 200 r/min to about 2 r/min. From this point, further despin and sun pointing are accomplished with all vanes negatively pitched ($\beta_{1,3} = -80°$, $\beta_{2,4} = -35.26°$) to produce maximum erecting and despin torque. When ω_z reaches .3 r/min, the motor is activated to spin the wheel up, thus completely despinning the spacecraft body. Initial roll orientation is then accomplished such that the antenna rotation axis is perpendicular to the ecliptic. All this time, the spacecraft has been moving from its initial ϕ_0 to its steady state equilibrium position $\phi = 180°$ at a rate given by Equation (5-16):

$$\dot{\phi} = \omega_{is} \cot\theta \sin\phi \qquad (5\text{-}72)$$

When ϕ reaches 180°, $\dot{\phi} = 0$, and the motion reaches its steady state where the z axis limits cycle in the ecliptic between θ^{ss} and θ^{ss}.

A computer simulation was carried out using the described vane pitching scheme. The spacecraft configuration is shown in Figure 5.10. The following constants were used:

Vane dimensions: $\ell_{vv} = 140$ cm.

$h = 140$ cm.

The torque equations for the vanes system were put into the equations of motion and numerical integration was carried out to obtain the resulting motion.

$$\dot{\phi} = \omega_{is} \cos\theta \sin\phi \tag{5-73}$$

$$\dot{\theta} = -\frac{N_v}{C\Omega} - \omega_{is} \cos\phi \tag{5-74}$$

$$\dot{\Omega} = \frac{N_s}{C} \tag{5-75}$$

The results for the initial phase ($\dot{\phi} \neq 0$) for two different starting conditions are shown in Figure 5.11 and 5.12. They show that the initial despin from 2 r/min down to .3 r/min, can be expected to take about 5 days. At this point, the momentum wheel is activated and the antennas properly oriented. Note that at this stage in the motion, $\dot{\phi}$ is not yet zero in general, so that solar sensing is not an accurate roll orientation reference. In fact, the results show that "steady state" motion ($\phi = 180°$) is not reached until as much

as another fifteen days. Thus it seems that an RF uplink method for roll determination is very desirable because it would enable initial antenna orientation and roll up-dating during this stage. Although this method can be employed only about once a day, it is noted that $\dot{\phi}$ is quite small ($\lesssim 20°$/day) so that roll errors can never grow too large. Once the "steady state" ($\phi = 180°$) is reached, the spacecraft γ axis remains in the ecliptic plane and limit cycles between 2° and 10°. A typical motion is shown below:

TIME (days)	N_x	N_y (dyne-cm)	N_z	Ω (r/min)	ϕ	θ	β_{13} ($\pm 60°$)	β_{24} ($\pm 35.26°$)
36.3	0	5.91	-50.74	6500	180	2.77	-	-
36.8	0	5.95	-50.72	6000	180	2.55	-	-
37.0	0	4.99	-50.71	5500	180	2.34	-	-
37.2	0	4.54	-50.69	5000	180	2.13	-	-
37.4	0	4.09	-50.68	4500	180	1.92	+	-
37.6	0	-5.80	50.74	5000	180	2.72	+	+
37.8	0	-7.78	50.83	5500	180	3.65	+	+
38.0	0	-10.06	50.97	6000	180	4.73	+	+
38.2	0	-12.62	51.17	6500	180	5.95	+	+
38.4	0	-15.47	51.45	6830	180	7.32	+	+
38.6	0	-18.57	51.82	7330	180	8.83	+	+
38.8	0	-21.92	52.31	7830	180	10.48	+	+
39.0	0	7.83	15.23	8000	180	10.22	-	+

TIME	N_x	N_y	N_z	Ω	ϕ	Θ	β_{13}	β_{24}
39.2	0	7.65	15.37	8170	180	9.98	-	+
39.4	0	7.48	15.50	8330	180	9.76	-	+
39.6	0	7.33	15.62	8500	180	9.56	-	+
39.8	0	7.19	15.72	8500	180	9.37	-	+
40.0	0	7.07	15.81	8670	180	9.20	-	+
40.2	0	6.95	15.90	8830	180	9.04	-	+
40.4	0	6.84	15.97	9000	180	8.90	-	+
40.6	0	6.75	16.04	9170	180	8.77	-	+
40.8	0	6.66	16.10	9340	180	8.65	-	+
41.0	0	6.58	16.16	9500	180	8.54	-	+
41.2	0	6.50	16.21	9670	180	8.44	-	+
41.4	0	6.44	16.25	9670	180	8.36	-	+
41.6	0	6.38	16.29	9840	180	8.28	-	+
41.8	0	6.32	16.32	10,000	180	8.20	-	+
42.0	0	16.00	-51.51	9500	180	7.58	-	-
42.2	0	14.75	-51.37	9170	180	6.97	-	-
42.4	0	13.56	-51.26	8670	180	6.40	-	-

Note that the vanes are switched only about once every three or four days.

There are several possible modifications to the above control scheme. First, note that β_{13} is almost always pitched at -80° to maintain sun pointing; +80° is used only when θ goes below 2°. Thus if the vanes were designed such that θ^{*} is always greater than 2° but less than 10°, the absorbing vanes could be fixed at -80° to always produce

a positive erecting torque. In this case, the equilibrium position would cycle between θ^{*} and $\theta^{**} \sim 20^{*}$ as the wheel speed varies between its minimum and maximum values. With such a scheme, however, we essentially lose direct contol of θ .

Another modification is possible to reduce the time required for initial despin and sun pointing. Using vanes, it takes about five days for the spacecraft to despin and erect from initial conditions $\omega_z = 2$ r/min and $\theta = 60°$ to $\omega_z = .3$ r/min and $\theta \approx 10°$. During this period, the antennas are unoriented and hence signal strength at earth would be very irregular. Thus it is desirable to minimize the duration of this phase. This can be accomplished by using actively pitched thrusters which achieve both despin and sun pointing as described in Chapter 4. Because the thrusters can provide much larger torques, this initial period may be reduced to less than one day. Of course, this method would incur a penalty of additional weight and complexity.

The above control scheme was formulated only under the conditions imposed by the yagi antennas, thus the results found are for a specific set of requirements and hence tend to mask the generality of the solution. For example, θ was allowed to cycle within the interval 2° to 10° because the beamwidth of the antenna ($\sim 47°$) allows it.

However, on board experiments may require that sun pointing be maintained within much smaller tolerances, say between 2° and 3°. This would simply entail more frequent switching of the absorbing vanes. In fact, if the vanes could be varied in pitch continuously, it is theoretically possible to maintain θ constant.

5.6 Disturbances to the Motion

Disturbances stem from three principal causes: (1) error torques, (2) antenna rotation, and (3) micrometeoritic impact.

Small errors in N_y and N_z are not critical to the motion; however, precession error torques resulting in a net $N_x \neq 0$ will cause the spacecraft equilibrium position to move out of the ecliptic plane ($\phi = 180°$) to some ϕ^* given by

$$\sin \phi^* = - \frac{N_x}{C \Omega \omega_{is} \cos \theta} \qquad (5\text{-}76)$$

Of course N_x will normally be much smaller than $C \Omega \omega_{is} \cos \theta$ so that ϕ^* will be close to 180°. For example for a net N_x of .5 dyne-cm., the resulting equilibrium position is:

$$\phi^* \simeq 187°$$

With the given antenna beamwidth, an error of 7° is quite acceptable. This error would not be detected by the sun

sensor; however, by using the RF uplink phase comparison method approximately once every day to "update" roll orientation, this error can effectively be eliminated.

If the antennas are controlled by a signal from earth which commands antenna rotation by small incremental steps every several days, a small doublet impulse reaction torque will be exerted on the spacecraft at each rotation. Because there is no net torque, the spacecraft angular momentum remains constant and the resulting motion is a small nutation which is quickly damped out.

The angular momentum imparted to the spacecraft due to impact with a meteoritic particle of mass m having velocity $\vec{v}$ is

$$\Delta\left[\vec{H}\right] = \vec{\ell}_m \times \left[\Delta\left(m\vec{v}\right)\right] \tag{5-77}$$

In most cases, the effect is negligible, showing up as a tiny nutation which the damper eliminates. In the unlikely case that a very large torque disturbance occurs which actually causes the angular momentum vector to move from its equilibrium point, the motion will return, albeit slowly, to the equilibrium position in the ecliptic.

5.7 Engineering Considerations

This thesis has been almost entirely concerned with the theoretical aspects of the problem, while the ultimate test of any design is its engineering applicability. Actually, this consideration was kept in mind throughout so that the final configuration requires no engineering technology beyond present day capabilities. The momentum wheel system, for example, is certainly a proven concept.

Perhaps one of the most critical engineering problems in any long duration mission is that of bearings. Despite much work in this area, rotating bearings subject to the space environment remain a serious source of failure. The only continuous bearing required in this configuration is that for the momentum wheel. However, since it is contained within the spacecraft, the entire system can be sealed and thus not subject to the space environment. The other two rotations required are those for the antennas through γ and the vanes through $\pm\beta$. Note that in neither case is continuous rotation necessary. For the antennas, a total rotation of about 270° relative to the spacecraft body is required to track earth from launch to superior conjunction. The vanes only need to rotate in pitch between $\pm\beta$ and hence the maximum required rotation is 160°. Thus, a true rotary joint is unnecessary. The motions can be accomplished by a single joint permitting a limited rotation, such as a flexible

spring driven by a thermally controlled bimetallic strip. Note that such a device has no parts in contact which move relative to each other and hence the problems of lubrication are eliminated.

Active thrusters, if they are to be used during the initial orientation period, present no difficulties. Much work has been done in the field of microthrusters (see reference 13); motors using subliming solid propellants can be made very small, lightweight, and simple.

So far, little mention has been made of the problems of deployment of the vanes and the antennas. The vanes can be deployed in the same manner as in the Sunblazer spacecraft where they are stored in a rolled configuration and then released. Deployment of the massive antennas present more of a problem. Although the spacecraft is spinning at a relatively high rate at deployment, this can still cause an appreciable disturbance to the motion if it is done very suddenly. Schemes in which deployment is slow and controllable have been investigated and shown to be feasible. Note that if the two yagi antennas are deployed synchronously, their reaction torques will tend to cancel and hence minimize disturbance to the spacecraft motion. Thus although further work must be done in this area, the problem of antenna deployment is not felt to be a critical one.

5.8 Conclusion

It is concluded that the dual spin, dual vanes configuration presents a highly satisfactory design which meets all the dynamic and attitude control requirements while retaining the features of engineering simplicity and low weight.

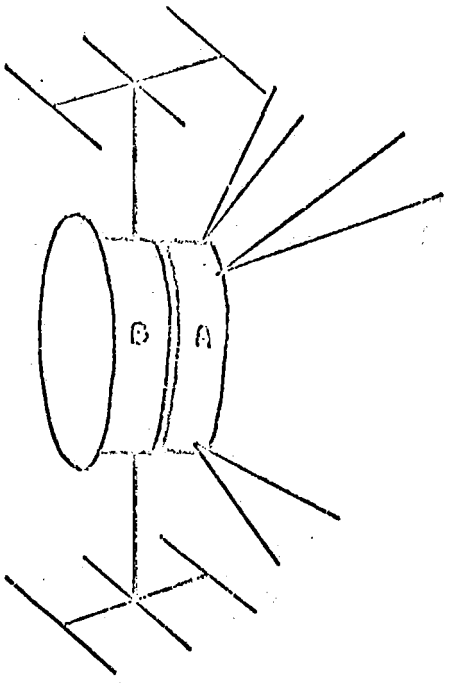

Figure 5.1 Two body dual spin system

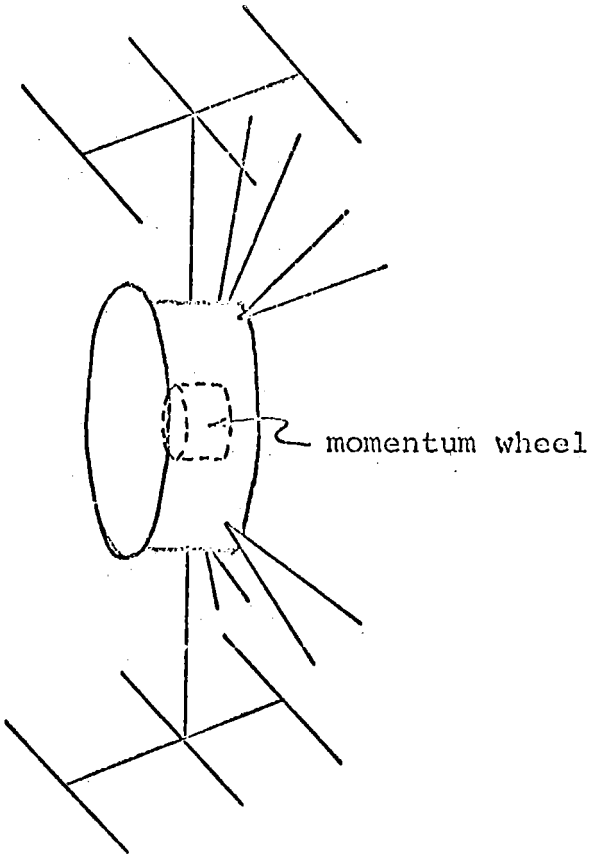

Figure 5.2 Momentum wheel system

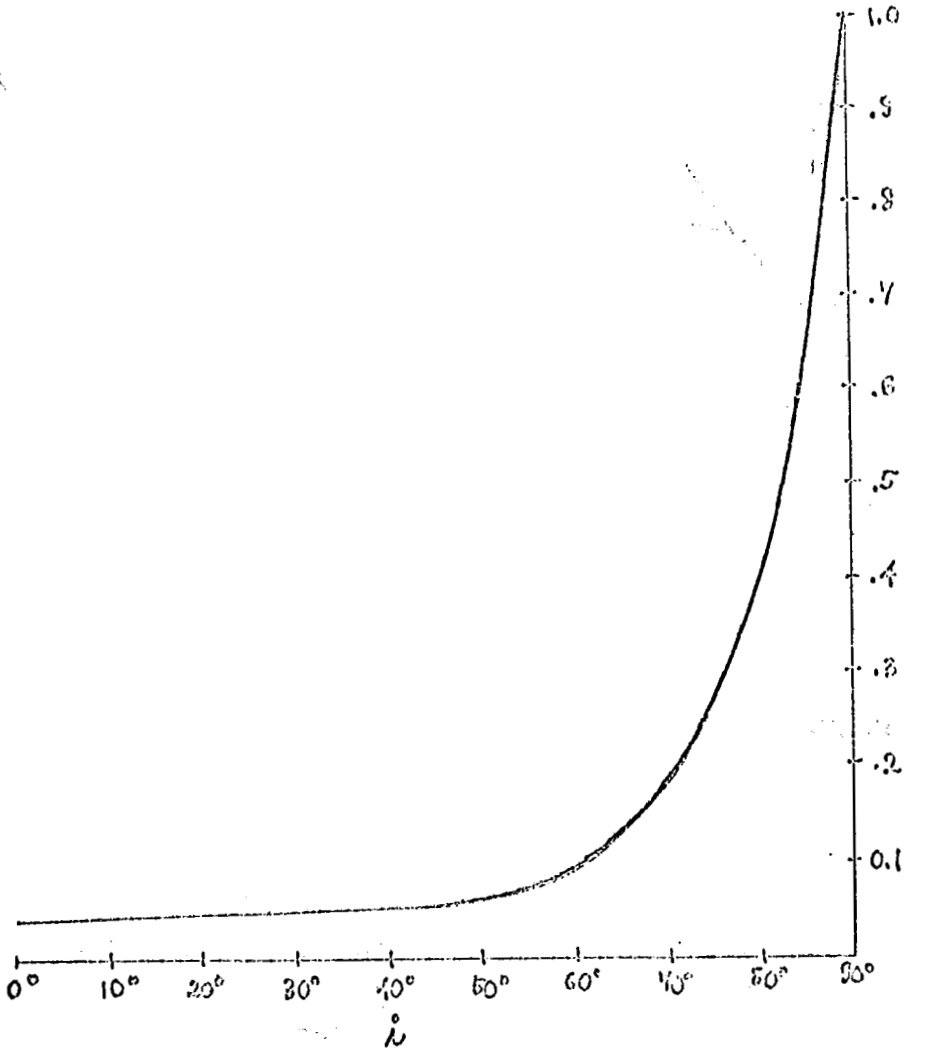

Figure 5.3 Intensity of reflected light as a function of the angle of incidence (n= 1.52)

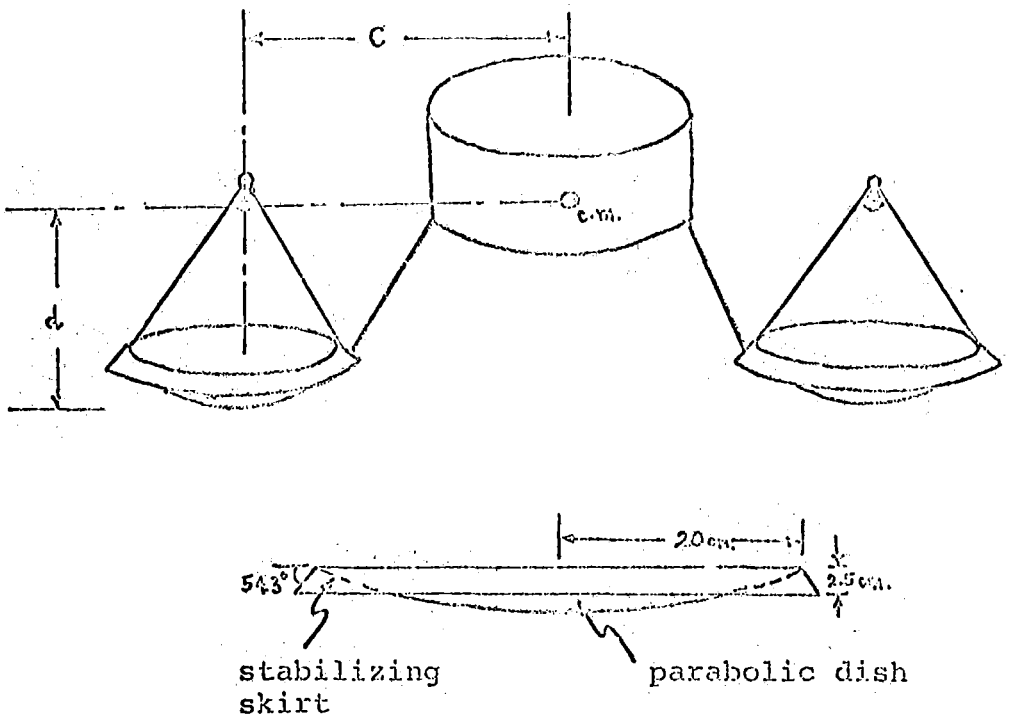

Figure 5.4 System for producing roll torques using light pipes

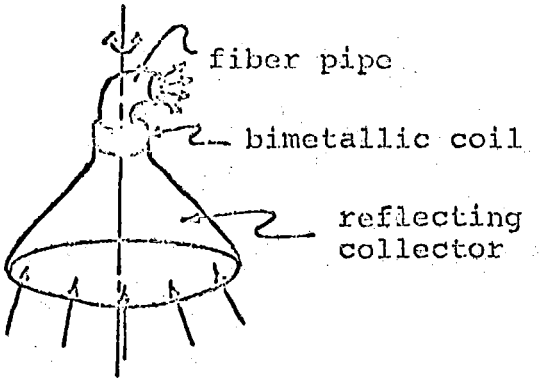

Figure 5.5 Rotating fiber pipe to produce +, -, or 0 roll torque

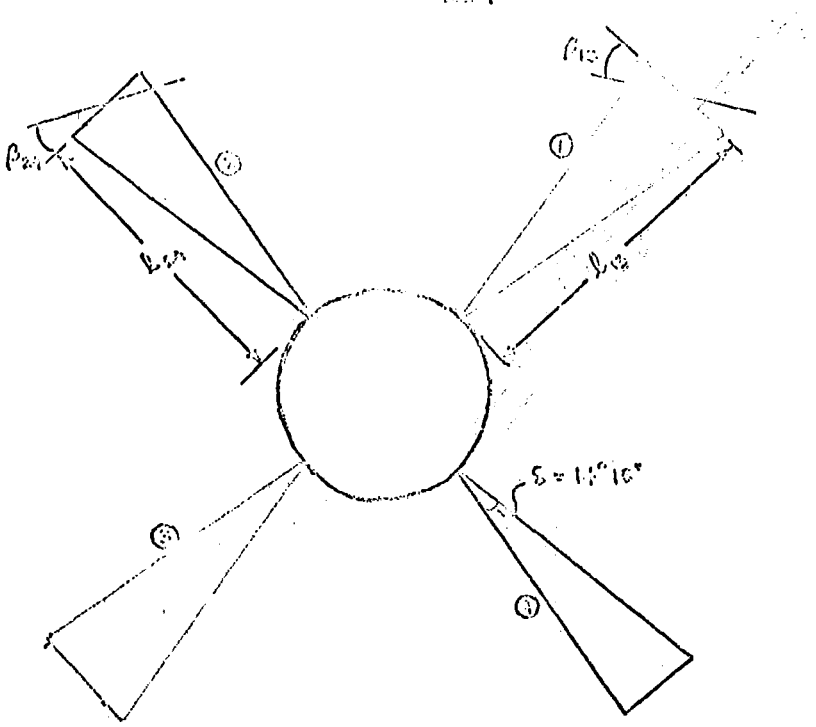

Figure 5.6 Configuration with pairs of reflecting and absorbing vanes

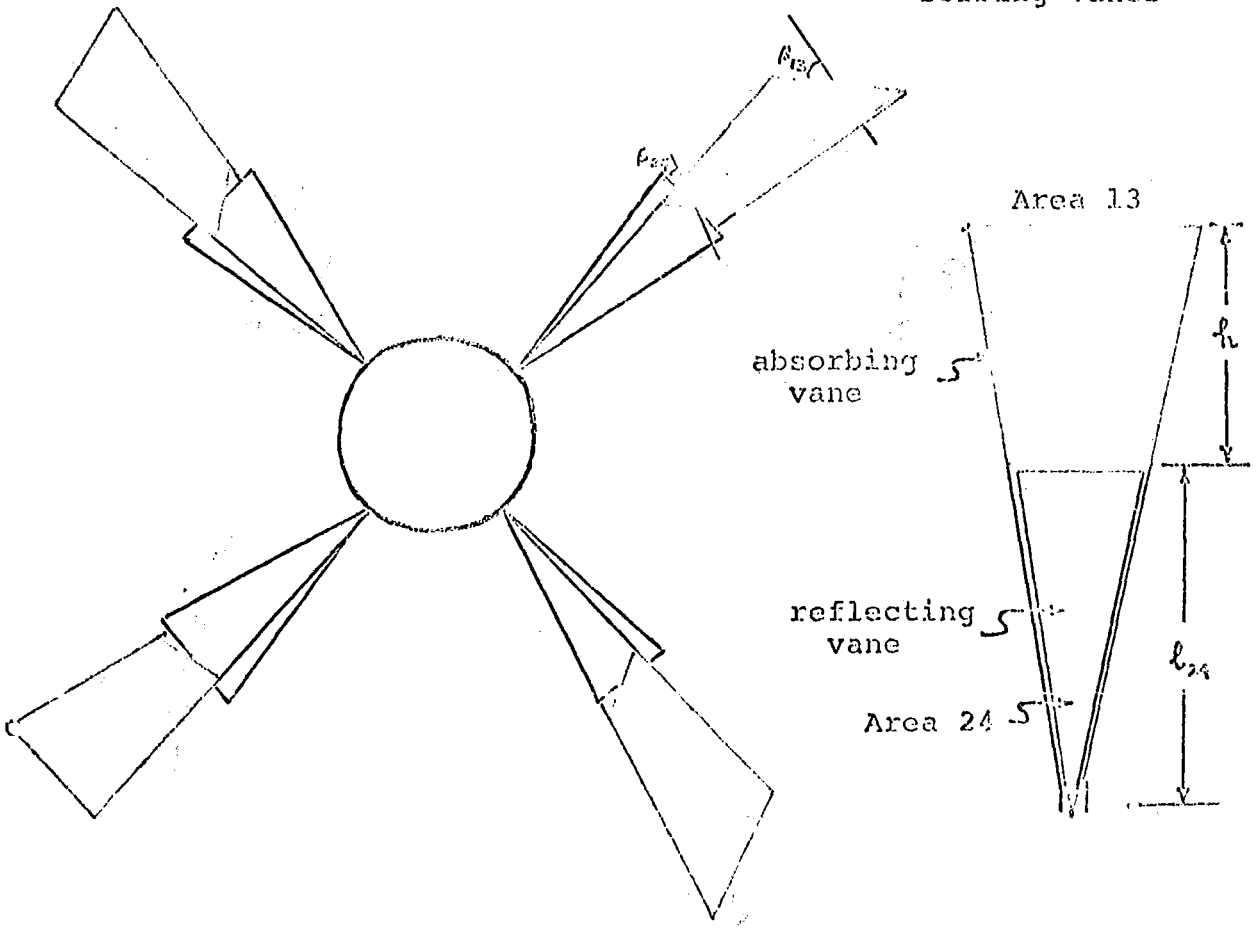

Figure 5.9 Dual vanes configuration

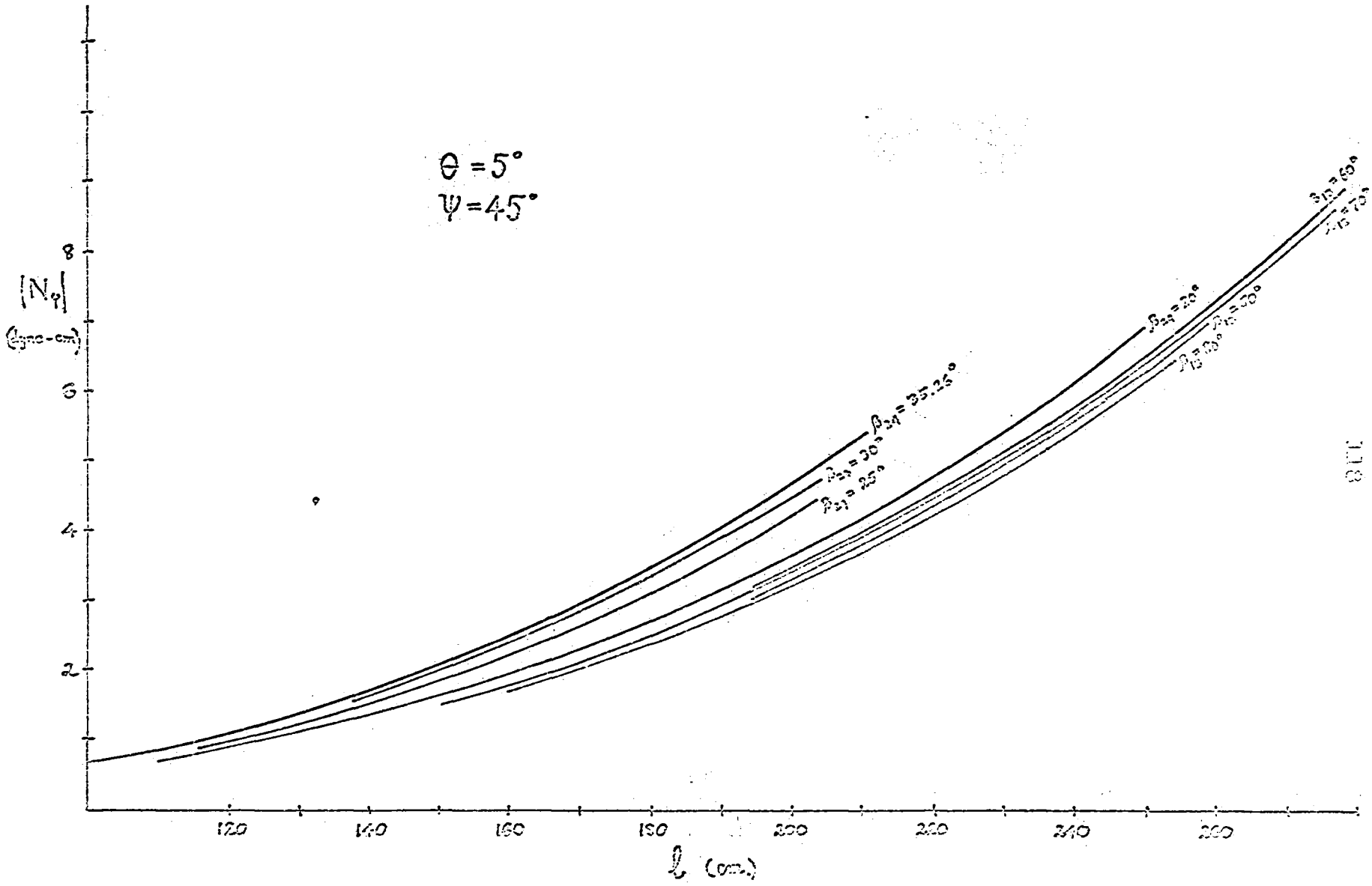

Figure 5.7 Erecting torques produced by absorbing and reflecting vanes versus length

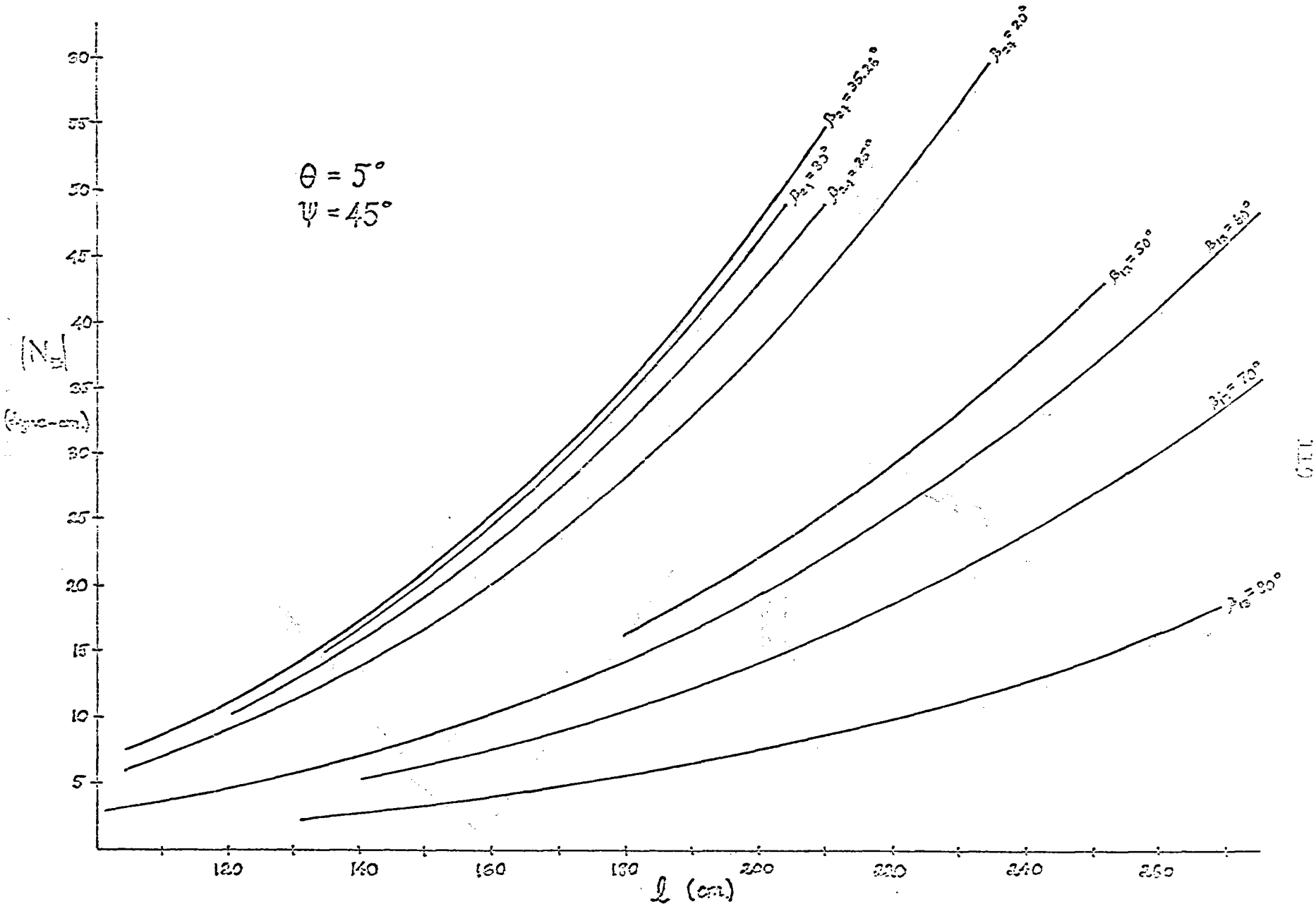

Figure 5.8 Spin torques produced by reflecting and absorbing vanes versus length

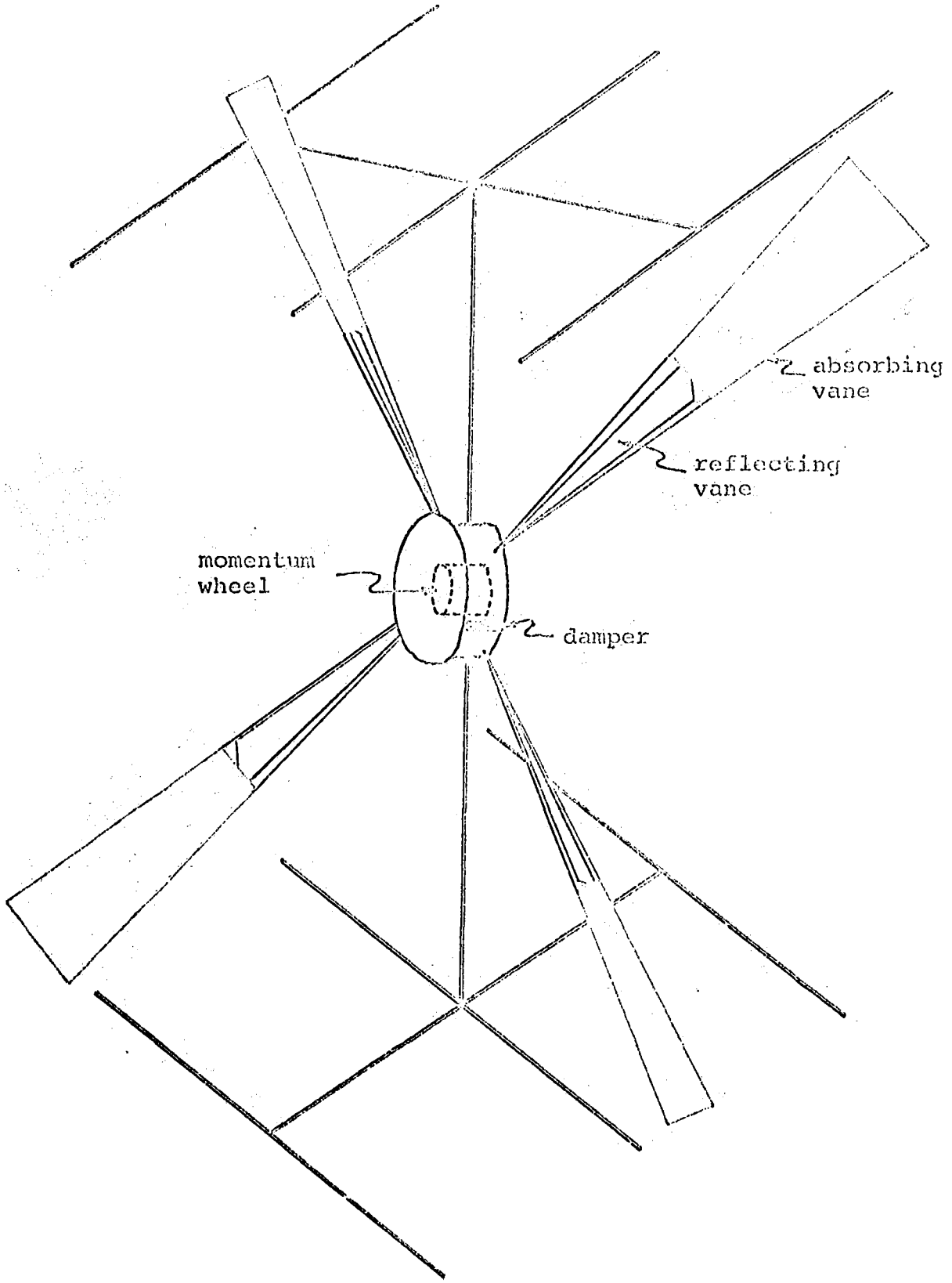

Figure 5.10 Dual spin dual vanes spacecraft configuration

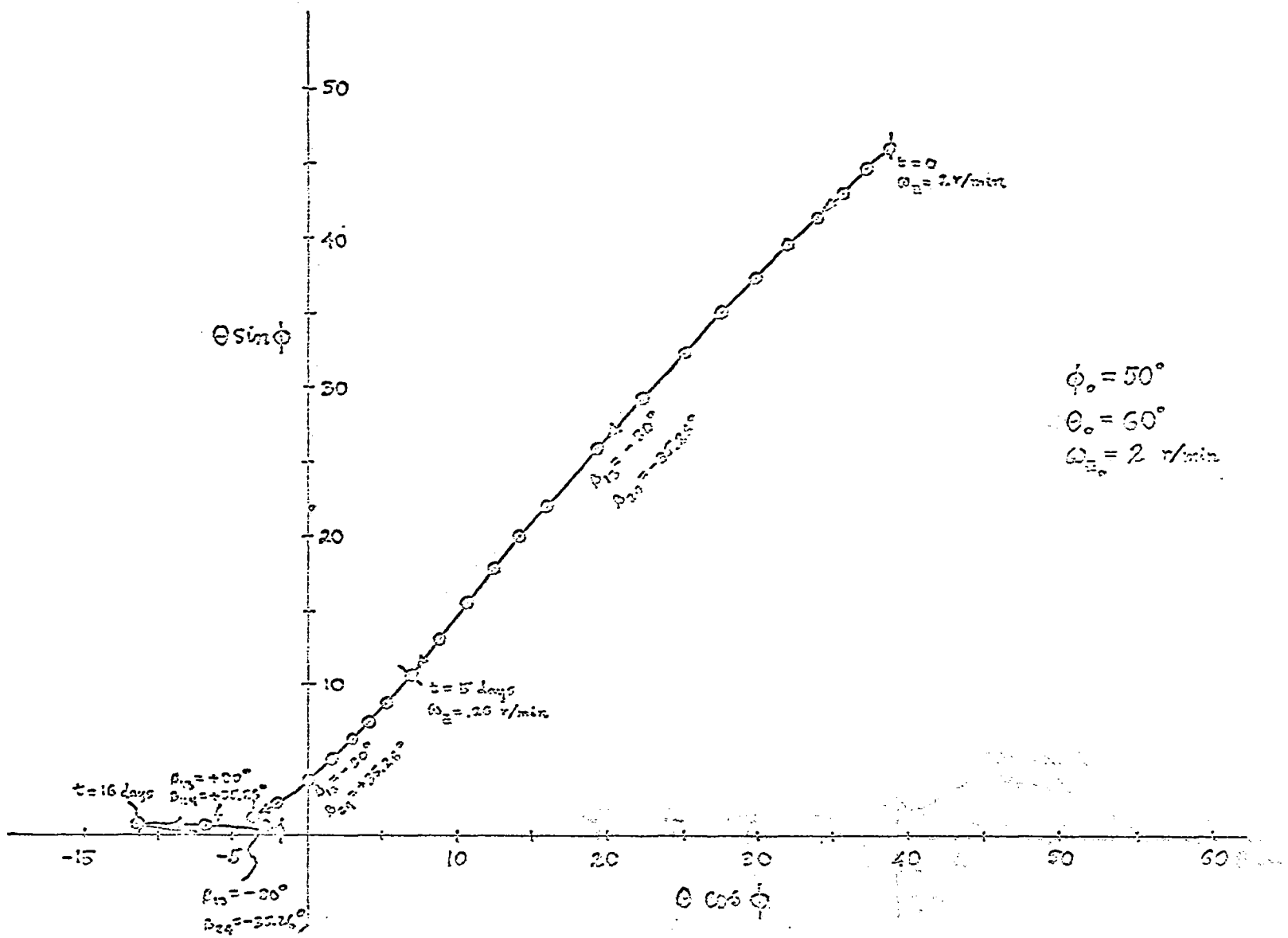

Figure 5.11 Initial orientation phase

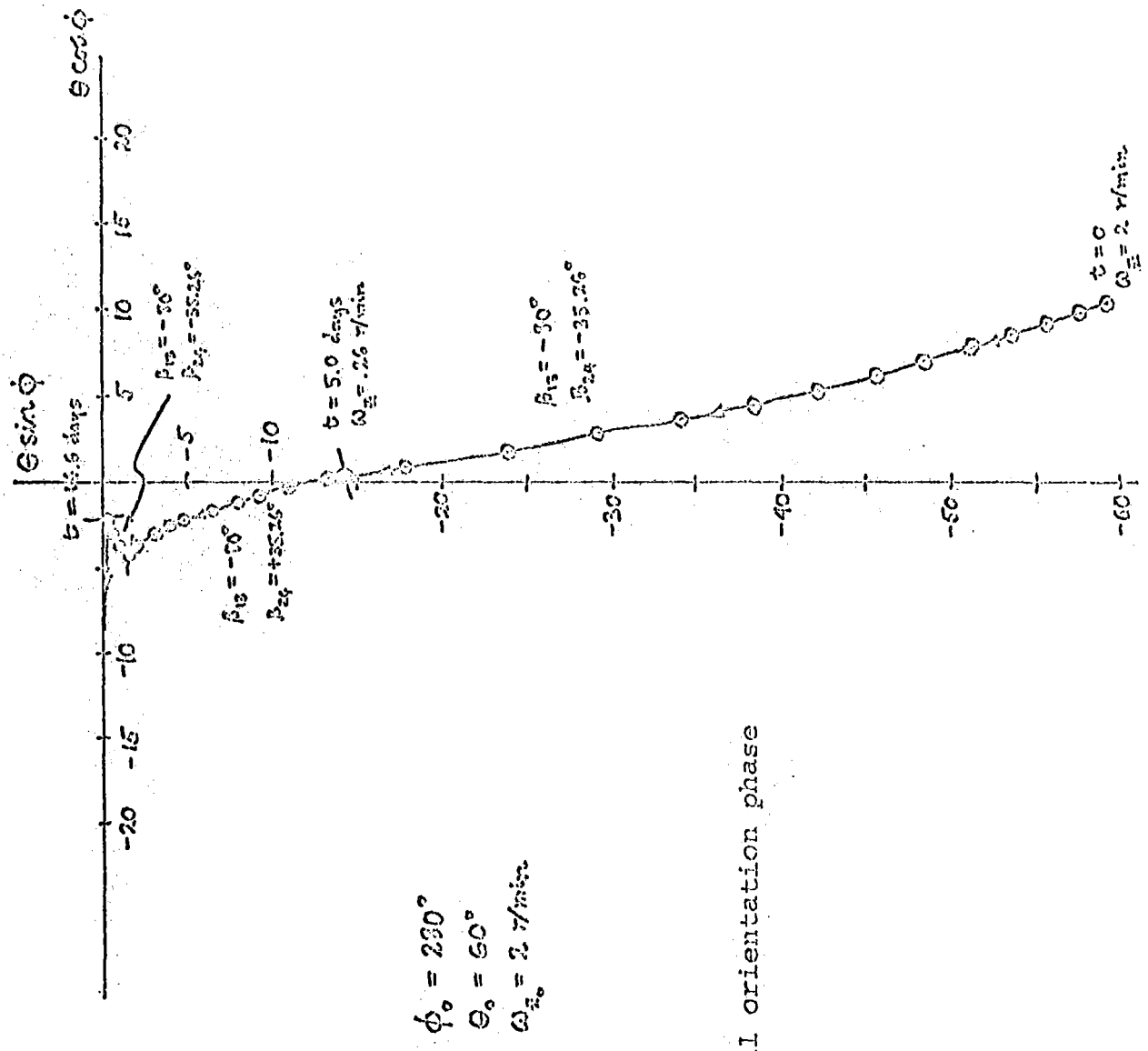

Figure 5.12 Initial orientation phase

CHAPTER 6

CONCLUSIONS AND RECOMMENDED FURTHER STUDIES

The main results of this study may be summarized as follows:

(1) For a non-precessing spacecraft, attitude sensing using only the solar radiation vector is sufficient.

(2) A completely despun spacecraft is undesirable for the following reasons: (a) difficulty in maintaining a stable despin at very low rates; (b) difficulty in sensing zero spin rate; (c) inherent sensitivity to torque disturbances.

(3) A dual spin configuration meets all the basic attitude control requirements. The spacecraft uses only solar radiation pressure for the generation of control torques. Specifically, a set of reflecting vanes are controlled in pitch to produce roll torques (positive and negative) while another set of absorbing vanes are controlled in pitch to produce erecting torques (positive or negative). The vanes are uncanted so that no precession torque is generated. The spacecraft uses only a sun sensor measurement of the Euler angles θ and ψ to determine its attitude. The precession angle ϕ is known because in the steady state the spacecraft equilibrium position is in the ecliptic plane ($\phi = 180°$). A back-up roll reference scheme using phase

comparison of an RF uplink provides roll sensing during the initial orientation phase and serves as an "updating" source to eliminate roll error build up due to sun sensor inaccuracies and error torques. The uplink also provides for ground control of antenna rotation. This entire configuration achieves full three-axis orientation and stabilization with minimum weight and complexity (it is surmised that the spacecraft will weight roughly 35 pounds more, due mainly to the massive antennas, than the Sunblazer configuration).

It is recommended that further studies be made in the following areas: (1) optimization of vane pitching scheme to minimize time to reach steady state equilibrium position; (2) more detailed analysis of the effects of torque disturbances to spacecraft motion; (3) deployment schemes for vanes and antennas; (4) analysis of the effects of shadowing of vanes and the exposures of backs of vanes at large Θ's; (5) analysis and design of the RF uplink phase comparison method for roll attitude determination.

APPENDIX A

VANE TORQUES

An analysis of solar pressure torques on four triangular vanes is contained in Reference 1, and is repeated here for convenience.

Solar radiation can be considered as a flux of momentum which is absorbed and reflected according to the laws of geometrical optics. The flux of momentum hitting the vane is proportional to the cosine of the angle between the normal to the vane and the incident radiation. Light striking the vanes causes a resultant force vector which has three physically distinct components: (1) a reflected momentum, normal to the vane $\vec{P}$; (2) an absorbed momentum component, in the direction of the incident radiation $\vec{I}$; and (3) a reradiated component, also normal to the vane $\vec{P}$. Define:

$\vec{P}$ = unit normal vector to vane

$\vec{I}_o$ = unit vector to sun

I = solar radiation intensity

C = velocity of light

α_{abs} = absorptivity of vane

ϵ_{miss} = emissivity of vane

α = cant angle of vane

β = pitch angle of vane

With these definitions, and with reference to Figure A.1:

$$\vec{P} = \vec{\imath}_K(c\alpha c\beta c\psi + s\beta s\psi) + \vec{\jmath}_K(c\alpha c\beta s\psi - s\beta c\psi) + \vec{k}_K(s\alpha c\beta) \tag{A-1}$$

or $$\vec{P} = \vec{\imath}_K a c\psi'' + \vec{\jmath}_K a s\psi'' + \vec{k}_K b \tag{A-2}$$

where $$a = \sqrt{1 - s^2\alpha c^2\beta} = \sqrt{1 - b^2} \tag{A-3}$$

$$b = s\alpha c\beta \tag{A-4}$$

$$\psi'' = \psi - A \tag{A-5}$$

$$A = \tan^{-1}\left(\frac{s\beta}{c\alpha \cdot c\beta}\right) \tag{A-6}$$

$$\vec{I}_o = \vec{\jmath}_K s\theta + \vec{k}_K c\theta \tag{A-7}$$

Using these expressions, the angle between the normal to the vane and the incident radiation is:

$$C(\theta) = \vec{P}\cdot\vec{I}_o = a s\theta s\psi'' + b c\theta \tag{A-8}$$

Using this cosine, the reflected and absorbed radiation pressure components are given by

$$\vec{F}_{\text{reflected}}(\psi'') = \text{Area}\cdot(1 - \text{emiss})\cdot\frac{2I}{C}\cdot(\vec{P}\cdot\vec{I}_o)^2\cdot(-\vec{P}) \tag{A-9}$$

$$\vec{F}_{\text{absorbed}}(\psi'') = \text{Area}\cdot\text{abs}.\cdot\frac{I}{C}\cdot(\vec{P}\cdot\vec{I}_o)\cdot(-\vec{I}_o) \tag{A-10}$$

For a reradiative force, resulting from a reradiated intensity I_R, assuming isotropic radiation according to

Lambert's law, the effective normal component of the intensity and force is given by:

$$I_N = I_R \frac{\int_0^{\frac{\pi}{2}} s\theta c^2\theta \, d\theta}{\int_0^{\frac{\pi}{2}} s\theta c\theta \, d\theta} = \frac{2}{3} I_R \qquad \text{(A-11)}$$

$$\underset{\text{reradiated}}{\vec{F}(\psi'')} = Area \cdot \frac{I_N}{C} \cdot (-\vec{P}) \qquad \text{(A-12)}$$

The torque produced by the vanes are then obtained by taking $\vec{r} \times \vec{F}$. Define:

$\vec{r}$ = vector from spacecraft center of mass to center of pressure of vane (A-13)

$$\vec{r} = \vec{\iota}_K r_1 c\psi + \vec{\jmath}_K r_1 s\psi - \vec{k}_K z_1 \qquad \text{(A-14)}$$

$$r_1 = r_o + \ell_o s\alpha \qquad \text{(A-15)}$$

$$z_1 = \ell_o c\alpha \qquad \text{(A-16)}$$

Thus:
$$\begin{aligned}\vec{P} \times \vec{r} = {} & \vec{\iota}_K \left[-(a z_1 + b r_1 cA) s\psi'' - b r_1 sA c\psi'' \right] \\ & + \vec{\jmath}_K \left[(a z_1 + b r_1 cA) c\psi'' - b r_1 sA s\psi'' \right] \\ & + \vec{k}_K r_1 s\beta\end{aligned} \qquad \text{(A-17)}$$

And from (A-8):

$$(\vec{P} \cdot \vec{I}_o)^2 = s^2\theta \left(a^2 s^2\psi'' - b^2 \right) + 2ba \, s\theta c\theta \, s\psi'' + b^2 \qquad \text{(A-18)}$$

Hence the reflected torque is:

$$\underset{\text{reflected}}{\vec{N}(\psi'')} = Area \cdot (1 - emiss) \cdot \frac{2I}{C} \cdot (\vec{P} \cdot \vec{I}_o)^2 \cdot (\vec{P} \times \vec{r}) \qquad \text{(A-19)}$$

where $(\vec{P}\cdot\vec{I}_o)^2$ and $(\vec{P}x\vec{r})$ are given by Equations (A-18) and (A-12) respectively.

The absorbed torque is:

$$\vec{N}(\psi)_{\text{absorbed}} = \text{Area}\cdot\text{abs}\cdot\frac{I}{c}\cdot(\vec{P}\cdot\vec{I}_o)\cdot(\vec{I}_o\times\vec{r}) \tag{A-20}$$

where, from (A-1) and (A-14):

$$\vec{I}_o\times\vec{r} = \vec{\imath}_K(-z_1 s\theta - r_1 co\, s\psi) + \vec{\jmath}_K(r_1 co\, c\psi) - \vec{k}_K r_1 s\theta\, c\psi \tag{A-21}$$

$$\vec{P}\cdot\vec{I}_o = s\theta\,(c\alpha\, c\beta\, s\psi - s\beta\, c\psi) + co(s\alpha\, c\beta) \tag{A-22}$$

The reradiated torque is given by:

$$\vec{N}(\psi)_{\text{rerad.}} = \frac{2}{3}\cdot\text{Area}\cdot\text{abs}\cdot\frac{I}{c}\cdot(\vec{P}\cdot\vec{I}_o)(\vec{P}\times\vec{r})\cdot\frac{(\text{emiss } 1 - \text{emiss } 2)}{(\text{emiss } 1 + \text{emiss } 2)} \tag{A-23}$$

where $\vec{P}.\vec{I}_o$ is given by (A-8); and using (A-1) and (A-14):

$$\begin{aligned}\vec{P}\times\vec{r} = {} & \vec{\imath}_K\{-z_1(c\alpha\, c\beta\, s\psi - s\beta\, c\psi) - r_1\, s\alpha\, c\beta\, s\psi\} \\ & + \vec{\jmath}_K\{r_1\, s\alpha\, c\beta\, c\psi + z_1(c\alpha\, c\beta\, c\psi + s\beta\, s\psi)\} \\ & + \vec{k}_K\{r_1 s\psi\,(c\alpha\, c\beta\, c\psi + s\beta\, s\psi) - r_1 c\psi\,(c\alpha\, c\beta\, s\psi - s\beta\, c\psi)\}\end{aligned} \tag{A-24}$$

For a system of four triangular vanes, the effective center of pressure of each vane is at a point 2/3 of the distance along the longitudinal axis of the triangular vane.

$$l_o = \frac{\int_o^l f\lambda^2\, d\lambda}{\int_o^l f\lambda\, d\lambda} = \frac{2}{3}l \tag{A-25}$$

Also, if the spacecraft is rotating uniformly and fast enough then we can average the torques for $0 < \psi < 2\pi$ thus eliminating the ψ dependence:

$$\vec{N}^{av}_{reflected} = \frac{1}{2\pi}\int_0^{2\pi} \vec{N}_{ref}(\psi'')\, d\psi'' \qquad \text{(A-26)}$$

$$= \text{Area}(1-\text{emiss}_2)\frac{2\pi}{C}\Big[-\vec{i}_K\big(s^2\alpha\, c\alpha\, c^2\beta\, r_1 + s\alpha c\beta(1-s^2\alpha c^2\beta)\tfrac{r_1}{2}\big)s\theta c\theta$$

$$-\vec{j}_K\big(s^2\alpha\, s\beta\, c^2\beta\, r_1\big)s\theta c\theta + \vec{k}_K\big(s^2\alpha s\beta c^2\beta + s\beta\big(\tfrac{1}{2\pi} - \tfrac{3}{2}s^2\alpha c^2\beta\big)s^2\theta\big)r_1\Big]$$

$$\vec{N}^{av}_{absorbed} = \frac{1}{2\pi}\int_0^{2\pi} \vec{N}_{ab}(\psi)\, d\psi \qquad \text{(A-27)}$$

$$= \text{Area}\cdot abs.\cdot\frac{I}{C}\Big\{\vec{i}_K\Big[-\tfrac{r_1}{2}s\alpha c\beta - \tfrac{r_1}{2}c\alpha c\beta\Big]s\theta c\theta + \vec{j}_K\Big[-\tfrac{r_1}{2}s\beta s\theta c\theta\Big]$$

$$+ \vec{k}_K\Big[\tfrac{r_1}{2}s\beta s^2\theta\Big]\Big\} \qquad \text{(A-28)}$$

$$\vec{N}^{av}_{rerad.} \simeq C_r\Big\{\vec{j}_K\Big[\tfrac{1}{2}(a\tfrac{r_1}{2}+b\tfrac{r_1}{2}cA)\frac{as\theta}{\left(\frac{\omega}{\omega_{opt}}+\frac{\omega_{opt}}{\omega}\right)}\Big] + \vec{k}_K\tfrac{r_1}{2}s\beta c\theta\Big\}$$

$$\text{(A-29)}$$

$$C_r = \frac{2}{3}\cdot\frac{I}{C}\cdot\text{Area}\cdot abs.\cdot\frac{(\text{emiss}_1-\text{emiss}_2)}{(\text{emiss}_1+\text{emiss}_2)}$$

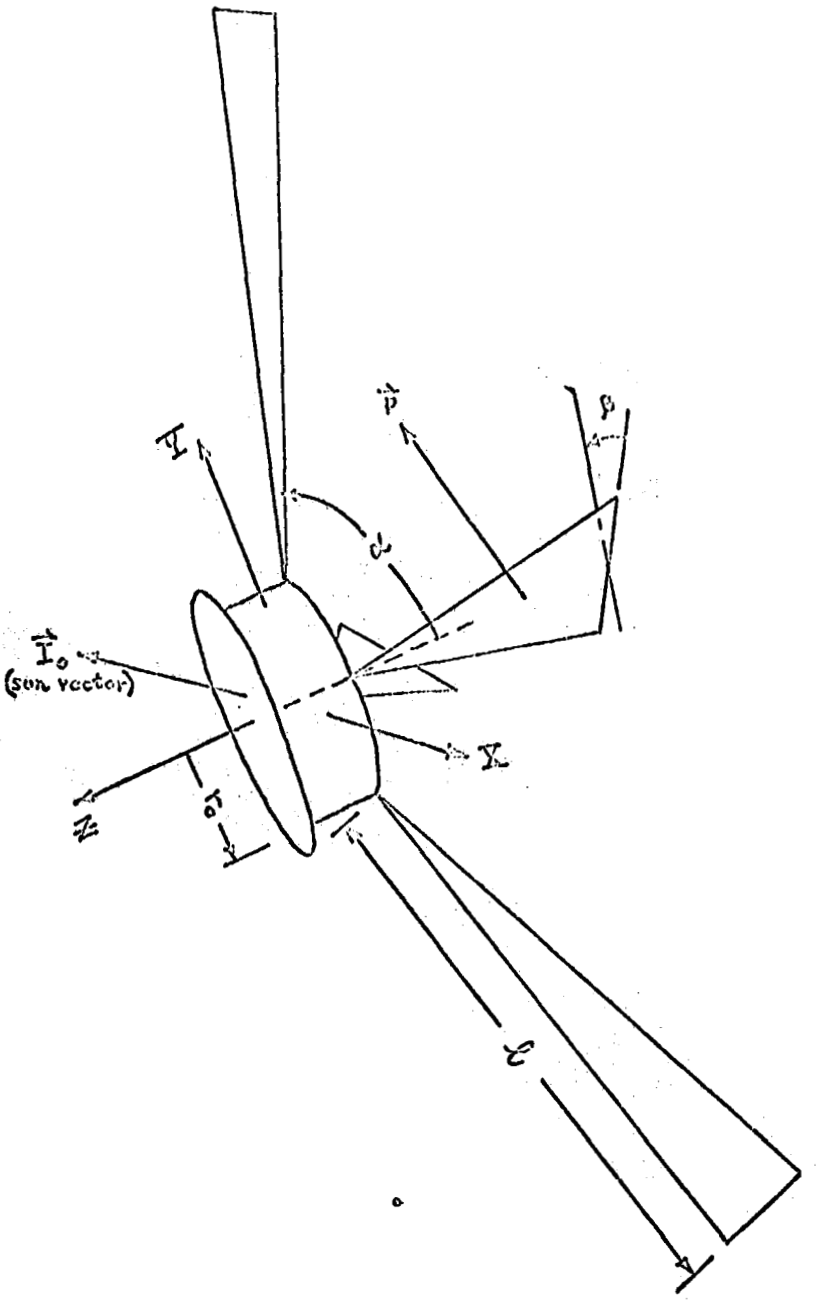

Figure A.1 Definition of spacecraft parameters

APPENDIX B

DUAL SPIN STABILITY

Nutational stability for the given spacecraft configuration will be investigated. From first principles the rotational equations of motion will be developed. In addition, two scalar equations describing the internal motion of the wheel and damper mass are found. A solution which satisfies this set of equations is established. Linearized variational equations about this solution are written, and a Routh stability analysis is used to determine stability of the solution.

Consider the dual spin spacecraft configuration shown in Figure B.1, consisting of the main asymmetric body "A", the internally contained symmetric momentum wheel "S", and a mass-spring-dashpot damper aligned with the spin axis. When the damper mass is in its neutral position (spring undeformed), the mass center of the total system defines the point 0, and m lies on the x axis. As the mass m moves a distance z in the $\mathcal{Y}$ direction, the system mass center, C, moves a distance $\bar{z}$ from 0 in the same direction, where

$$\bar{z} = \frac{m}{M} z = \mu z \qquad \text{(B-1)}$$

where M is the total system mass.

The basic equation of motion is:

$$\vec{N} = \dot{\vec{H}} \tag{B-2}$$

where a dot over a vector indicates rate of change with respect to inertial space. The angular momentum $\vec{H}$ is defined as:

$$\vec{H} = \int \vec{R} \times \dot{\vec{R}}\, dm \tag{B-3}$$

where $\vec{R}$ is the vector from the system mass center, C, to a differential mass element, dm.

$$\dot{\vec{R}} = \mathring{\vec{R}} + \vec{\omega}_{ib} \times \vec{R} \tag{B-4}$$

An over circle represents the time derivative in the body frame and $\vec{\omega}_{ib}$ is the angular velocity of the body frame with respect to inertial space. Since the only angular velocity that we will be interested in is $\vec{\omega}_{ib}$, the subscript will henceforth be dropped for convenience. Thus, Equation (B-3) becomes:

$$\vec{H} = \int \vec{R} \times (\vec{\omega} \times \vec{R})\, dm + \int \vec{R} \times \mathring{\vec{R}}\, dm \tag{B-5}$$

Since point C is moving with respect to the body fixed axes, it is more convenient to work with vectors relative to point 0. If $\vec{R}_o$ is the vector from C to 0, and $\vec{r}$ is the vector from 0 to the incremental mass,

$$\vec{R} = \vec{R}_o + \vec{r} \tag{B-6}$$

and $\vec{H}$ becomes:

$$\begin{aligned}\vec{H} &= \int (\vec{R}_o + \vec{r}) \times [\vec{\omega} \times (\vec{R}_o + \vec{r})]\, dm + \int (\vec{R}_o + \vec{r}) \times (\dot{\vec{R}}_o + \dot{\vec{r}})\, dm \\ &= \vec{R}_o \times \left[\vec{\omega} \times \int (\vec{R}_o + \vec{r})\, dm\right] + \int \vec{r} \times (\vec{\omega} \times \vec{r})\, dm \\ &\quad - (\vec{\omega} \times \vec{R}_o) \times \int \vec{r}\, dm + \vec{R}_o \times \frac{d}{dt_n} \int (\vec{R}_o + \vec{r})\, dm \\ &\quad - \dot{\vec{R}}_o \times \int \vec{r}\, dm + \int \vec{r} \times \dot{\vec{r}}\, dm\end{aligned} \tag{B-7}$$

From the definition of center of mass,

$$\int (\vec{R}_o + \vec{r})\, dm = \int \vec{R}\, dm = 0 \tag{B-8}$$

Hence,

$$\int \vec{r}\, dm = -M\vec{R}_o \tag{B-9}$$

Using (B-8) and (B-9) in (B-7):

$$\vec{H} = \int \vec{r} \times (\vec{\omega} \times \vec{r})\, dm + [\dot{\vec{R}}_o + \vec{\omega} \times \vec{R}_o] \times M\vec{R}_o + \int \vec{r} \times \dot{\vec{r}}\, dm \tag{B-10}$$

Recognizing that $\int \vec{r} \times (\vec{\omega} \times \vec{r})\, dm$ is simply the definition of $[\![] \cdot \vec{\omega}$ where $[\![]$ is the inertia diadic of the spacecraft with respect to the body axes system "b" centered at 0.

Also,

$$[\dot{\vec{R}}_o + \vec{\omega} \times \vec{R}_o] = \dot{\vec{R}}_o \tag{B-11}$$

Thus Equation (B-10) becomes

$$\vec{H} = [\![] \cdot \vec{\omega} + M\dot{\vec{R}}_o \times \vec{R}_o + \int \vec{r} \times \dot{\vec{r}}\, dm \tag{B-12}$$

Differentiating:

$$\dot{\vec{H}} = \dot{\mathbb{I}} \cdot \vec{\omega} + \mathbb{I} \cdot \dot{\vec{\omega}} + M\ddot{\vec{R}}_o \times \vec{R}_o + \frac{d}{dt_1}\int \vec{r} \times \dot{\vec{r}}\, dm \qquad \text{(B-13)}$$

Remembering that $$\dot{\mathbb{I}} \cdot \vec{\omega} = \mathring{\mathbb{I}} \cdot \vec{\omega} + \vec{\omega} \times (\mathbb{I} \cdot \vec{\omega}) \qquad \text{(B-14)}$$

And $$\ddot{\vec{R}}_o = \mathring{\ddot{\vec{R}}}_o + 2\vec{\omega} \times \mathring{\vec{R}}_o + \dot{\vec{\omega}} \times \vec{R}_o + \omega \qquad \text{(B-15)}$$

(B-13) becomes:

$$\dot{\vec{H}} = \vec{N} = \mathring{\mathbb{I}} \cdot \vec{\omega} + \mathbb{I} \cdot \dot{\vec{\omega}} + \vec{\omega} \times (\mathbb{I} \cdot \vec{\omega}) + M\left[\mathring{\ddot{\vec{R}}}_o + 2\vec{\omega} \times \mathring{\vec{R}}_o + \dot{\vec{\omega}} \times \vec{R}_o + \vec{\omega} \times (\vec{\omega} \times \vec{R}_o)\right] \times \vec{R}_o$$
$$+ \int \vec{r} \times \mathring{\ddot{\vec{r}}}\, dm + \vec{\omega} \times \int \vec{r} \times \mathring{\dot{\vec{r}}}\, dm \qquad \text{(B-16)}$$

Equation (B-16) is the general dynamical equation for a non-rigid body. To apply it to our case, the contribution of the three components A, S, and m must be found.

To evaluate the wheel contribution, let $\vec{c}$ be the vector from 0 to the wheel mass center C_s, and $\vec{\rho}$ be the vector from C_s to the individual wheel mass elements. Thus,

$$\vec{r} = \vec{c} + \vec{\rho} \qquad \text{(B-17)}$$

$$\mathring{\vec{r}} = \mathring{\vec{\rho}} \qquad \text{(B-18)}$$

The wheel contribution to the last term in (B-16) is:

$$\vec{\omega} \times \int_s \vec{r} \times \mathring{\dot{\vec{r}}}\, dm = \vec{\omega} \times \int_s \left[(\vec{c} + \vec{\rho}) \times \mathring{\dot{\vec{\rho}}}\right] dm$$
$$= \vec{\omega} \times \int_s \vec{\rho} \times (\vec{\omega}_{AS} \times \vec{\rho})\, dm \qquad \text{(B-19)}$$

where $\vec{\omega}_{AS}$ is the angular velocity of the wheel with respect to the body axes system "b". The above integral is simply the angular momentum, $\vec{h}_{AS}$, of the wheel with respect to the body. Thus (B-9) can be expressed as:

$$\vec{\omega} \times \int_S \vec{r} \times \mathring{\vec{r}}\, dm = \vec{\omega} \times \vec{h}_{AS} \tag{B-20}$$

Next, consider the wheel contribution to the term $\int \vec{r} \times \ddot{\vec{r}}\, dm$ in (B-16):

$$\begin{aligned} \int_S \vec{r} \times \ddot{\vec{r}}\, dm &= \frac{d}{dt_A} \int_S \vec{r} \times \mathring{\vec{r}}\, dm = \frac{d}{dt_A} \int_S (\vec{c} + \vec{\rho}) \times \mathring{\vec{\rho}}\, dm \\ &= \frac{d}{dt_A} \int_S \vec{\rho} \times \mathring{\vec{\rho}}\, dm \\ &= \mathring{\vec{h}}_{AS} \end{aligned} \tag{B-21}$$

Thus combining Equations (B-20) and (B-21), the total contribution of the rotor is:

$$\mathring{\vec{h}}_{AS} + \vec{\omega} \times \vec{h}_{AS} = \dot{\vec{h}}_{AS} \tag{B-22}$$

We can now rewrite the general Equation (B-16) for the case of a rigid body with K attached wheels and Q attached particles:

$$\begin{aligned} \vec{N} = {} & \mathring{[I]} \cdot \vec{\omega} + [I] \cdot \dot{\vec{\omega}} + \vec{\omega} \times [I] \cdot \vec{\omega} + M\left[\ddot{\vec{R}}_o + 2\vec{\omega} \times \mathring{\vec{R}}_o + \dot{\vec{\omega}} \times \vec{R}_o + \vec{\omega} \times (\vec{\omega} \times \vec{R}_o)\right] \times \vec{R}_o \\ & + \sum_{i=1}^{K} \dot{\vec{h}}_{AS} + \sum_{i=1}^{Q} m_i \left[(\vec{r}_i \times \ddot{\vec{r}}_i) + \vec{\omega} \times (\vec{r}_i \times \mathring{\vec{r}}_i)\right] \end{aligned} \tag{B-23}$$

For our particular configuration:

$$\vec{R}_o = \mu z \vec{k}_b \tag{B-24}$$

and,

$$\dot{\vec{R}}_o = \mu \dot{z} \vec{k}_b \qquad \ddot{\vec{R}} = \mu \ddot{z} \vec{k}_b \tag{B-25}$$

Thus the term involving $\vec{R}_o$ in Equation (B-23) becomes:

$$\begin{aligned} M[\ddot{\vec{R}}_o + 2\vec{\omega}\times\dot{\vec{R}}_o + \dot{\vec{\omega}}\times\vec{R}_o + \vec{\omega}\times(\vec{\omega}\times\vec{R}_o)]\times\vec{R}_o = \\ \vec{i}_b[\omega_y\omega_z\mu m z^2 - 2\omega_x\mu m z\dot{z} - \dot{\omega}_x\mu m z^2] \\ + \vec{j}_b[-\omega_x\omega_z\mu m z^2 - 2\omega_y\mu m z\dot{z} - \dot{\omega}_y\mu m z^2] \end{aligned} \tag{B-26}$$

Now to evaluate the last term of (B-23):

$$\begin{aligned} m[(\vec{r}\times\ddot{\vec{r}}) + \vec{\omega}\times(\vec{r}\times\dot{\vec{r}})] &= m(d\vec{j}_b + z\vec{k}_b)\times\dot{z}\vec{k}_b + m\vec{\omega}\times[(d\vec{j}_b + z\vec{k}_b)\times\dot{z}\vec{k}_b] \\ &= m(\vec{i}_b d\ddot{z} + \vec{j}_b\omega_z d\dot{z} - \vec{k}_b\omega_y d\dot{z}) \end{aligned} \tag{B-27}$$

Next, to evaluate the wheel term in (B-23):

$$\vec{h}_{AS} = C\Omega\vec{k}_b \tag{B-28}$$

where C is the wheel inertia about the spin axis, and Ω is the angular speed relative to the body A. Thus,

$$\dot{\vec{h}}_{AS} = C\dot{\Omega}\vec{k}_b + C\omega_y\Omega\vec{i}_b - C\omega_x\Omega\vec{j}_b \tag{B-29}$$

The inertia dyadic for the total system can be written out as:

$$
\begin{aligned}
I_{xx} &= I_x + mZ^2 \\
I_{yy} &= I_y + mZ^2 \\
I_{zz} &= I_z \\
I_{xy} &= I_{xz} = 0 \\
I_{yz} &= I^{\zeta}_{yz} - mdZ
\end{aligned}
\qquad \text{(B-30)}
$$

The single subscript and the superscript ζ indicate moments and products of inertia of the undeformed system (Z=0). Thus the inertia dyadic can be written as

$$
\begin{aligned}
\mathbb{I} = {} & (I_x + mZ^2)\vec{\tau}_b\vec{\tau}_b + (I_y + mZ^2)\vec{\gamma}_b\vec{\gamma}_b + (I^{\gamma}_{yz} - mdZ)\vec{\gamma}_b\vec{\kappa}_b + (I^{\gamma}_{yz} - mdZ)\vec{\kappa}_b\vec{\gamma}_b \\
& + I_z\vec{\kappa}_b\vec{\kappa}_b
\end{aligned}
$$

$$
\dot{\mathbb{I}} = 2mZ\dot{Z}\vec{\tau}_b\vec{\tau}_b + 2mZ\dot{Z}\vec{\gamma}_b\vec{\gamma}_b - md\dot{Z}\vec{\gamma}_b\vec{\kappa}_b - md\dot{Z}\vec{\kappa}_b\vec{\gamma}_b \qquad \text{(B-31)}
$$

Hence the terms involving $\mathbb{I}$ in Equation (B-23) can be written as:

$$
\begin{aligned}
& \dot{\mathbb{I}}\cdot\vec{\omega} + \mathbb{I}\cdot\dot{\vec{\omega}} + \vec{\omega}\times(\mathbb{I}\cdot\vec{\omega}) = \\
& \vec{\tau}_b\{2mZ\dot{Z}\omega_x + (I_x + mZ^2)\dot{\omega}_x + \omega_y^2(I^{\gamma}_{yz} - mdZ) + I_z\omega_y\omega_z - (I_y + mZ^2)\omega_y\omega_z \\
& \qquad - (I^{\gamma}_{yz} - mdZ)\omega_z^2\} \\
& + \vec{\gamma}_b\{2mZ\dot{Z}\omega_y - md\dot{Z}\omega_z + (I_y + mZ^2)\dot{\omega}_y + (I^{\gamma}_{yz} - mdZ)\dot{\omega}_z + \omega_x\omega_z(I_x + mZ^2) \\
& \qquad - \omega_x\omega_y(I^{\zeta}_{yz} - mdZ) - I_z\omega_x\omega_z\} \\
& + \vec{\kappa}_b\{-md\dot{Z}\omega_y + (I^{\gamma}_{yz} - mdZ)\dot{\omega}_y + I_z\dot{\omega}_z + (I_y + mZ^2)\omega_x\omega_y + (I^{\gamma}_{yz} - mdZ)\omega_x\omega_z \\
& \qquad - (I_x + mZ^2)\omega_x\omega_y\}
\end{aligned}
\qquad \text{(B-32)}
$$

Now, summing all the contributions from Equations (B-26), (B-27), (B-29), and (B-32) into the general equations of motion (B-23) and imposing the condition $\vec{N}=0$, we obtain three scalar equations from setting the $\vec{\imath}_b$, $\vec{\jmath}_b$, $\vec{k}_b$ components equal to zero individually:

$$I_x\dot{\omega}_x + (I_z - I_y)\omega_y\omega_z + C\omega_y\Omega + m(1-\mu)\bar{z}^2\dot{\omega}_x - m(1-\mu)\bar{z}^2\omega_y\omega_z + 2m(1-\mu)\bar{z}\dot{\bar{z}}\omega_x + md\ddot{\bar{z}} + (I^Y_{yz} - md\bar{z})\omega_y^2 - (I^S_{yz} - md\bar{z})\omega_z^2 = 0 \quad \text{(B-33)}$$

$$I_y\dot{\omega}_y + (I_x - I_z)\omega_x\omega_z - C\omega_x\Omega + m(1-\mu)\dot{\omega}_y\bar{z}^2 + m(1-\mu)\bar{z}^2\omega_x\omega_z + 2m(1-\mu)\bar{z}\dot{\bar{z}}\omega_y + (I^Y_{yz} - md\bar{z})\dot{\omega}_z - (I^Y_{yz} - md\bar{z})\omega_x\omega_y = 0 \quad \text{(B-34)}$$

$$I_z\dot{\omega}_z + C\dot{\Omega} + (I_y - I_x)\omega_x\omega_y - 2md\dot{\bar{z}}\omega_y + (I^Y_{yz} - md\bar{z})\dot{\omega}_y + (I^Y_{yz} - md\bar{z})\omega_x\omega_z = 0 . \quad \text{(B-35)}$$

Two more equations are necessary to completely specify the five unknowns $\omega_x, \omega_y, \omega_z, \Omega, \bar{z}$. These two additional equations come from the specification of the behavior of the wheel and damper mass. For the wheel:

$$C\dot{\omega}^S_z = L \quad \text{(B-36)}$$

where L is the spin moment applied to the wheel and is made up of the combination of bearing friction and motor torque.

$$\omega^S_z = \omega_z + \Omega \quad \text{(B-37)}$$

Therefore, (B-36) becomes:

$$C(\dot{\omega}_3 + \dot{\Omega}) = I_3 \tag{B-38}$$

Applying F = ma to the damper mass:

$$-f\dot{z} - kz = m\vec{k}_b \cdot \left[\frac{d^2}{dt_i^2}\left(d\vec{i}_b + z(1-\mu)\vec{k}_b\right)\right] \tag{B-39}$$

But

$$\frac{d}{dt_i}\left[d\vec{i}_b + z(1-\mu)\vec{k}_b\right] = \dot{z}(1-\mu)\vec{k}_b + \vec{\omega}\times\left[d\vec{i}_b + z(1-\mu)\vec{k}_b\right]$$

And

$$\begin{aligned}\frac{d^2}{dt_i^2}\left[d\vec{i}_b + z(1-\mu)\vec{k}_b\right] &= \ddot{z}(1-\mu)\vec{k}_b + \dot{\vec{\omega}}\times\left[d\vec{i}_b + z(1-\mu)\vec{k}_b\right] + 2\vec{\omega}\times\left[\dot{z}(1-\mu)\vec{k}_b\right] \\ &\quad + \vec{\omega}\times\left\{\vec{\omega}\times\left[d\vec{i}_b + z(1-\mu)\vec{k}_b\right]\right\} \\ &= \vec{i}_b\left\{\dot{\omega}_y z(1-\mu) - d\dot{\omega}_3 + 2\omega_y\dot{z}(1-\mu) + \omega_x\omega_y d + z(1-\mu)\omega_x\omega_3\right\} \quad \text{(B-40)} \\ &\quad + \vec{j}_b\left\{-z(1-\mu)\dot{\omega}_x - 2\omega_x\dot{z}(1-\mu) + z(1-\mu)\omega_y\omega_3 - d\omega_3^2 - \omega_x^2 d\right\} \\ &\quad + \vec{k}_b\left\{\ddot{z}(1-\mu) + d\dot{\omega}_x - z(1-\mu)\omega_x^2 - z(1-\mu)\omega_y^2 + d\omega_y\omega_3\right\}\end{aligned}$$

Hence,

$$\begin{aligned}m\vec{k}_b \cdot \left\{\frac{d^2}{dt^2}\left(d\vec{i}_b + z(1-\mu)\vec{k}_b\right)\right\} &= m\ddot{z}(1-\mu) + md\dot{\omega}_x - mz(1-\mu)\omega_x^2 \\ &\quad - mz(1-\mu)\omega_y^2 + md\omega_y\omega_3 \quad \text{(B-41)}\end{aligned}$$

Putting (B-41) into (B-39):

$$m(1-\mu)\ddot{z} + f\dot{z} + kz - m(1-\mu)(\omega_x^2 + \omega_y^2)z + md\omega_y\omega_3 + md\dot{\omega}_x = 0 \tag{B-42}$$

Equations (B-33), (B-34), (B-35), (B-38) and (B-42) comprise a set of five coupled equations in the five unknowns. Assuming the motor torque balances bearing

friction so that L = 0, these equations are satisfied by the solution

$$\omega_x = \omega_y = \omega_z = 0$$
$$\Omega = \Omega_s \qquad \text{(B-43)}$$
$$\dot{z} = 0$$

To establish necessary and sufficient conditions for the assymptotic stability of the solution, we construct the variational equations about this solution, linearize these equations in the variational coordinates, and subject them to a Routh stability analysis. The variational coordinates are represented by $\omega_x^*, \omega_y^*, \omega_z^*, z^*, \Omega^*$. Terms above the first degree in all these terms and their derivatives are dropped, resulting in the following equations:

$$I_x \dot{\omega}_x^* + C\Omega_s \omega_y^* + md\ddot{z}^* = 0 \qquad \text{(B-44)}$$

$$I_y \dot{\omega}_y^* - C\Omega_s \omega_x^* + I_{yz}^y \dot{\omega}_z^* = 0 \qquad \text{(B-45)}$$

$$I_z \dot{\omega}_z^* + C\dot{\Omega}_s^* + I_{yz}^y \dot{\omega}_y^* = 0 \qquad \text{(B-46)}$$

$$C(\dot{\omega}_z^* + \dot{\Omega}^*) = 0 \qquad \text{(B-47)}$$

$$m(1-\mu)\ddot{z}^* + f\dot{z}^* + kz^* + md\dot{\omega}_x^* = 0 \qquad \text{(B-48)}$$

Using (B-47) to eliminate $\dot{\omega}_z^*$:

$$I_x \dot{\omega}_x^* + C\Omega_s \omega_y^* + md\ddot{z}^* = 0 \qquad \text{(B-49)}$$

$$I_y \dot{\omega}_y^* - C\Omega_s \omega_x^* - I_{yz}^y \dot{\Omega}_s^* = 0 \tag{B-50}$$

$$-I_z \dot{\Omega}_s^* + C\dot{\Omega}_s^* + I_{yz}^z \dot{\omega}_y^* = 0 \tag{B-51}$$

$$m(1-\mu)\ddot{z}^* + f\dot{z}^* + kz^* + md\dot{\omega}_x^* = 0 \tag{B-52}$$

Using (B-51) to eliminate $\dot{\Omega}^*$:

$$I_x \dot{\omega}_x^* + C\Omega_s \omega_y^* + md\ddot{z}^* = 0 \tag{B-53}$$

$$I_y \dot{\omega}_y^* - C\Omega_s \omega_x^* - \frac{I_{yz}^{y2}}{I_z - C}\dot{\omega}_y^* = 0 \tag{B-54}$$

$$m(1-\mu)\ddot{z}^* + f\dot{z}^* + kz^* + md\dot{\omega}_x^* = 0 \tag{B-55}$$

Taking the Laplace transform, the equations can be written in matrix form as:

$$\begin{bmatrix} I_x s & C\Omega_s & md s^2 \\ -C\Omega_s & \left(I_y - \frac{I_{yz}^{y2}}{I_z - C}\right)s & 0 \\ md s & 0 & m(1-\mu)s^2 + fs + k \end{bmatrix} \begin{Bmatrix} \omega_x^* \\ \omega_y^* \\ z^* \end{Bmatrix} = \begin{Bmatrix} 0 \end{Bmatrix} \tag{B-56}$$

By expanding the determinant, the characteristic equation is found to be:

$$s^4\left(I_y - \frac{I_{yz}^{y2}}{I_z - C}\right)\left[I_x m(1-\mu) - m^2 d^2\right] + s^3\left[I_x\left(I_y - \frac{I_{yz}^{y2}}{I_z - C}\right)f\right]$$
$$+ s^2\left[I_x k\left(I_y - \frac{I_{yz}^{y2}}{I_z - C}\right) + m(1-\mu)C^2\Omega_s^2\right] + C^2\Omega_s^2 fs + C^2\Omega_s^2 k = 0 \tag{B-57}$$

Applying Routh's criteria, the coefficients must all be positive, thus:

$$I_y > \frac{I_{yz}^{y2}}{I_z - C}$$

$$I_x > \frac{md^2}{1-\mu}$$

To construct the Routhian array, first define

$$\gamma \equiv \left(I_y - \frac{I_{yz}^2}{I_z - C}\right) \tag{B-58}$$

$$h_o^2 \equiv C^2 \Omega_s^2 \tag{B-59}$$

The array becomes

$\gamma[I_x m(1-\mu) - m^2 d^2]$	$[I_x h \gamma + h_o^2 m(1-\mu)]$	$h_o^2 h_z$
$I_x \gamma f$	$h_o^2 f$	0
$\dfrac{I_x^2 \gamma h + m^2 d^2 h_o^2}{I_x}$	$h_o^2 h$	0
$\dfrac{h_o^4 f + m^2 d^2}{I_x^2 \gamma h + m^2 d^2 h_o^2}$	0	0
$h_o^2 h_z$	0	0

Thus the two necessary and sufficient conditions for stability are:

$$I_x > \frac{m d^2}{1-\mu} \tag{B-60}$$

$$I_y > \frac{I_{yz}^2}{I_z - C} \tag{B-61}$$

Both the conditions are always met for the given spacecraft configurations.

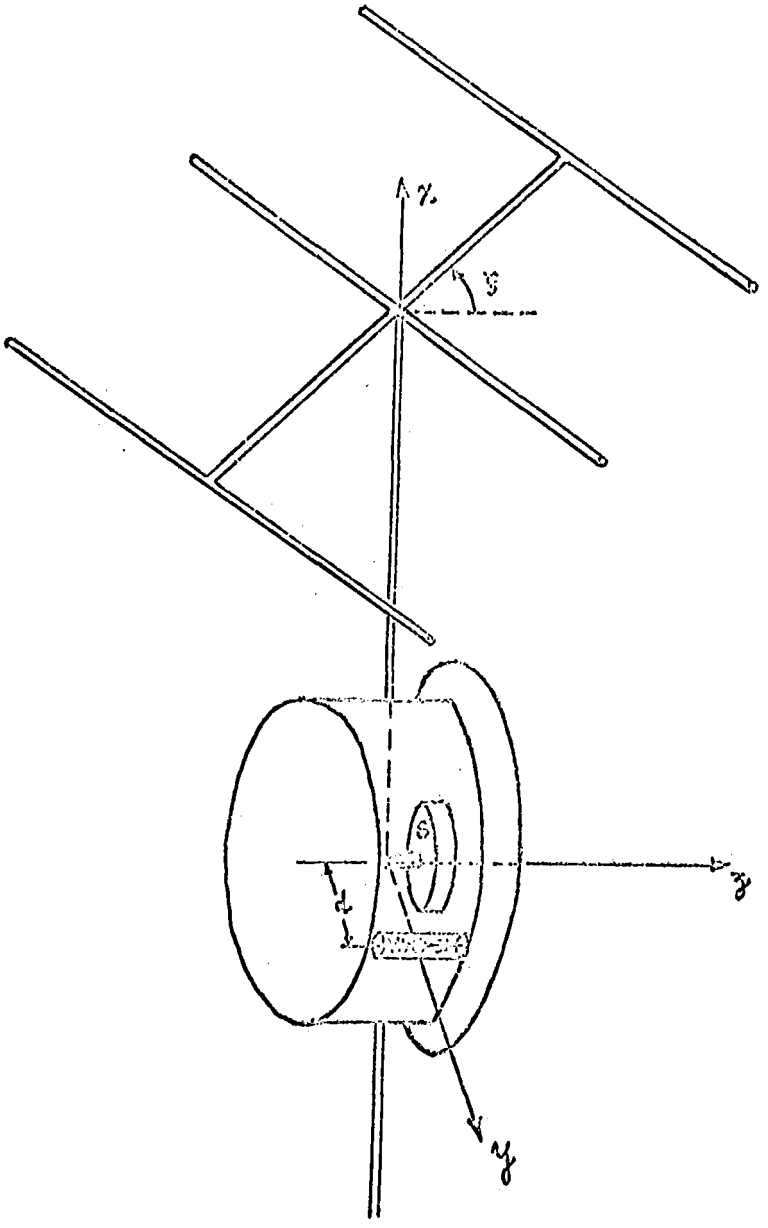

Figure B.1 Dual spin configuration

APPENDIX C

ANTENNA INERTIAS

Consider each antenna to be made up of five individual elements as shown below:

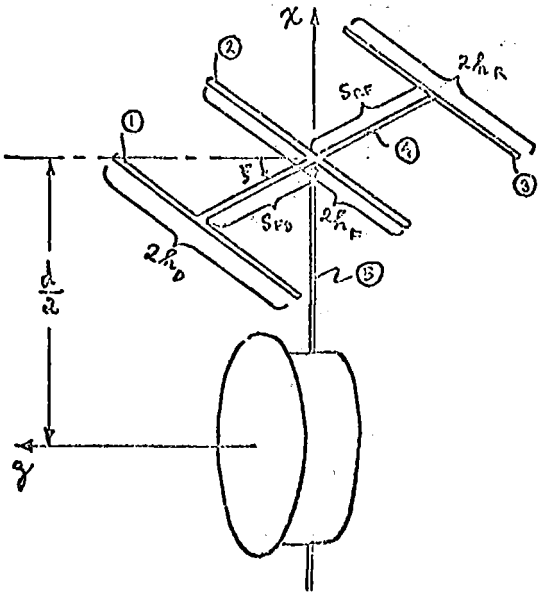

Each element can be considered as a thin long rod. For a uniform long rod of mass m and length 1, the moments of inertia are:

(1) normal to the length at one end, $m\frac{l^2}{3}$ (C-1)

(2) normal to the length at the center, $m\frac{l^2}{12}$ (C-2)

Using these results:

$$I_{x_{①}} = m_{①}\frac{(2h_D)^2}{12} + m_{①}(S_{FD})^2 \qquad (C-3)$$

$$I_{x_{②}} = m_{②}\frac{(2h_F)^2}{12} \qquad (C-4)$$

$$I_{x_{③}} = m_{③}\frac{(2h_R)^2}{12} + m_{③}(S_{RF})^2 \qquad (C-5)$$

$$I_{x_{④}} = m_{④}\frac{(S_{FD}+S_{RF})^2}{12} \qquad (C-6)$$

$$I_{x_{⑤}} \simeq 0 \qquad (C-7)$$

And $$I_x^a = I_{x_{①}} + I_{x_{②}} + I_{x_{③}} + I_{x_{④}} + I_{x_{⑤}} \qquad (C-8)$$

Note that I_x is independent of γ (x is a principal axis).

$$I_{y_{①}} = m_{①}\frac{(2h_D\sin\gamma)^2}{12} + m_{①}\left[\left(\frac{d}{2}\right)^2 + (S_{FD}\cos\gamma)^2\right] \qquad (C-9)$$

$$I_{y_{②}} = m_{②}\frac{(2h_F\sin\gamma)^2}{12} + m_{②}\left(\frac{d}{2}\right)^2 \qquad (C-10)$$

$$I_{y_{③}} = m_{③}\frac{(2h_R\sin\gamma)^2}{12} + m_{③}\left[\left(\frac{d}{2}\right)^2 + (S_{RF}\cos\gamma)^2\right] \qquad (C-11)$$

$$I_{y_{④}} = m_{④}\frac{[(S_{FD}+S_{RF})\cos\gamma]^2}{12} + m_{④}\left(\frac{d}{2}\right)^2 \qquad (C-12)$$

$$I_{y_{⑤}} = m_{⑤}\frac{\left(\frac{d}{2}\right)^2}{3} \qquad (C-13)$$

And $$I_y^a = I_{y_{①}} + I_{y_{②}} + I_{y_{③}} + I_{y_{④}} + I_{y_{⑤}}. \qquad (C-14)$$

$$I_{z_{①}} = m_{①}\frac{(2h_D\cos\gamma)^2}{12} + m_{①}\left[\left(\frac{d}{2}\right)^2 + (S_{FD}\sin\gamma)^2\right] \qquad (C-15)$$

$$I_{z_{②}} = m_{②}\frac{(2h_F\cos\gamma)^2}{12} + m_{②}\left(\frac{d}{2}\right)^2 \qquad (C-16)$$

$$I_{z_{③}} = m_{③}\frac{(2h_R\cos\gamma)^2}{12} + m_{③}\left[\left(\frac{d}{2}\right)^2 + (S_{RF}\sin\gamma)^2\right] \qquad (C-17)$$

$$I_{z\textcircled{3}} = m_{\textcircled{3}} \frac{[(S_{FD}+S_{RF})\sin\xi]^2}{12} + m_{\textcircled{3}} \left(\frac{d}{2}\right)^2 \qquad \text{(C-18)}$$

$$I_{z\textcircled{5}} = m_{\textcircled{5}} \frac{\left(\frac{d}{2}\right)^2}{3} \qquad \text{(C-19)}$$

And $$I_z^a = I_{z\textcircled{1}} + I_{z\textcircled{2}} + I_{z\textcircled{3}} + I_{z\textcircled{4}} + I_{z\textcircled{5}} \qquad \text{(C-20)}$$

$$J_{yz} = -\int yz\,dm \qquad \text{(C-21)}$$

$$J_{yz\textcircled{1}} = -m_{\textcircled{1}} \frac{(2h_D)^2}{12} \sin\xi\cos\xi + m_{\textcircled{1}} S_{FD}^2 \cos\xi\sin\xi \qquad \text{(C-22)}$$

$$J_{yz\textcircled{2}} = -m_{\textcircled{2}} \frac{(2h_F)^2}{12} \sin\xi\cos\xi \qquad \text{(C-23)}$$

$$J_{yz\textcircled{3}} = -m_{\textcircled{3}} \frac{(2h_R)^2}{12} \sin\xi\cos\xi + m_{\textcircled{3}} S_{RF}^2 \cos\xi\sin\xi \qquad \text{(C-24)}$$

$$J_{yz\textcircled{4}} = m_{\textcircled{4}} \frac{(S_{FD}+S_{RF})^2}{12} \sin\xi\cos\xi \qquad \text{(C-25)}$$

$$J_{yz\textcircled{5}} = 0 \qquad \text{(C-26)}$$

And $$J_{yz}^a = J_{yz\textcircled{1}} + J_{yz\textcircled{2}} + J_{yz\textcircled{3}} + J_{yz\textcircled{4}} + J_{yz\textcircled{5}} \qquad \text{(C-27)}$$

To get an indication of the actual values that can be expected, assume the following antenna dimensions:

$\frac{d}{2} = 150$ cm.

$2h_D = 2h_F = 2h_R = 200$ cm.

$\rho_R = \rho_F = \rho_D = 1.5$ cm.

$S_{RF} = S_{FD} = 64$ cm.

These figures were arrived at assuming a wavelength of 400 cm. For a three element yagi, only the center element is active, all the others being parasitic elements. Thus it is possible to make these much lighter. The following densities were assumed:

$$\rho_{②,③} = 2.7 \text{ gm/cm}^3$$

$$\rho_{①②③} = 2 \text{ gm/cm}^3$$

For $\gamma = 0$, the resulting inertias are:

$$I_y^a \simeq 2.9 \times 10^8 \text{ gm-cm}^2$$

$$I_x^a \simeq .312 \times 10^8 \text{ gm-cm}^2$$

$$I_z^a \simeq 3.0 \times 10^8 \text{ gm-cm}^2$$

Thus the spacecraft actually has almost equal inertias along two axes and a much smaller inertia along the remaining axis.

To get an idea of the maximum expected product of inertia, for $\gamma = 45°$,

$$|J_{yz}| \simeq 6 \times 10^6 \text{ gm-cm}^2$$

REFERENCES

1. The Conceptual Design of a Small Solar Probe (Sunblazer), M.I.T., CSR TR-69-1, Center for Space Research, M.I.T., January 1969.

2. Continued Study of a Small Solar Probe (Sunblazer), M.I.T., CSR TR-69-8, June 1969.

3. Harrington, J.V., "Dynamics of a Spinning Solar Pressure Stabilized Satellite with Precession Damping," Center for Space Research, M.I.T., CSR TR-66-6, June 1966.

4. Peterson, C.A., "Use of Thermal Reradiative Effects in Spacecraft Attitude Control," M.I.T., CSR T-66-3, May 1966.

5. Thomson, W.T., Introduction to Space Dynamics, John Wiley & Sons, New York, 1963.

6. Lim, W.K., Passive Damping of Spacecraft Rotational Motion., Ph.D. Thesis, M.I.T., October 1969.

7. Goldstein, H., Classical Mechanics, Addison-Wesley Co., London, 1964.

8. Acord, J.D., and Nicklas, J.C., "Theoretical and Practical Aspects of Solar Pressure Attitude Control for Interplanetary Spacecraft," Progress in Aeronautics and Astronautics, Vol. 13, Academic Press, New York, 1964.

9. Nercessian, H.J., "Optimum Design of a Stacked Pair of 3-element Yagis," Center for Space Research memorandum, July 16, 1969.

10. White, T.S., and Hansen, Q.M., "Study of Systems Using Inertia Wheels for Precise Attitude Control of a Satellite," NASA TN D-691, April 1961.

11. Schmidt, S.F., "The Analysis and Design of Continuous and Sampled-Data Feedback Control Systems with a Saturation Type Nonlinearity," NASA TN D-20, August 1959.

References (continued)

12. Lyon, E.F., "Sunblazer Orientation," Center for Space Research memorandum, July 10, 1969.

13. Sutherland, G.S., and Maes, M.E., "A Review of Micro-rocket Technology," Journal of Spacecraft and Rockets, August 1966.

14. Greensite, A.L., "Analysis and Design of Space Vehicle Flight Control Systems, Vol. 12, Attitude Control in Space," NASA CR-831, August 1967.

15. Likins, P.W., "Attitude Stability Criteria for Dual Spin Spacecraft," Journal of Spacecraft and Rockets, December 1967.

16. Velman, J.R., "Attitude Dynamics of Dual Spin Satellites," Hughes Aircraft Co., SSD 60419R, September 1966.

17. Landon, V.D., and Steward, B., "Nutational Stability of an Axisymmetric Body Containing a Rotor," Journal of Spacecraft and Rockets, November 1964.

18. Kapany, N.S., Fiber Optics: Principles and Applications, Academic Press, New York, 1967.

19. Strong, J., Concepts of Classical Optics., W.H. Freeman & Co., San Francisco, 1958.

20. Born, M., and Wolf, E., Principles of Optics, Pergamon Press, London, 1964.

21. Siegal, R., and Howell, Jr., "Thermal Radiation Heat Transfer," NASA SP-164, 1968.